Chemistry and biochemistry of *Populus* leaf bud resin

by

Eerik-Mikael Piirtola

B.Sc., University of Turku, Finland, 2016
M.Sc., University of Turku, Finland, 2019

A Dissertation Submitted in Partial Fulfillment
of the Requirements for the Degree of

DOCTOR OF PHILOSOPHY

In the Department of Biology

We acknowledge and respect the lək̓ʷəŋən peoples on whose traditional territory the university stands and the Songhees, Esquimalt and W̱SÁNEĆ peoples whose historical relationships with the land continue to this day.

Supervisory committee

Chemistry and biochemistry of *Populus* leaf bud resin

by

Eerik-Mikael Piirtola

B.Sc., University of Turku, Finland, 2016
M.Sc., University of Turku, Finland, 2019

Supervisory Committee

Dr. C. Peter Constabel, Supervisor
Department of Biology

Dr. Jürgen Ehlting, Departmental Member
Department of Biology

Dr. Greg Owens, Departmental Member
Department of Biology

Dr. Jeremy Wulff, Outside Member
Department of Chemistry

Abstract

Poplar trees, such as black cottonwood (*Populus trichocarpa*), balsam poplar (*Populus balsamifera*), and eastern cottonwood (*Populus deltoides*) are known to secrete resinous exudate from their leaf buds as their adaptation to temperate climate. The leaf bud resin protects the developing leaf buds from frost during winter dormancy. During bud break, the sticky resin coats the young leaves, protecting against insect herbivory during the early stages of leaf development. Leaf bud resins from different poplar species contain diverse phenolic secondary metabolites, especially hydrophobic flavonoids, which are biologically active. Due to their flavonoid-rich composition, poplar bud resins have been used widely in traditional medicine for their antimicrobial properties. Poplar leaf bud resins are also essential for honeybees, which utilize them as a building material and antibiotic protection for their hives in the form of propolis.

In this thesis, I characterized seasonal patterns of leaf bud resin accumulation, as well as genes involved in the biosynthesis of secreted flavonoids in leaf buds of *P. trichocarpa*, *P. balsamifera*, and *P. deltoides* using a combination of metabolomic analysis and transcriptomics. I used targeted and non-targeted analysis of the chemical composition of poplar bud resins to identify and quantify characteristic flavonoids in each poplar species. In parallel with the metabolomic analysis, transcriptomics and biochemical techniques were used to identify and characterize novel genes associated with the production of methoxylated and acylated flavonoids. The identified candidate genes were tested as recombinant proteins to characterize and verify their function. This work provides insight into the dynamic nature of poplar leaf bud resin biosynthesis and the enzymes involved in synthesizing characteristic flavonoids of poplar bud resin.

Table of Contents

List of Figures

Chapter 1

Chapter 2

Chapter 3

Chapter 4

Chapter 5

List of Tables

Acknowledgments

I want to start by thanking my supervisor, Dr. Peter Constabel, for providing me with this opportunity to grow as a scientist. The leap from being a chemist to becoming a plant biologist was bigger than I had initially anticipated, so I am grateful for Peter's support and guidance on this journey. I acknowledge the various organizations that have provided funding throughout the program, including the Natural Sciences and Engineering Research Council of Canada (NSERC), the University of Victoria, and the UVic Centre for Forest Biology.

I thank my committee members, Dr. Jürgen Ehlting, Dr. Greg Owens, and Dr. Jeremy Wulff, for our fruitful discussions. Your ideas and thorough explanations helped me set the frame for this thesis. I want to thank Dr. David Overy and the talented people at Agriculture and Agri-Food Canada for training and introducing me to the fascinating yet complicated world of metabolomics. I thank Dr. Ori Granot for assistance at the analytical chemistry lab. I extend my thanks to the past and present members of the Constabel lab, especially Dr. Dawei Ma, whose unparalleled experience and knowledge of countless methods have been invaluable help during my research. I also want to thank Sarah Lane for all the great conversations and ideas. I acknowledge the staff of the Biology office, especially Michelle Shen, for assisting me with a variety of paperwork I could not have figured out on my own.

I want to warmly thank my friends overseas, especially Aleksi Nyqvist and Thomas Keller, and my forever tutors, Salla Lahdenpohja and Isabella Pönkkä, for their support. I owe you guys a party. Lastly, I want to thank my family in Finland. Their love and support have helped me more than they could ever know.

Dedication

This journey has been a long and rocky road, and I could not have walked it alone.
Thank you, Winter, for bringing the summer and sunshine when the days were dark and cold.
You made all the difference.

List of Abbreviations

°C	degrees Celsius
2’,4’,6’,4-OH DHC	phloretin
2’,4’,6’-OH DHC	2’,4’,6’-trihydroxydihydrochalcone
2’,4’,6’-OH-4-OMe DHC	2’,4’,6’-trihydroxy-4-methoxydihydrochalcone
2’,6’,4-OH-4’-OMe DHC	asebogenin
2’,6’-OH-4,4’-OMe DHC	2’,6’-dihydroxy-4’,4-dimethoxydihydrochalcone
2’,6’-OH-4’-OMe DHC	2’,6’-dihydroxy-4’-methoxydihydrochalcone
4CL	4-coumaroyl-CoA ligase
AAFC	Agriculture and Agri-Food Canada
ANR	anthocyanidin reductase
ANS	anthocyanidin synthase
AT	acyltransferase
AU	absorbance unit
bp	base pairs
C4H	cinnamate 4-hydroxylase
cDNA	coding DNA
CHI	chalcone isomerase
CHS	chalcone synthase
cm	centimetre
CoA	coenzyme A
D	days
DAD	diode array detector
DFR	dihydroflavonol reductase
DTT	dithiothreitol
DW	dry weight
EIC	extracted ion chromatogram
eV	electron volts
F3H	flavanone 3-hydroxylase
FC	fold-change
Fig.	figure
FLS	flavonol synthase
FNS	flavone synthase
FW	fresh weight
g	gram
GC	gas chromatography
h	hours
HCDBR	hydroxycinnamoyl-CoA double-bond reductase
HRMS	high-resolution mass spectrometry

IPTG	isopropyl ß-D-thiogalactopyranoside
kDa	kilo Dalton
K_m	Michaelis–Menten constant (μM)
K_m/K_{cat}	enzyme specificity ratio
LAR	leucoanthocyanidin reductase
LB	Luria-Bertani broth
LC	liquid chromatography
LC/MS	liquid chromatography-mass spectroscopy
LD	long day
LT	low temperature
M	molar
m/z	mass to charge
mg	milligram
min	minute
mL	millilitre
mm	millimetre
mM	millimolar
MS	mass spectroscopy
n	sample size
nm	nanometers
OD	optical density
OH	hydroxy group
OMe	*O*-methoxy group
OMT	*O*-methyltransferase
PAL	phenylalanine ammonia-lyase
PC	principal component
PCA	principal component analysis
PCR	polymerase chain reaction
PdDAT1	*Populus deltoides* dihydroflavonol AT 1
PLS-DA	partial least squares-discriminant analysis
PtDOMT1	*Populus trichocarpa* dihydrochalcone OMT 1
PVDF	polyvinylidene difluoride
qPCR	qualitative PCR
RNA	ribonucleic acid
RNA-seq	RNA sequencing
rpm	revolutions per minute
RT	retention time
SAM	S-adenosyl-*L*-methionine
SD	short day
SDS-PAGE	sodium dodecyl sulfate-polyacrylamide gel electrophoresis

SE	standard error
SIR	selected ion recording
Spp.	species
TIC	total ion current
UPLC	ultra-high performance liquid chromatography
UV	ultraviolet
UVic	University of Victoria
VIP	variable importance in projection
Vmax	enzyme maximum velocity (pkat mg^{-1})
WT	warm temperature
µg	microgram
µL	microlitre
µM	micromolar

Chapter 1 – General introduction

1.1 Introduction

Plants are undoubtedly the best chemists and biochemists in the world. They produce an astonishing range of chemical compounds to grow, adapt, interact with their environment, and defend themselves. These metabolites are generally classified as primary metabolites and specialized metabolites. Primary metabolites are common metabolites across plants and are deemed essential for cell development, growth, and reproduction. Specialized metabolites, which constitute a much higher diversity of chemical compounds than primary metabolites, serve more adaptive functions such as pigments, signals, UV screens, and defence mechanisms. Many specialized metabolites are biologically active and have therapeutic and medicinal properties. Such metabolites have been harnessed by humans in the form of drugs, stimulants and pharmaceuticals. The types and profiles of specialized metabolites can differ dramatically between individual plant species. Sometimes, plants are defined by the characteristic classes of specialized metabolites they produce. This chemical diversity offers excellent potential for studying how plants produce and utilize such compounds. In this thesis, I describe several aspects of specialized metabolites, focusing on the metabolomic profiles as well as underlying enzymatic mechanisms relating to the intriguing world of plant resins.

1.2 Plant resins

In response to their environmental challenges and as part of their evolutionary adaptation, many plant species can produce complex resinous exudates of volatile and non-volatile specialized metabolites (Langenheim, 2003, 1990). These exudates are collectively referred to as plant resins. Plant resins are sometimes produced in response to stress, such as wounding or disease, or as a measure against herbivory (Phillips and Croteau, 1999; Langenheim, 2003). A classic example of an application of plant resin in defence is the production of resin by pine trees (Pinaceae) in their struggle against attack by bark beetles (*Dendroctonus* spp.), which are considered one of the most devastating tree-killing pests in North America (Kane and Kolb,

2010; Trapp and Croteau, 2001). As such, the production of resins demonstrates the constant evolutionary arms race of plants against insects and pathogens. Apart from defence against herbivores and pathogens, plant resins offer various ecological benefits to host plants. These include promoting wound healing, reducing transpiration, shielding against UV radiation, protecting seeds and pollen, and serving as a means of communication between plants (Langenheim, 2003).

Plant resins also have a long and rich history of economic, cultural, and medicinal importance for humans (Langenheim, 2003). They have been employed in numerous industrial applications, for example, as varnishes for paints and waterproofing (Colombini et al., 2000; Langenheim, 2003). Infusions of plant resins from various plant species have been widely used in traditional medicine (Langenheim, 2003; Moerman, 1998). Additionally, plant resins, such as those from cannabis, have a longstanding history of recreational and therapeutic use across different continents (Langenheim, 2003; Russo, 2007).

Plant resins are produced in specialized secretory tissues, which vary depending on the plant species. These secretary tissues include canals, pockets, cavities, trichomes, and epidermal cells (Langenheim, 2003). Generally, plant resins can be classified based on the type of specialized metabolites they are primarily composed of (Langenheim, 2003). This classification distinguishes resins from different plant species as terpenoid-type and phenolic-type resins. Terpenoid-type resins are rich in terpenoids, which are synthesized by terpene synthases derived from the mevalonate pathway and deoxyxylulose phosphate pathway (Trapp and Croteau, 2001; Langenheim, 2003). Phenolic-type resins are rich in phenolic compounds, such as phenylpropanoids, which are synthesized mainly via shikimic acid and malonic acid pathways (Langenheim, 2003; Lambert et al., 2021). It is important to note that despite this binary general classification, terpenoid-type resins can contain phenolic components and vice versa. They may also contain other classes of specialized metabolites, such as alkaloids and cannabinoids (Langenheim, 2003).

Importantly, plants can produce other exudates not classified as plant resins. Substances commonly mistaken as plant resins include gums, mucilages, essential oils, waxes, and latex (Langenheim, 2003; Lambert et al., 2021). These exudates can share some components with

plant resins but also contain groups of compounds not present in resins. Gums and mucilages contain primarily water-soluble polysaccharides, while essential oils and waxes are characteristically hydrophobic and contain fatty acids and their esters (Langenheim, 2003). Latex typically includes a mixture of compounds often found in plant resins, including terpenoids and phenylpropanoids, but also proteins and carbohydrates (Langenheim, 2003). Latex is sometimes intermixed with plant resin, explaining some of the chemical similarities (Langenheim, 2003). Moreover, latex is distinguished by its production in specialized secretory structures called laticifers, distinct from the tissues responsible for resin production (Langenheim, 2003).

1.2.1 Terpenoid-type plant resins

Terpenoid-type plant resins, also known as oleoresins, are common in gymnosperms, such as conifers. They are typically stored in interconnected canal-like resin ducts distributed throughout the wood and bark (Trapp and Croteau, 2001; Langenheim, 1990). Characteristically, terpenoid resins consist of volatile mono- and sesquiterpenes (turpentine fraction) and non-volatile di- and triterpenes (rosin fraction) (Fig. 1.1). In conifers and some angiosperms, the volatile fraction often consists of both mono- and sesquiterpenes, but the non-volatile fraction usually contains only either di- and triterpenes (Langenheim, 2003).

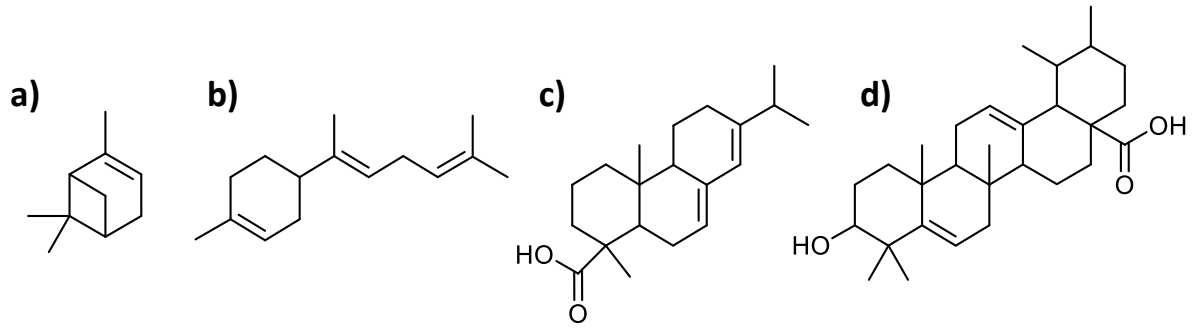

Figure 1.1. Examples of common terpenoids in terpenoid-type plant resins. Structures of a) monoterpene, α-pinene, b) sesquiterpene, bisabolene, c) diterpene, abietic acid, and d) triterpene, α-amyrin.

The relative proportion of volatile to non-volatile compounds can vary even within the same genus (Wang et al., 1997; Langenheim, 1990, 2003). This ratio can influence the ecological properties of the resins, as well as the physical properties of the resin, such as the fluidity and viscosity, and how easily it hardens (Langenheim, 1990, 2003). A higher proportion of the volatile components enhances resin flow, reducing viscosity, which allows the resin to engulf the invasive organisms. Resins rich in non-volatile components, such as diterpenoids, have higher viscosity but harden more quickly, allowing the resin to coat wounds on the plant's surface.

The regulatory mechanisms determining the ratio between the volatile and non-volatile fractions are not well known. However, the terpenoid composition of pine trees is known to vary in response to predation (Sturgeon, 1979; Langenheim, 2003). For example, when facing attacks from bark beetles, pine trees are observed to increase the production of toxic monoterpenes. These subtle yet efficient dynamic adjustments involved in terpenoid-type resin production underscore the adaptability of plant defence mechanisms in response to environmental challenges.

1.2.2 Phenolic-type plant resins

In contrast to terpenoid-type resins, phenolic-type resins are commonly found on the surface of plant tissues of angiosperms, such as leaf trichomes or secretary epidermis in leaf bud scales (Langenheim, 2003; Lambert et al., 2021). While the phenolic-type resins primarily consist of phenolic compounds, they are often intermixed with terpenoids (Langenheim, 2003).

Common phenolic components in these resins include simple phenolic acids, alcohols, and their esters (Langenheim, 2003). Simple phenolics include benzenoids, such as 4-hydroxybenzoic acid (Fig. 1.2a) and their derivatives, such as benzyl salicylate (Fig. 1.2b), and hydrocinnamic acids derived from *p*-coumaric acid (Fig. 1.2c). These compounds have been identified in the resins produced by various plant genera, such as *Liquidambar*, *Myroxylon* and *Xanthorrhoea* (Langenheim, 2003), as well as in leaf bud resins of *Populus* (English et al., 1991; Greenaway and Whatley, 1990; English et al., 1992). These simple phenolics often act as precursors for more complex phenolic compounds, such as phenylpropanoids, which have a wide

range of roles in plants, including providing structural support through lignin and acting as natural sunscreens against UV light and antioxidants via flavonoids (Vogt, 2010).

Phenylpropanoids in phenolic-type resins often include flavonoid aglycones (Wollenweber and Dietz, 1981; Langenheim, 2003). In contrast to water-soluble flavonoid glycosides found in many parts of the plant, the flavonoid aglycones in plant resins are generally hydrophobic. The addition of hydrophobic substitutions, such as varying degrees of *O*-methylation (Fig. 1.2d) (Wollenweber and Dietz, 1981), or hydrophobic of side chains, such as acylation (Fig. 1.2e) or prenylation (Fig. 1.2f), further increases the hydrophobicity of these flavonoids (Langenheim, 2003). Bioactive acylated flavonoids have been identified in leaf bud resins of eastern cottonwood (*Populus deltoides*) (Wilson et al., 2017), and prenylated chalcones have been studied in hops (*Humulus lupulus*) (Nagel et al., 2008). Flavonoid aglycone-rich phenolic-type resin is commonly found as secreted exudates from leaves and buds (Wollenweber and Dietz, 1981), especially on deciduous trees, such as birches (*Betula* spp.) (Valkama et al., 2004) and poplars (*Populus* spp.) (English et al., 1992, 1991; Greenaway et al., 1991).

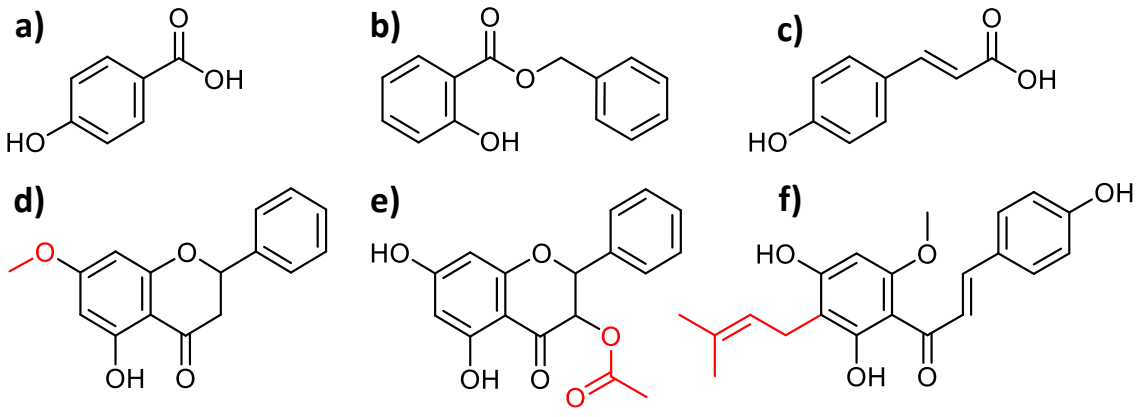

Figure 1.2. Examples of phenolic compounds found in phenolic-type resins. Structures of a) 4-hydroxybenzoic acid, b) benzyl salicylate, c) *p*-coumaric acid, d) methoxylated flavanone, pinostrobin, e) acylated dihydroflavonols, and f) prenylated chalcone, xanthohumol. Methoxy, acyl, and prenyl groups are highlighted in red.

This thesis investigates specialized metabolites found in phenolic-type resins, particularly flavonoid aglycones. Although significant contributions have been made in characterizing plant resins chemically, our comprehension of the underlying biochemical processes and mechanisms governing resin synthesis remains incomplete. To uncover the biochemical pathways responsible for the production of phenolic-type resin, we must understand the processes involved at the gene level. To achieve this, we can harness the knowledge of selected well-studied resin-producing plants, considered model species. One of the best-studied genera of resin-producing perennial trees is *Populus*.

1.3 Poplar as model species for studying specialized metabolism

The genus *Populus* belongs to the Salicaceae family, which includes poplars, willows, cottonwoods, and aspens. Poplars are widely distributed species in the Northern Hemisphere, especially in North America and Europe (Mitton and Grant, 1996; Cooke and Rood, 2007), often acting as keystone species (Rogers et al., 2020). In the world of poplar, Canada possesses a rather unique position as the center of poplar diversity, with seven of the 29 global poplar species occurring naturally as native species (Cooke and Rood, 2007).

Extensive genomic research, enabled by the high-quality sequenced and annotated genome (Sjödin et al., 2009; Tuskan et al., 2012), as well as efficient genetic transformation methods, has made *Populus* an important model for tree molecular biology (Jansson and Douglas, 2007). *Populus* are also ecologically important species and chemically rich in specialized metabolites, especially phenolics, making them an attractive genus for studies of phenolic biochemistry and chemical ecology.

Poplar trees face various abiotic stresses such as drought, seasonal temperature fluctuations, and biotic stress from insect herbivory. As evolutionary adaptations, poplar trees have devised different ways of utilizing specialized metabolites as defence compounds. Poplars accumulate condensed tannins, phenolic glycosides, and hydroxycinnamate esters in response to biotic and abiotic stresses and under nitrogen-limiting growing conditions (Tsai et al., 2006; Philippe and Bohlmann, 2007; Constabel and Lindroth, 2010). The most characteristic class of

phenolic defence compounds, specific to the Salicaceae family, is the salicinoids, a group of phenolic glycosides consisting of glycosylated and esterified derivatives of salicyl alcohol. These metabolites in poplar leaves, bark, and roots are important for anti-herbivore defence (Boeckler et al., 2011). The poplar genome and transcriptomes have been successfully leveraged for functional analyses to identify genes involved in the biosynthesis of these defence compounds (Gordon et al., 2022; Fellenberg et al., 2020).

In addition to salicinoids, many poplar species produce sticky resin from their leaf buds as a defence mechanism. The resin is thought to prevent dehydration and freezing of the leaf buds during overwintering dormancy and protect young leaves from insect herbivory (Curtis and Lersten, 1974). Poplar leaf bud resin is considered phenolic-type resin, as the main metabolites include common phenolics, such as benzonoids and flavonoids (Langenheim, 2003). Leaf bud resin synthesis takes place in a specialized secretary epidermis on the inner surface of the bud scales and developing leaves (Curtis and Lersten, 1974). Overwintering buds contain abundant amounts of resin, and in the spring, during bud break, the resin is secreted out with the emerging leaves, coating them with a layer of resin, which dries up as the leaves unroll and expand (Curtis and Lersten, 1974). While the chemical composition of resins produced by different poplar trees has been previously studied, the biosynthesis of the specialized metabolites found in the resin has not been investigated.

1.3.1 Chemistry of poplar leaf bud resin

Poplar bud resins are complex mixtures of specialized metabolites, including non-volatile phenolics and volatile compounds, such as terpenoids and phenylpropanoid cinnamyl cinnamate, which give poplar bud resin a strong characteristic fragrance (Langenheim, 2003). The main non-volatile phenolic metabolites are hydrophobic phenylpropanoids, benzenoids, and several classes of flavonoid aglycones (English et al., 1991; Greenaway and Whatley, 1990; English et al., 1992; Kuś et al., 2018; Isidorov and Vinogorova, 2003). The chemical composition of poplar leaf bud resin can vary significantly among *Populus* species, and distinct resin components are characteristic of many poplars. To date, English, Greenaway, and colleagues have conducted the most comprehensive analysis of the bud resins of different poplar species. Analyzed poplar

species include *P. trichocarpa* (English et al., 1991), *P. balsamifera* (Greenaway and Whatley, 1990), *P. nigra* (Greenaway et al., 1992a), *P. alba* (Greenaway et al., 1992a), *P. tremuloides* (Greenaway et al., 1992a), *P. deltoides* (English et al., 1992), *P. fremontii* (English et al., 1992), *P. sieboldii* (Greenaway et al., 1991), and *P. maximowiczii* (Greenaway et al., 1989a).

The most prevalent classes of flavonoids in poplar bud resins include flavanones, dihydroflavonols, and dihydrochalcones (English et al., 1991, 1992; Greenaway et al., 1992a), including *O*-acylated or *O*-methylated compounds. Characteristic resin compounds include pinostrobin (Figure 1.3a), pinobanksin-3-acetate (Figure 1.3b), and 2',6'-dihydroxy-4'-methoxydihydrochalcone (Figure 1.3c), as well as related compounds with different substitution patterns. This thesis will focus on the *O*-methylated dihydrochalcones and *O*-acylated dihydroflavonols, given their abundance in poplar bud resin (Greenaway et al., 1989b; English et al., 1992, 1991; Kuś et al., 2018) and the potential biological activities these types of compounds (Tyśkiewicz et al., 2019; Wilson et al., 2017).

O-methylated dihydrochalcones are found in the bud resins of *P. trichocarpa* and *P. balsamifera*, which belong to the *Tacamahaca* section of poplars (English et al., 1991; Greenaway and Whatley, 1990). These compounds are absent in the bud resin of other poplar species. Similar *O*-methylated derivatives of dihydrochalcones have been identified in the leaves of plants belonging to the Piperaceae (Rivière, 2016). *O*-acylated flavanones, on the other hand, are found in the bud resin of the *Aigeiros* section of poplars, including *P. deltoides*, *P. fremontii*, and *P. nigra*. These poplars contain characteristic acylated pinobanksin derivatives, such as pinobanksin-3-acetate, pinobanksin-3-propanoate, and pinobanksin-3-butanoate (English et al., 1992; Kuś et al., 2018). Similar *O*-acylated pinobanksin derivatives have been previously identified in other plant species, such as *Eremophila alternifolia* (Biva et al., 2016) and *Pinus armandii* (Fang et al., 1988).

Despite well-studied chemical profiles of different poplar resins, the exact timing of resin synthesis and accumulation is not known. Additionally, potential seasonal changes in the chemical composition of poplar bud resin over the growth and dormancy cycle have not been previously studied.

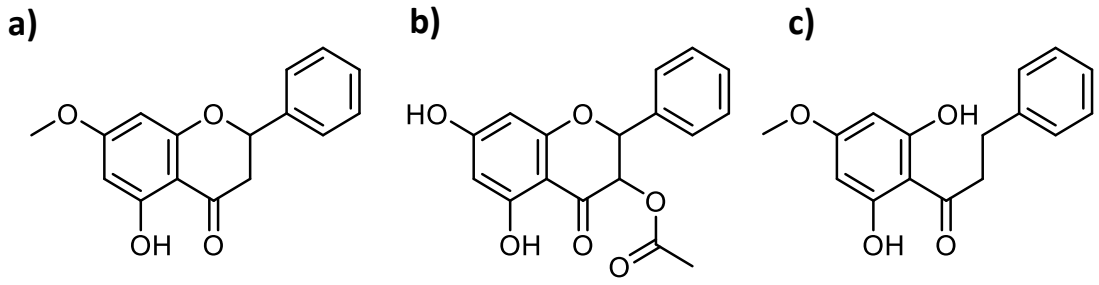

Figure 1.3. Characteristic flavonoid aglycones found in poplar bud resin. Example structures of poplar resin flavonoids investigated in this thesis, including a) flavanone, pinostrobin, b) dihydroflavonol, pinobanksin-3-acetate, and c) dihydrochalcone, 2',6'-dihydroxy-4'-methoxydihydrochalcone.

1.3.2 Seasonal growth cycle of poplar leaf buds

Due to their perennial and deciduous nature, poplars experience an annual cycle of growth and dormancy (Rinne et al., 2010). The key developmental stages of the annual growth cycle of poplar consist of active growth, growth cessation, dormancy, and reactivation of growth (Singh et al., 2017) (Fig. 1.4). The annual growth cycle in trees is influenced by environmental factors, such as changes in temperature and photoperiod (Tanino et al., 2010; Goffinet and Larson, 1981; Böhlenius et al., 2006). This cycle is also affected by hormonal responses, such as the stress hormone abscisic acid, which potentially regulates the induction of cold hardiness-related genes during the induction of dormancy (Druart et al., 2007). These different triggers induce transcriptome-level changes during the different stages of leaf bud development (Rohde et al., 2007; Ruttink et al., 2007; Conde et al., 2017).

The life cycle of leaf buds in poplar begins with active growth stimulated by increasing photoperiod in the late spring and early summer. During the active growth phase, the leaf primordia and the surrounding stipules elongate, developing into embryonic leaves and bud scales, which together form a leaf bud (Curtis and Lersten, 1974; Rohde et al., 2002; Singh et al., 2017; Goffinet and Larson, 1981). Terminal leaf buds form later in the summer, following the cessation of growth (Goffinet and Larson, 1981). Growth cessation is initiated by short days in the fall (Conde et al., 2017; Rinne et al., 2010). During cessation of growth, the elongation of the leaf primordia is gradually arrested, and the bud scales formed from the stipules form a

protective outer layer surrounding the leaf buds (Rohde et al., 2002; Goffinet and Larson, 1981). Since this transition is affected by the photoperiod, the timing of the growth cessation is affected by the latitude where the trees grow (Böhlenius et al., 2006).

Exposure to low temperatures, in addition to shortening photoperiod, initiates the induction of dormancy (Singh et al., 2017; Shim et al., 2014). During this stage, the leaf buds acclimate to overwintering dormancy and develop cold hardiness (Cooke et al., 2012). During dormancy, leaf buds become unresponsive to growth-promoting signals (Singh et al., 2017). The accumulated leaf bud resin protects the dormant leaf buds against dehydration and freezing temperatures (Curtis and Lersten, 1974).

The release from dormancy is coordinated by environmental signals, mainly by the length of exposure to non-freezing low temperatures (Rinne et al., 2010; Conde et al., 2017). In perennial trees, an increase in the photoperiod length, after sufficient exposure to low temperatures, signals the reactivation of growth in the spring, which leads to swelling of the leaf buds and bud break (Basler and Körner, 2014; Singh et al., 2017). After the bud break, the life cycle of a new generation of leaf buds begins with the formation of leaf primordia.

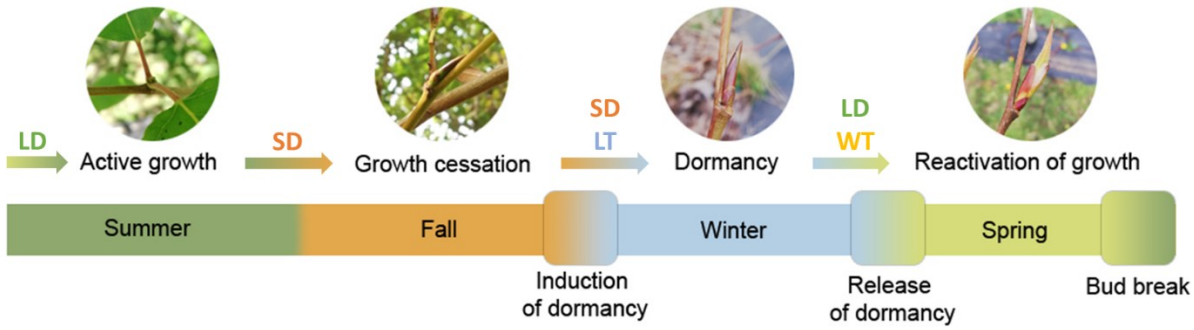

Figure 1.4. Annual growth cycle in poplar trees. Different stages of the growth-dormancy cycle in poplars are indicated above the time scale. Significant stages in the development of the leaf buds are indicated below. Short days (SD) induce the transition from active growth to growth cessation in early fall. Low temperatures (LT) and SD in the fall initiate the transition to dormancy. The overwintering dormancy is released in late winter/early spring after sufficient exposure to LT by warm temperatures (WT) and long days (LD), leading to bud break. Adapted from Singh et al. (2017) and Shim et al. (2014).

1.4 Biochemistry of poplar bud resin

Flavonoids in poplar leaf bud resin are derived from the phenylpropanoid pathway (Winkel-Shirley, 2001; Tsai et al., 2006; Yonekura-Sakakibara et al., 2019), which is also involved in the production of other important plant metabolites, such as lignin (Whetten and Sederoff, 1995). Different subgroups of flavonoids include chalcones, dihydrochalcones, flavanones, flavones, dihydroflavonols, flavonols, anthocyanins, and flavan-3-ols (Winkel-Shirley, 2001). The flavonoid genes and gene families encoding the flavonoid pathway enzymes (Fig. 1.5) have been characterized (Winkel-Shirley, 2001; Liu et al., 2016).

The first enzyme involved in the biosynthetic pathway of flavonoids is phenylalanine ammonia-lyase (PAL), which catalyzes the conversion of L-phenylalanine to cinnamic acid. In the subsequent step, cinnamate 4-hydroxylase (C4H) is involved in the catalysis of *p*-coumaric acid by the addition of a hydroxy group in the para position of cinnamic acid. However, in the case of hydrophobic flavonoids, this step of biosynthesis is omitted, as the B-ring of hydrophobic flavonoid structures does not have hydroxy groups. Consecutively, 4-coumarate-CoA ligase (4CL) and 4CL-like enzymes catalyze the conversion of *p*-coumaric acid and other substituted hydroxycinnamates into their respective coenzyme A (CoA) esters. All core phenylpropanoid and flavonoid gene families have been cataloged in-depth in poplar (Tsai et al., 2006).

1.4.1 Biochemistry of flavonoids

In many plant species, the first flavonoid products of this pathway are the chalcones, which are synthesized by condensation of three malonyl-CoA units on *p*-coumaroyl-CoA in a reaction catalyzed by chalcone synthase (CHS). In the main flavonoid pathway, chalcones are first converted to flavanones by chalcone isomerase (CHI). These compounds can be hydroxylated to dihydroflavonols by flavonoid hydroxylase (F3H) or are reduced into flavones by flavone synthase (FNS). Dihydroflavonols can be further processed to flavonols by flavonol synthase (FLS) or leucoanthocyanidins by dihydroflavonol reductase (DFR). Leucoanthocyanidins are precursors for anthocyanidins and flavan-3-ols. Flavan-3-ols are produced via two alternative routes at the downstream flavonoid pathway. They can form from

leucoanthocyanidins through a reductase enzyme (LAR) or anthocyanidins via a respective reductase enzyme (ANR). Condensation of flavan-3-ol subunits gives rise to proanthocyanidins downstream of the flavonoid pathway.

A separate pathway yielding dihydrochalcones diverging from the main flavonoid pathway has more recently been described (Ibdah et al., 2018). In the presence of hydroxycinnamoyl-CoA carbon double-bond reductases (HCDBR), *p*-coumaroyl-CoA can be reduced into *p*-dihydrocoumaroyl-CoA (Dare et al., 2013; Ibdah et al., 2014). This intermediate product is further modified by the addition of three malonyl-CoA units in a reaction catalyzed by a CHS or CHS-like gene to produce dihydrochalcones (Yahyaa et al., 2017; Ibdah et al., 2018). The HCDBR or CHS-like genes specific to dihydrochalcone synthesis have not yet been identified in *Populus*.

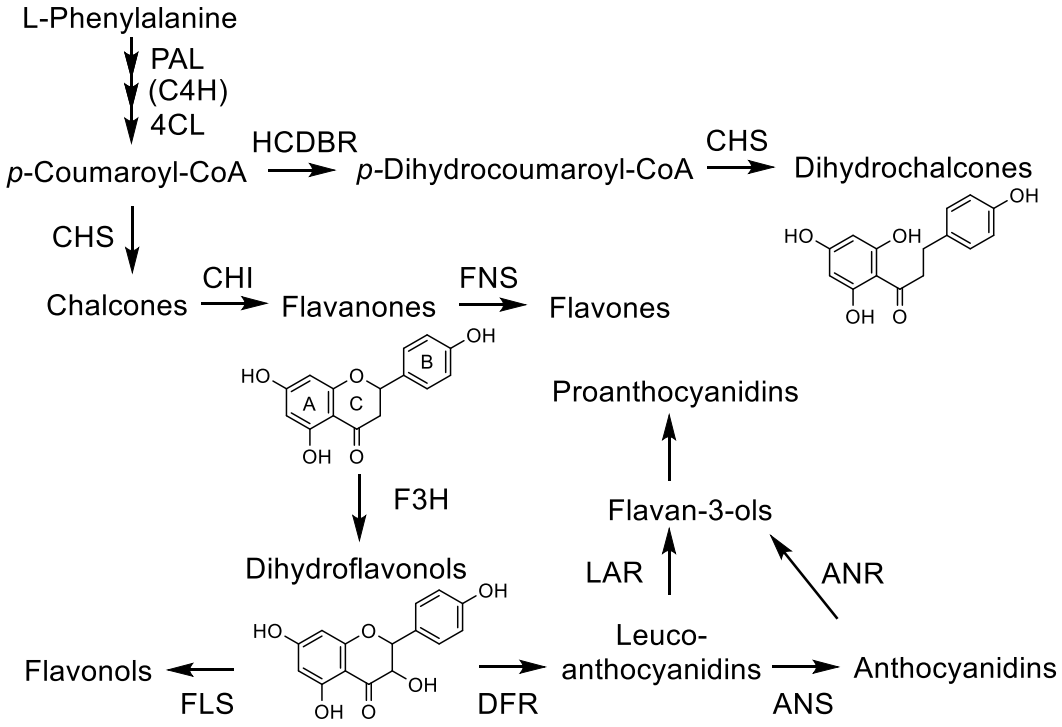

Figure 1.5. Biosynthetic pathway flavonoids. Enzymes involved in the biosynthesis of different classes of flavonoids. Name abbreviations: PAL, phenylalanine ammonia-lyase; C4H, cinnamate 4-hydroxylase; 4CL, 4-coumarate-CoA ligase; HCDBR, hydroxycinnamoyl-CoA double-bond reductase; CHS, chalcone synthase; CHI, chalcone isomerase; FNS, flavone synthase; F3H, flavanone 3-hydroxylase; DFR, dihydroflavonol reductase; FLS, flavonol synthase; LAR, leucoanthocyanidin reductase; ANS, anthocyanidin synthase; and ANR, anthocyanidin reductase.

1.4.2 Flavonoid acyltransferases and *O*-methyltransferases

While the biosynthesis of core flavonoids and the identity of biosynthetic genes is generally well-established in *Populus*, the occurrence of modified flavonoid aglycones in poplar leaf bud resins implies additional modifications of flavonoid structures by yet uncharacterized enzymes that are involved in the biosynthesis of flavonoids. The abundance and diversity of *O*-acylated and *O*-methylated flavonoids in poplar leaf bud resin suggest the existence of flavonoid *O*-acyltransferases (ATs) and *O*-methyltransferases (OMTs). These postulated enzymes modify the core flavonoids by adding hydrophobic side groups as a part of poplar bud resin biosynthesis.

ATs are a biochemically diverse and significant group of enzymes which catalyze the addition of acyl groups to metabolites, including flavonoids. In particular, enzymes that use CoA thioesters as donor molecules for acylation reactions of plant metabolites belong to the family of BAHD-type ATs (Kruse et al., 2022; Wang et al., 2022; D'Auria, 2006; Tuominen et al., 2011). The BAHD family was named based on the first four characterized enzymes in this family, including benzyl alcohol *O*-acetyltransferase (BEAT) (Dudareva et al., 1998), anthocyanin O-hydroxycinnamoyltransferase (AHCT) (Fujiwara et al., 1998), N-hydroxycinnamoyl/ benzoyltransferase (HCBT) (Yang et al., 1997), and deacetylvindoline 4-*O*-acetyltransferase (DAT) (St-Pierre et al., 1998). BAHDs are usually located in the cytosol of plant cells (Bontpart et al., 2015). Generally, BAHDs are classified into clades based on their function and the types of substrates they accept (D'Auria, 2006). However, these clades are not entirely homogenous in terms of substrate-specificity of the BAHDs, and these clades can be further divided into subclades (Kruse et al., 2022; D'Auria, 2006). Annotation of characterized BAHDs based on substrate classes comprises up to eight groups (A-H) (Table 1.1) within the BAHD family (Kruse et al., 2022).

Table 1.1. Classification of BAHD-type acyltransferases. Groups of characterized BAHD-ATs based on their substrate classes. Adapted from Kruse et al. (2022).

Substrate classes	Group	# of characterized genes
Aromatic alcohols, amines	A	67
Aliphatic alcohols, amines	B	60
Monoterpenoids, Sesquiterpenoids	C	8
Anthocyanins, Flavonoids, Phenolic glucosides	D	31
Diterpenoids	E	5
Triterpenoids	F	3
Sugar derivatives	G	14
Alkaloids	H	14

Another important structural modification of flavonoids is *O*-methylation. *O*-methyltransferases found in plants can act on hydroxy groups of phenolic specialized metabolites, catalyzing the methoxylation of these groups (Barakat et al., 2011). Methoxylation is a common substitution in phenolic specialized metabolites, and *O*-methylation has been reported in phenylpropanoids, including hydrocinnamic acids, stilbenes, and flavonoids (Roje, 2006; Ibrahim et al., 1998). Flavonoid OMTs have been previously described in various plant species, including sweet basil (*Ocimum basilicum*) (Berim et al., 2012) and peach (*Prunus percia*) (Cheng et al., 2014). As of yet, only a single OMT acting on flavones has been characterized in poplar (Kim et al., 2006). Generally, OMTs share structural similarities, but subtle differences in their gene sequences lead to functional differentiation, which results in distinct substitution patterns on their preferred substrates (Berim et al., 2012). This differentiation in the substitution patterns results from the regioselectivity of the OMT enzymes (Berim et al., 2012). The selectivity contributes to structural diversity and the accumulation of different specialized metabolites in plants (Cheng et al., 2014).

1.5 Biological and ecological significance of poplar resins

Beyond the beneficial properties of plant resins for the host plants, resin-producing poplar species have been widely used in traditional medicine in North America (Moerman, 1998; Ghisalberti, 1979; Uprety et al., 2012). Poplar resins are commonly utilized in human medicine as infusions, such as boiled extracts or mixtures with animal fats (Moerman, 1998). The resin

preparations have been used for various purposes, such as disinfectants and dermatological aids as topical ointments for dressing wounds (Langenheim, 2003; Moerman, 1998). However, humans are not the only species to benefit from poplar resins. One of the biggest beneficiaries of the specialized metabolites produced by poplar is honey bees, which use it to prepare propolis (Simone-Finstrom and Spivak, 2010).

Propolis, the collective apicultural term for bee glue, has also been used in human medicine, and its use dates back as far as 300 BC (Braakhuis, 2019; Burdock, 1998; Ghisalberti, 1979). Bees make propolis by mixing plant resins from different plant origins with beeswax to make a sticky substance utilized as a building material for their nests (Bastos et al., 2008; Simone-Finstrom et al., 2017; Wilson et al., 2013). In addition to honey bees (*Apis mellifera*), stingless bees (*Tetragonilla* spp.) make propolis (Ishizu et al., 2018; Leonhardt and Blüthgen, 2009).

Due to the varying availability of resin-secreting plant species, honey bees utilize plant resins from specific plant species in different regions as the main components of propolis (Kumazawa et al., 2004; Salatino et al., 2011). Hence, plant resins responsible for the diversity of biological activities differ between propolis types of different geographical origins. Propolis types from different geographical origins have demonstrated a wide range of pharmacological properties, including antioxidant (Kumazawa et al., 2004), antibacterial (Kujumgiev et al., 1999; Veloz et al., 2019), antifungal (Kujumgiev et al., 1999), anticancer (Akao et al., 2003), and antiviral (Kujumgiev et al., 1999) activities.

In the Northern Hemisphere, *Populus* species are a primary source of plant resins in propolis (Salatino et al., 2011; Bankova et al., 2000, 2018). In Europe, one of the most studied species identified as one of the major sources of propolis plant resins is *P. nigra* (Dudonné et al., 2011; Rubiolo et al., 2013; Kuś et al., 2018). In contrast, studies conducted in North American apiaries have identified leaf bud resins from *P. trichocarpa*, *P. balsamifera*, and *P. deltoides* as the main sources of biologically active components of propolis (Wilson et al., 2015, 2013).

For honey bee colonies, propolis compounds derived from the plant resins provide antimicrobial protection against various bee pathogens (Bastos et al., 2008; Simone-Finstrom et al., 2017; Wilson et al., 2015; Simone-Finstrom and Spivak, 2010). The diversity of biologically

active specialized metabolites in poplar bud resin, utilized by both humans and pollinators as a source of natural remedy, underlines the pharmacological significance of poplar resins. By extension, due to the antimicrobial nature of the flavonoids, propolis and poplar resins can be considered both ecologically and economically important, as honey bee pollination is a significant contributor to global agriculture (Gallai et al., 2009; Johnson, 2010).

1.6 Research objectives

This dissertation seeks to bridge a significant knowledge gap between the chemistry and biosynthesis of poplar bud resin. The seasonal changes in the chemistry of bud resin and the genes related to the biosynthesis of the major resin components have not been previously investigated. This work thus expands on the previous research on poplar resin components, which focused on quantifying the major resin flavonoids in different poplar species. In addition, my work aims to identify the seasonal patterns in bud resin composition using targeted and non-targeted metabolomic approaches. I focus on identifying and characterizing key enzymes responsible for the biosynthesis of lipophilic flavonoids found in poplar bud resin, specifically OMTs and BAHD-type ATs. To do this, I use RNA sequencing (RNA-seq) and differential gene expression analyses combined with phylogenetic analysis to identify candidate genes expressed in poplar buds.

The overall objective of this research is to study the flavonoids related to poplar bud resin biosynthesis and provide an in-depth understanding of the enzymes involved. By identifying the enzymes acting on bud resin dihydrochalcones and dihydroflavonols, this research will elucidate the first characterized steps in leaf bud resin synthesis and contribute to localizing the sites of resin production in poplar bud tissues, representing a significant step forward in understanding the biosynthesis of poplar bud resin. By utilizing state-of-the-art tools and methods, this research will significantly advance our knowledge of the chemical composition, seasonal dynamics, and biosynthetic processes of poplar bud resin.

1.7 Dissertation outline

This introductory chapter provides a background for specialized metabolites in different types of plant resin, as well as the ecological importance of poplar leaf bud resin. More specifically, I introduced the chemical and biochemical properties of leaf bud resin flavonoids produced by poplars. The data chapters of this thesis aim to assess the chemistry and biochemistry of major leaf bud resin components. The overall objectives of this thesis are to characterize the seasonal patterns of poplar bud resin accumulation and the biochemical characterization of OMTs and ATs, namely *O*-methylated dihydrochalcones and acylated dihydroflavonols, in poplar bud resin of verified genotypes of *P. trichocarpa*, *P. balsamifera*, and *P. deltoides*. The data chapters are written in the form of manuscripts, which will be submitted for publication.

In Chapter 2, I aim to identify the seasonal shifts in poplar leaf bud resin in *P. trichocarpa* over the growth-dormancy cycle. I used targeted metabolite analysis to identify seasonal patterns in the accumulation of dihydrochalcones in poplar leaf buds and the secreted surface resin. I also conducted a non-targeted metabolomic analysis to investigate the seasonal changes in the total metabolites. The non-targeted metabolomics study established metabolomic shifts in the chemical composition of whole leaf buds and the surface resin over the growth-dormancy cycle. Overall, the chemical analysis demonstrated the importance of *O*-methylated dihydrochalcones and flavonoids as significant components of poplar bud resin. The abundance of *O*-methylated dihydrochalcones provided preliminary evidence for candidate genes for leaf bud resin-related OMTs, which I describe in Chapter 3.

In Chapter 3, I describe the identification and biochemical characterization of an OMT, which acts on leaf bud resin-specific dihydrochalcones. I studied *P. trichocarpa* and *P. balsamifera* as parallel systems because the two species contain similar dihydrochalcones in their leaf bud resin. I used RNA-seq and differential gene expression analysis between the two species to identify candidate genes. I expressed the candidate genes as recombinant proteins in *E. coli* to test their activities, and I identified PtDOMT1, which specifically produces *O*-methylations on various dihydrochalcone substrates. I studied the gene expression dynamics of PtDOMT1 in poplar leaf buds collected over the growth-dormancy cycle. This analysis revealed a seasonal

expression pattern, coinciding with the dihydrochalcones accumulation described in Chapter 2. In addition, tissue-specific expression analysis suggested localization of PtDOMT1 in the leaf bud scales. Overall, identifying PtDOMT1 as an OMT related to the production of major resin components in *P. trichocarpa* and *P. balsamifera* established the first characterized step of poplar bud resin synthesis.

Chapter 4 of this thesis describes the identification and preliminary biochemical characterization of bud resin-related BAHD-type AT in *P. deltoides*. The approach described in this chapter follows largely a similar approach presented in Chapter 3. I used UPLC-MS analysis to confirm the presence of acylated dihydroflavonols in different tissues of *P. deltoides* leaf buds and flower buds. I conducted RNA-seq analyses with a time series of leaf buds induced to flush in a growth chamber and different tissues of leaf and flower buds to identify candidates for bud resin-related BAHD-ATs. I conducted differential gene expression analyses to identify tissue-specific expression patterns and expression dynamics of the candidate genes. The candidate genes were tested as recombinant proteins to study their interaction with pinobanksin. Overall, these experiments identified PdDAT1 with the capacity to use different acyl donors to produce acylated pinobanksin derivatives found in *P. deltoides*, connecting it to the synthesis of bud resin. Additionally, PdDAT1 is the first identified BAHD-type AT capable of acting on flavonoid aglycones.

Chapter 5 summarizes the general conclusions from my analyses of poplar leaf bud resin. I aim to relate the analysis of dihydrochalcone accumulation results performed in Chapter 2 with the gene expression analysis of a leaf bud resin-related gene characterized in Chapter 3. I present conclusions regarding the significance of the contributions made in this thesis in research of secreted plant resins and the field of flavonoid biosynthesis. Lastly, I aim to present my suggestions for the future directions of poplar leaf bud resin research.

Chapter 2 - Poplar leaf bud resin metabolomics – seasonal patterns and developmental changes in leaf bud chemistry

2.1 Abstract

Poplar trees (*Populus* spp.) are known to secrete resinous exudate from their leaf buds. *Populus trichocarpa* leaf bud resin contains diverse phenolic specialized metabolites, including characteristic hydrophobic dihydrochalcone aglycones. The ecological function of the hydrophobic leaf bud resin compounds is to protect the leaf buds and developing leaves from insect herbivory and frost. The synthesis of poplar leaf bud resin occurs in special secretary structures on the inner surface of the bud scales. The accumulated resin coats the developing leaves, and a part of it is secreted on the surface of the leaf buds. However, potential changes in the leaf bud resin composition during the growing season and at different stages of leaf bud development have not been previously studied. We analyzed the dihydrochalcone composition in whole leaf buds and the secreted surface resin extracts over the yearly growth cycle using targeted UPLC-MS. We also applied a non-targeted metabolomics approach by UPLC-HRMS to analyze seasonal patterns in leaf buds and the surface resin. Our results demonstrate the role of dihydrochalcones as major components in the leaf bud resin in dormant leaf buds and differences in the timing of dihydrochalcone accumulation between the whole buds and surface resin. Furthermore, our results indicate shifts in the chemical composition of leaf bud resin over the different stages of leaf bud development.

2.2 Introduction

Trees in the genus *Populus* (poplars, cottonwoods, and aspens) are widely distributed species in North America and Europe (Mitton and Grant, 1996; Cooke and Rood, 2007). The ecological significance of poplar trees and the diversity of phenolic specialized metabolites produced by *Populus* as defence compounds make it an attractive genus for studies of phenolic biochemistry and chemical ecology. The most characteristic classes of phenolic compounds for poplars are salicinoids, hydroxycinnamate derivatives, and condensed tannins (Constabel and

Lindroth, 2010). Salicinoids, a group comprising glycosylated and esterified derivatives of salicyl alcohol, are important specialized metabolites associated with anti-herbivore defence (Boeckler et al., 2011). Salicinoids are especially abundant in poplar leaves, bark, and root tissues (Donaldson et al., 2006; Fellenberg et al., 2020). Hydroxycinnamate derivatives include chlorogenic acid isomers and shikimate esters (Babst et al., 2014; Tsai et al., 2006). Hydroxycinnamate esters in poplar have radical scavenging properties, acting as a type of high-light sunscreen. However, they are also important in part of the biosynthesis of other metabolites, such as lignin (Tsai et al., 2006). Condensed tannins act as an inducible defence against oxidative stress and herbivory (Gourlay and Constabel, 2019). Besides the non-volatile phenylpropanoids, poplars are also capable of producing volatile terpenes (Irmisch et al., 2014) and benzoic acid esters (Chedgy et al., 2015; Babst et al., 2010), which may act as herbivore-induced signalling compounds.

In temperate regions, a particularly characteristic feature of many poplar species is the fragrant resin produced in the leaf buds. The function of leaf bud resin is associated with protecting developing tissues, working as an antidesiccant by reducing water loss and protecting against freezing damage in these tissues during winter and early spring (Langenheim, 2003). Based on anatomical observation, the leaf bud resin is proposed to be mainly synthesized in a special secretary epidermis on the inner surface of the bud scales (Curtis and Lersten, 1974). Overwintering dormant buds contain abundant amounts of resin, and in the spring, the resin is secreted on the young leaves, coating the leaves with a layer of resin, which dries up as the leaves unroll and expand (Curtis and Lersten, 1974). The surface resin protects young leaves against insect herbivory (Curtis and Lersten, 1974).

Poplar leaf bud resin is a complex mixture of phenolic specialized metabolites (English et al., 1991, 1992; Greenaway et al., 1991). The abundance of the phenolic compounds distinguishes the resins produced by poplar trees from resin produced by conifers, which typically produce resin rich in terpenoids (Langenheim, 2003). The chemical composition of poplar leaf bud resin can vary significantly among *Populus* species, and distinct resin components are characteristic of different poplar species (Greenaway and Whatley, 1990; Greenaway et al., 1992b, 1989b; English et al., 1992). Generally, the main components of leaf bud resin include non-volatile phenolics (Jerković and Mastelić, 2003; English et al., 1991) and

volatile compounds, such as cinnamic acid esters, which are thought to give poplar bud resin a strong characteristic fragrance (Langenheim, 2003). The main non-volatile phenolic metabolites include hydrophobic phenylpropanoids and several classes of flavonoids, including flavanones, dihydroflavonols, and dihydrochalcones (Fig. 2.1) (English et al., 1991, 1992; Isidorov and Vinogorova, 2003; Greenaway and Whatley, 1990). Unlike the intracellular flavonoids, the flavonoids in poplar leaf bud resin are found as aglycones, which makes them hydrophobic. In addition to poplars, flavonoid aglycones have been previously identified in bud exudates of various plants, such as *Betula* spp. and *Alnus* spp. (Wollenweber and Dietz, 1981). Flavonoid aglycones detected in the surface resin of poplar buds often contain further hydrophobic modifications, such as a varying degree of *O*-methylation (English et al., 1991), which reduces water-solubility and contributes to the hydrophobic nature of the secreted surface resin. In addition to poplars, flavonoid aglycones and *O*-methylated flavonoids have been previously described in secreted surface exudates of *Betula* spp. leaves (Valkama et al., 2004).

Populus trichocarpa (black cottonwood) leaf bud resin contains dihydrochalcones aglycones as the characteristic class of phenylpropanoids, as well as benzoic acid and phenylpropanoic acid esters constituting the major phenolic components of the leaf bud resin (English et al., 1991; Greenaway et al., 1989b). Dihydrochalcones are a unique class of flavonoids as their biosynthesis diverges early from the main flavonoid pathway (Ibdah et al., 2018). Dihydrochalcones have been found in over 46 plant families, and approximately 256 dihydrochalcone structures have been identified (Rivière, 2016). Dihydrochalcone aglycones with varying degrees of *O*-methylation and hydroxylation substitution patterns were identified in *P. trichocarpa* leaf bud extract (English et al., 1991), as well as in the leaf bud resin of *P. balsamifera*, which is a closely related species in the *Tacamahaca* section of poplars (Greenaway et al., 1992; Greenaway and Whatley, 1990). Strikingly, these compounds are largely absent in the leaf bud resin of other sections of poplars (Greenaway and Whatley, 1990; Greenaway et al., 1992a, 1989b). Similar *O*-methylated dihydrochalcones have also been previously described in plant extracts of other plant species, such as *Piper aduncum* (Orjala et al., 1994) and *Piper dennisii* (Cabanillas et al., 2012), both of which have been shown to possess medicinal significance (Holdsworth and Damas, 1986; Céline et al., 2009). Although the main components of poplar leaf bud resins have been identified, seasonal changes in the chemical composition at different stages of leaf bud development have not been previously studied.

In this study, we investigated seasonal patterns and changes in the chemical composition of *P. trichocarpa* lateral leaf buds and the secreted resin monthly over a one-year growth-dormancy cycle. The phenological stages of the sampled leaf buds included actively growing newly developed buds in the summer, mature leaf buds during cessation of growth and induction of dormancy in the fall, dormant leaf buds in the winter, and opening leaf buds during the release of dormancy and reactivation of growth in the spring (Singh et al., 2017). We used ultra-high performance chromatography (UPLC) coupled with mass spectrometry (MS) for targeted analysis of dihydrochalcones and non-targeted metabolomics using high-resolution mass spectrometry (HRMS) to identify changes in the total metabolites in the leaf bud extracts. Here, we found that the leaf bud resin composition displayed distinct seasonal patterns over the growing season, potentially coinciding with different stages of leaf bud development and the accumulation of *O*-methylated dihydrochalcones. We detected an accumulation of dihydrochalcones in the whole leaf buds during summer. In contrast, in the surface resin, the accumulation of dihydrochalcones was observed in the early spring and late fall. These shifts in the specialized metabolite profiles and the total amount of dihydrochalcones could imply that the production of specialized metabolites derived from the phenylpropanoid pathway could be subject to seasonal regulation.

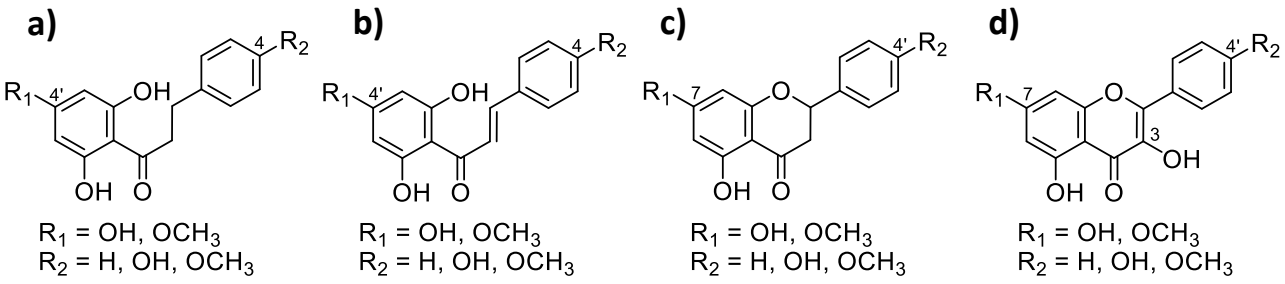

Figure 2.1. Common flavonoid classes in *P. trichocarpa* leaf bud resin. General structures and common substitution patterns of a) dihydrochalcones, b) chalcones, c) flavanones, and d) flavonols.

2.3 Materials and Methods

2.3.1 Analytical standards

Analytical standards for 2',4',6'-trihydroxydihydrochalcone (2',4',6'-OH DHC), 2',4',6'-trihydroxy-4-methoxydihydrochalcone (2',4',6'-OH-4-OMe DHC), 2',6'-dihydroxy-4,4'-dimethoxydihydrochalcone (2',6'-OH-4,4'-OMe DHC), salicortin, and tremulacin were acquired from Biosynth Carbosynth (San Diego, USA). Phloretin (2',4',6',4-OH DHC), asebogenin (2',6',4-OH-4'-OMe DHC), and 2',6'-dihydroxy-4'-methoxydihydrochalcone (2',6'-OH-4'-OMe DHC) were acquired from TransMIT (Giessen, Germany). Pinocembrin chalcone and naringenin chalcone were acquired from Extrasynthese (Lyon, France). Salicin was acquired from Sigma-Aldrich (Oakville, Canada).

2.3.2 Sampling of *P. trichocarpa* leaf buds

Poplar leaf bud samples of *P. trichocarpa* (Nisqually-1) were collected from the University of Victoria Research Compound. Intact leaf buds of *P. trichocarpa* were collected every month (mid-month) for 12 months to examine seasonal patterns of leaf bud resin accumulation (Supplemental Figure S2.1). Samples were collected from three adjacent clonal trees as biological replicates. For the whole leaf bud extraction, 10 lateral leaf buds were sampled from each biological replicate tree and frozen immediately in liquid nitrogen to prevent sample degradation. For the extraction and chemical analysis of the surface resin, three replicate sets of five similarly sized lateral leaf buds were collected from individual branches of each tree. During the sampling of surface resin between May and July, due to the small size of the developing leaf primordia, the whole leaf nodes, including the leaves and developing leaf primordia, were collected to account for the total amount of surface resin. The harvested leaf buds were homogenized into a fine powder in liquid nitrogen using a ceramic mortar and pestle and stored at -80°C before extraction to prevent sample degradation.

2.3.3 Extraction of *P. trichocarpa* leaf bud surface resin

The surface resin extracts of *P. trichocarpa* leaf buds were collected by accurately weighing 0.5 g (fresh weight) of intact lateral leaf buds and submerging them in 0.1 mL of HPLC-grade methanol per 10 mg of sample. The leaf buds were stirred for 1 min, after which the supernatant was collected. The methanol extract was filtered using a 0.20 µm PTFE filter to remove any solid particles. The extract was dried by transferring 2 mL of methanol extract into pre-weighed Eppendorf tubes and evaporating the samples using an Eppendorf concentrator until dry. The dried samples were accurately weighed to determine the dry weight of the surface resin extracts. The dry extracts were stored at -20 °C prior to the analysis.

2.3.4 Extraction of *P. trichocarpa* whole leaf bud resin

The extraction of whole leaf buds was performed by accurately weighing 40 mg (fresh weight) of frozen ground poplar leaf buds and adding 1 mL of methanol. The samples were vortexed, sonicated for 10 min in a sonicating water bath, and centrifuged for 10 min at 15000 rpm to pellet the plant material. The supernatant was collected, and the extraction protocol was repeated. The two extractions were combined, and the pooled samples were dried using an Eppendorf concentrator for 2 hours until dry. The dried extracts were stored at -20 °C until the analysis. For the non-targeted metabolomic analysis, nine extraction blanks were prepared using the same extraction protocol without the leaf buds.

2.3.5 Targeted quantification of dihydrochalcones *P. trichocarpa* in leaf bud resin extracts by UPLC-MS

The whole leaf bud extracts were reconstituted in 1 mL of methanol. These samples were normalized by the fresh weight of the extracted whole buds. The secreted surface resin samples were reconstituted to 100 µg/mL concentration based on dry extract weight. The samples were analyzed using a Waters Acquity UPLC System coupled to an Acquity PDA eLambda Detector and an Acquity QDa single quadrupole mass spectrometer (Waters, Milford, MA, USA). The

column used for separation was Acquity BEH C_{18} (50 mm x 2.1 mm ID, 1.7 µm). The column manager temperature was set to 40°C, and the autosampler temperature was 10°C. The two-solvent gradient consisted of solvent A (ddH_2O with 0.1% formic acid (v/v)) and solvent B (acetonitrile with 0.1% formic acid (v/v)) at a flow rate of 0.5 ml/min. The gradient was as follows: 0.1% B (0–0.5 min), 0.1–50% B (0.5–5 min), 50–90% B (5–8 min), 90% B column wash (8–9 min), 90–0.1% B (9–9.1 min), and 0.1% B for column equilibration (9.1–11 min). The UV detector range was 190–800 nm. The MS conditions were as follows: capillary voltage 0.8 kV, probe temperature 600°C, source temperature 150°C, and cone gas (N_2) flow. The MS full scan range was 50–1000 *m/z,* and the MS analysis was performed using the negative ionization mode.

The compound-specific MS data were collected using SIR methods optimized for the predominant molecular ion $[M+H]^-$ of each compound of interest. The optimized SIR methods were as follows: phloretin (273 *m/z*, 15 V), asebogenin (287 *m/z*, 15 V), 2',4',6'-trihydroxydihydrochalcone (257 *m/z*, 15 V), 2',6'-dihydroxy-4'-methoxydihydrochalcone (271 *m/z*, 15 V), 2',6'-dihydroxy-4,4'-dimethoxydihydrochalcone (301 *m/z*, 15 V), and 2',4',6'-trihydroxy-4-methoxydihydrochalcone (285 *m/z*, 15 V). Calibration curves for each compound were prepared by using a concentration range of 0.05–100 µg/mL. MS data were processed, and the peak areas were integrated using TargetLynx (Version 4.2).

2.3.6 Non-targeted metabolomics of *P. trichocarpa* leaf bud resin extracts

UPLC-HRMS analyses of poplar leaf bud extracts were carried out as previously described by Witte et al. (2021). Samples were resuspended in methanol based on the dry weight (surface resin samples) or fresh weight (whole leaf bud extract) to yield a final concentration of 500 µg/mL. Extraction blanks and methanol blanks were used as quality controls for data preprocessing. The samples were analyzed in a randomized injection order. Chromatographic separation of the samples was achieved using Thermo Ultimate 3000 UPLC coupled with Thermo LTQ Orbitrap XL high-resolution spectrometer for MS analysis. The UPLC-HRMS analysis was carried out using a Phenomenex C_{18} Kinetex column (50 mm x 2.1 mm ID, 1.7 µm). The two-solvent gradient for the flow gradient consisted of solvent A (ddH_2O with 0.1%

formic acid (v/v)) and solvent B (acetonitrile with 0.1% formic acid (v/v)) at a flow rate of 0.35 mL/min. The gradient was as follows: 1% B (0–0.5 min), 1–99% B (0.5–4.5 min), 99% B (4.5–8 min), 99-1% B (8–8.5 min), and 1% B (8.5–11.5 min) to equilibrate the column to starting conditions. The electron spray ion (ESI) source for the MS analysis used the following parameters: capillary voltage of 34 kV, ionization voltage of 4.0 kV, tube lens voltage of 100V, sheath gas 40, auxiliary gas 5, and sweep gas 2. The MS full scan range was 100–2000 *m/z,* and the MS analysis was performed using positive ionization modes. ThermoFisher Xcalibur (version 4.6.6717) was used for reviewing the raw data files.

2.3.7 Metabolomics data processing

The raw UPLC-HRMS data files were processed using MZmine2 (version 2.53) (Pluskal et al., 2010). Data pre-processing algorithms included mass detection, Automated Data Analysis Pipeline (ADAP) chromatogram builder, local minimum search for chromatogram deconvolution, isotopic peak grouper, peak alignment, and gap filling. Data pre-processing parameters are described in detail in the supplemental data (Supplemental Table S2.1). In summary, UPLC-HRMS raw data files were used to determine noise level cut-off for the Full Width at Half Maximum (FWHM) exact mass algorithm for mass detection. ADAP chromatogram builder was used to build a chromatogram for each mass feature detected continuously over the scans. The group intensity threshold was set to noise level, and the minimum highest intensity was set to three times the noise level, with mass tolerance set to 5 ppm. Chromatogram deconvolution was performed using a local minimum search algorithm and optimizing the algorithm parameters by previewing the data files. The Isotopic Peak Grouper algorithm was used to find peaks that form an isotope pattern and to remove isotopes besides the highest one. The join aligner method was used for signal alignment with a mass tolerance of 5 ppm, weight for *m/z* to RT ratio of 20:10, and retention time tolerance of 0.1 min. The peak finder method was used for gap filling to review the aligned data and fill in the detected mass variable values below the noise threshold.

Pre-processed sample data was curated in Microsoft Excel and visualized by plotting a heatmap highlighting mass features detected above the noise level threshold. As part of data

curation, duplicate mass features were removed. The mass features above the noise level in extraction and methanol blanks were eliminated from the data set to account for contaminations.

2.3.8 Mass feature annotation

Detected mass features were defined by retention time (RT) and exact mass. Mass features corresponding to dihydrochalcones were identified by comparison of the exact *m/*z and RT to analytical standards. When available, unknown mass features were annotated by comparing their observed exact *m/z* to the theoretical *m/z* of compounds that had been previously reported in poplar literature (Gordon et al., 2022; English et al., 1991; Greenaway et al., 1992b; English et al., 1992; Greenaway et al., 1992a, 1989a; Nissinen et al., 2017). Pseudo-molecular ionic annotations were assigned to mass features with an identical mass (mass error < 5 ppm) compared to predicted structures.

2.3.9 Statistical analysis

For the statistical analysis of the non-targeted metabolomic samples, the data were normalized by sample mass and centred using Pareto scaling. Hierarchical cluster analysis, principal component analysis (PCA), and univariate and multivariate analyses were conducted using MetaboAnalyst 5.0 (Pang et al., 2021). Statistical analyses, including two-way ANOVA and Tukey's post hoc HSD, were done in GraphPad Prism (Version 8.4.3).

2.4 Results

2.4.1 Dihydrochalcone accumulation in *P. trichocarpa* whole leaf bud follows a seasonal pattern

A UPLC-MS approach was used for the targeted quantification of dihydrochalcones in *P. trichocarpa* whole leaf bud extracts normalized by dry weight and surface resin extracts normalized by dry weight (Fig. 2.2, Supplemental Figures S2.2-2.3). The seasonal patterns displayed by the dihydrochalcone accumulation differed drastically between the two sample sets over the growth-dormancy cycle.

Dihydrochalcone concentration in lateral leaf buds was highest in samples harvested between August and March (Fig. 2.2a). In contrast, a significant reduction in all measured dihydrochalcones was observed in April and May, coinciding with the leaf bud break marked by the rapid expansion of leaves and the formation of new leaf buds. Subsequently, we noted a gradual increase in dihydrochalcone accumulation within the developing leaf buds from June to August. The relative proportions of the different dihydrochalcones remained constant throughout the seasons. For example, 2',4',6'-OH-4-OMe DHC was the most abundant detected dihydrochalcones at all time points. In contrast, 2',4',6',4-OH DHC, which acts as a precursor for the *O*-methylated dihydrochalcones, was consistently detected at the lowest concentration per fresh weight.

Dihydrochalcones in the surface resin displayed a distinct accumulation profile compared to the whole leaf bud extracts (Fig. 2.2b). We observed a steady increase in the accumulation of surface dihydrochalcones between January and April, coinciding with the release of leaf buds from their overwintering dormancy. The highest dihydrochalcone content in the spring was observed in April, at the time of bud break. Surprisingly, a second peak in dihydrochalcone accumulation was observed in October during leaf drop. There was a reduction in the abundance of dihydrochalcones in the surface resin from November to January. The lowest concentration of surface resin dihydrochalcones was observed between May and September. Consistent with our analysis of whole leaf bud extracts, 2',4',6'-OH-4-OMe DHC was observed as the most

abundant and 2’,4’,6’,4-OH DHC as the least abundant dihydrochalcone in the secreted surface resin.

Overall, the *O*-methylated dihydrochalcones were more prevalent than their non-methylated counterparts in both types of samples. The most substantial dihydrochalcone accumulation in whole leaf buds was observed during the summer, whereas the most marked accumulation was noted in the spring and fall. The bud break in April had a profound impact on the total dihydrochalcone content in both sample types.

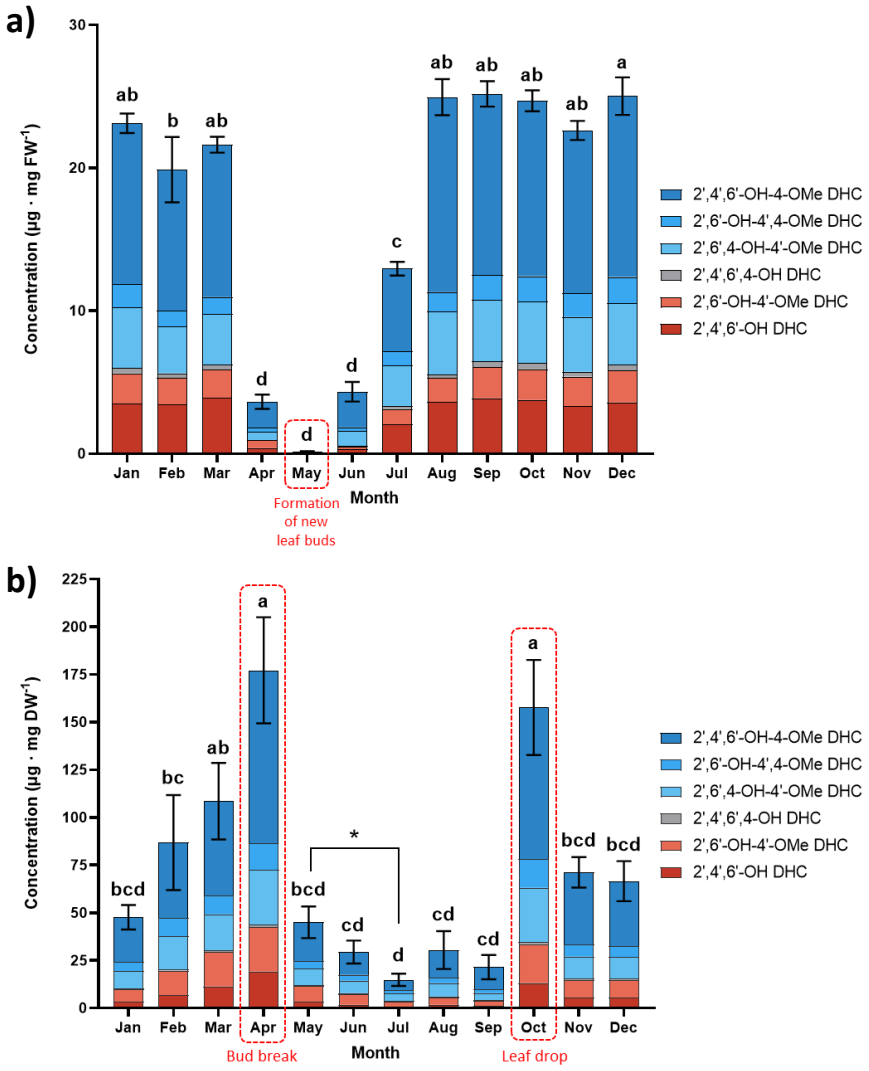

Figure 2.2. Quantification of the total amount of dihydrochalcones in poplar bud resin extracts. Quantification of dihydrochalcones in a) whole leaf buds normalized by fresh weight and b) secreted surface resin normalized by dry extract weight. The data display means ± cumulative SE. For whole leaf buds (n = 3) and surface resin (n = 9). Quantified analytes include 2',4',6'-4'-OMe DHC (2',4',6'-trihydroxy-4-methoxydihydrochalcone), 2',6'-OH-4,4'-OMe DHC (2',6'-dihydroxy-4,4'-dimethoxydihydrochalcone), asebogenin (2',6',4-OH-4'-OMe DHC), 2',4',6',4-OH DHC (phloretin), 2',6'-4'-OMe DHC (2',6'-dihydroxy-4'-methoxydihydrochalcone), and 2',4',6'-OH DHC (2',4',6'-trihydroxydihydrochalcone). Significant differences ($P < 0.05$) between the sample groups are indicated by different letters as determined by Tukey's post hoc HSD. Major phenological stages of the leaf bud development are annotated and indicated by red dashed lines. May corresponds to the first stage of the leaf bud development, while April corresponds to the bud break. October coincides with the leaf drop. Surface resin samples collected between May and July indicated by (*) included the whole leaf nodes, including the leaf primordia and the flushed leaves. Quantification of the individual compounds is presented in Supplemental Figures S2.2-2.3.

2.4.2 Non-targeted metabolomics analysis reveals seasonal patterns in *P. trichocarpa* whole leaf bud extracts

We next investigated the seasonal changes of the total metabolite profiles of *P. trichocarpa* whole leaf bud extracts using non-targeted metabolomic analysis by UPLC-HRMS. In this analysis, we detected 298 mass features above the noise threshold.

Hierarchical cluster analysis was performed to inspect the grouping of the samples based on similarities in the mass feature profiles (Fig. 2.3a). This analysis identified four distinct clusters of samples: April-May, June, July-August, and September-March. The sample grouping appeared to follow a linear pattern where the groups consisted of subsequent sampling time points. The April-May group directly coincided with the initiation of bud break and the emergence of new leaf buds. April represented fully opened leaf buds and emerging leaves, while May samples comprised the newly formed leaf primordia. June samples formed a distinctive cluster, signifying an early stage in the development of leaf buds. The July-August cluster was characterized by the active growth and development of leaf buds. In contrast, the largest group, spanning from September to March, was aligned with the overwintering dormancy of the leaf buds.

Partial least-squares discriminate analysis (PLS-DA) displayed a similar separation between these four sample groups (Fig. 2.3b). The loadings plot for the PLS-DA analysis is shown in Supplemental Figure S2.4a. The first two components explained a cumulative 79% of the variability in the data model.

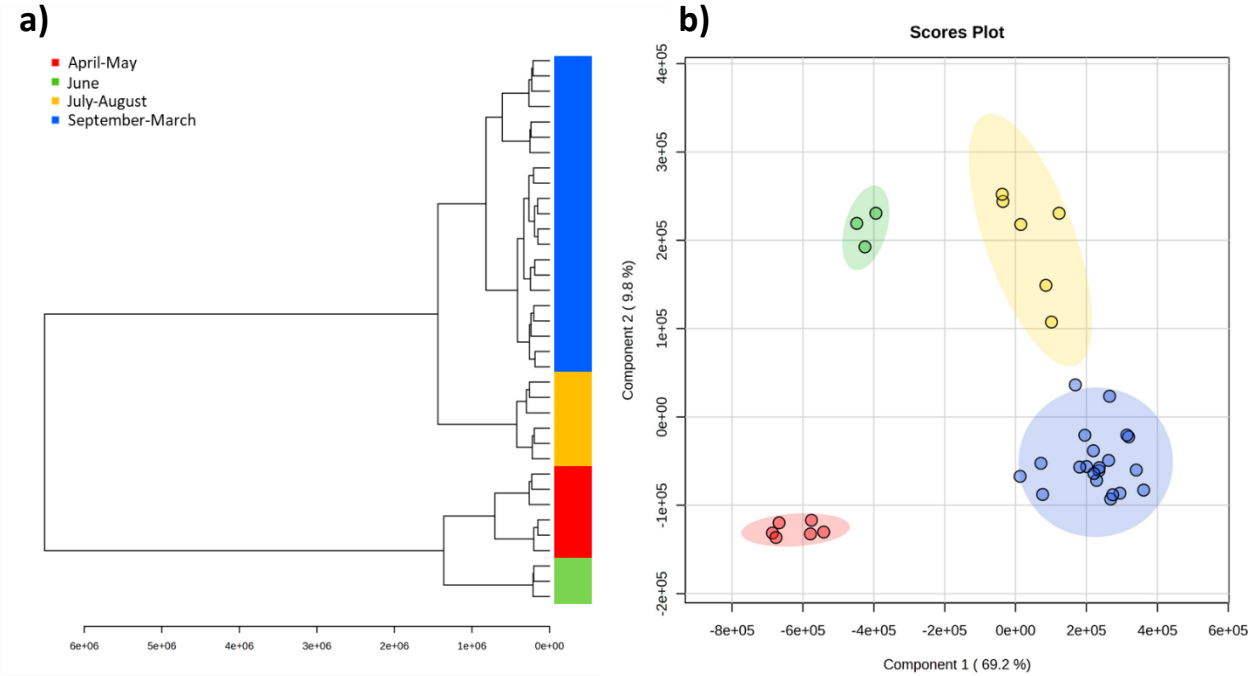

Figure 2.3. Non-targeted metabolomics analysis of *P. trichocarpa* whole leaf bud extracts. a) Hierarchical cluster dendrogram and b) partial least-squares discriminate analysis (PLS-DA) scores plot of *P. trichocarpa* whole leaf bud extracts metabolites detected in positive ionization mode. Samples clustered together are identified by colour coding and named based on their sampling months. Multivariate analysis was conducted using MetaboAnalyst 5.0 (Pang et al., 2021). The highlighted area around the data points signifies the 95% confidence regions.

We conducted a qualitative differential analysis to explore the distribution of mass features among the four sample groups (Fig. 2.4). Visualization of the intersecting mass features between the sample groups was performed using the UpSet package on R (Lex et al., 2014). Of the 298 detected mass features, 155 were common to all four sample groups. The July-August group had the highest metabolite diversity, with 272 detected mass features, whereas the April-May group had the lowest diversity, with 186 detected mass features. Notably, samples collected between April and May contained the highest number of unique mass features, followed by June, September-March, and July-August groups. In pairwise comparisons, the July-August and September-March groups showed the most overlap. At the same time, September-March and June, as well as September-March and April-May groups, shared only one common unique mass feature. This suggests clear distinctions in the metabolite profiles between these sample groups. Overall, this analysis suggests that most mass features are qualitatively consistent across the groups, with the separation between these groups likely driven by quantitative differences in the accumulation of these metabolites.

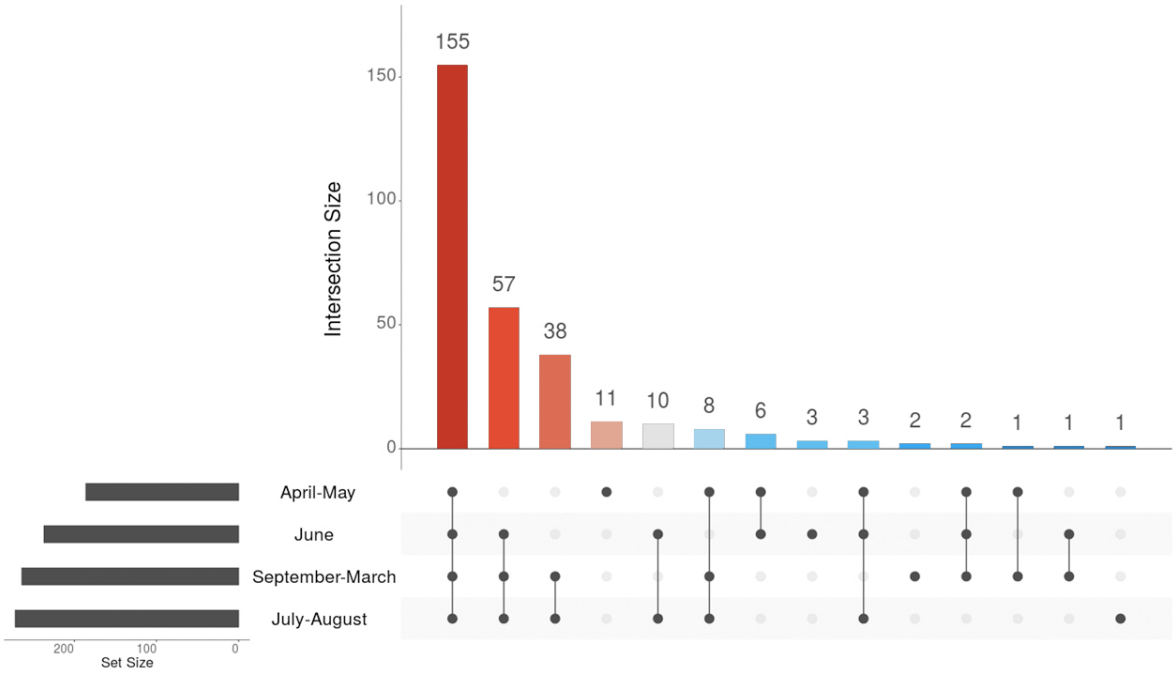

Figure 2.4 Non-targeted metabolomic differential analysis of the whole leaf bud resin extracts. UpSet plot of the metabolite intersection of 298 mass features detected above the noise threshold (peak height > 2e6) in each sample group. Set size refers to the total number of mass features detected in each sample group. Intersection size denotes the number of mass features shared by the sample groupings indicated by the connected dots.

To further explore the distribution of metabolites among the sample groups, we conducted a hierarchical cluster analysis of the mass features. We generated a heatmap displaying the relative abundances of the detected mass features (Fig. 2.5a). This analysis showed distinct clusters of mass features within the four sample groups, displaying significant quantitative variations in metabolite profiles over the sampling time points in whole leaf buds. In parallel, we employed PLS-DA analysis to identify mass features with the highest Variable Importance in Projection (VIP) scores for component 1 (Fig. 2.5b) and component 2 (Supplemental Table S2.2). Mass features with a high VIP score significantly contributed to the separation between the sample groups.

In this analysis, within the 15 highest-scoring mass features, we identified several dihydrochalcones and putative *O*-methylated flavonoids (Fig. 2.5b). Notably, the highest VIP score was attributed to 2',4',6'-OH-4-OMe DHC, which is the most prevalent dihydrochalcone in the targeted analysis of the whole leaf bud extracts. *O*-methylated dihydrochalcones with high VIP scores were found abundant in the September-March group. In addition to dihydrochalcones, we putatively identified the second highest-scoring mass feature with *m/z* 285.0762 as 3,7-dihydroxy-5-methoxyflavonol, previously reported as a component of bud resin in *P. balsamifera* (Greenaway and Whatley, 1990). The mass feature with the highest VIP score for the July-August group was *m/z* 287.0915, which was putatively identified as 2',4',6'-trihydroxy-4-methoxychalcone based on accurate mass. The identity of this mass feature could not be confirmed due to the lack of an analytical standard. However, it has been previously reported in *P. trichocarpa* leaf buds (English et al., 1991). Another unidentified mass feature with *m/z* 267.0664 achieved the highest VIP score out of the mass features with high abundance in the April-May group. The top 15 mass features with the highest VIP scores were largely identical between component 1 and component 2.

In total, 63 mass features with a VIP score ≥ 1 (component 1), signifying their role in distinguishing between the sample groups, are catalogued in Supplemental Table S2.4. In addition to flavonoids, we putatively identified salicinoids, salicortin and tremulacin, as well as benzyl benzoate in the whole leaf buds. These compounds have been previously reported in *P. trichocarpa* (English et al., 1991; Fellenberg et al., 2020).

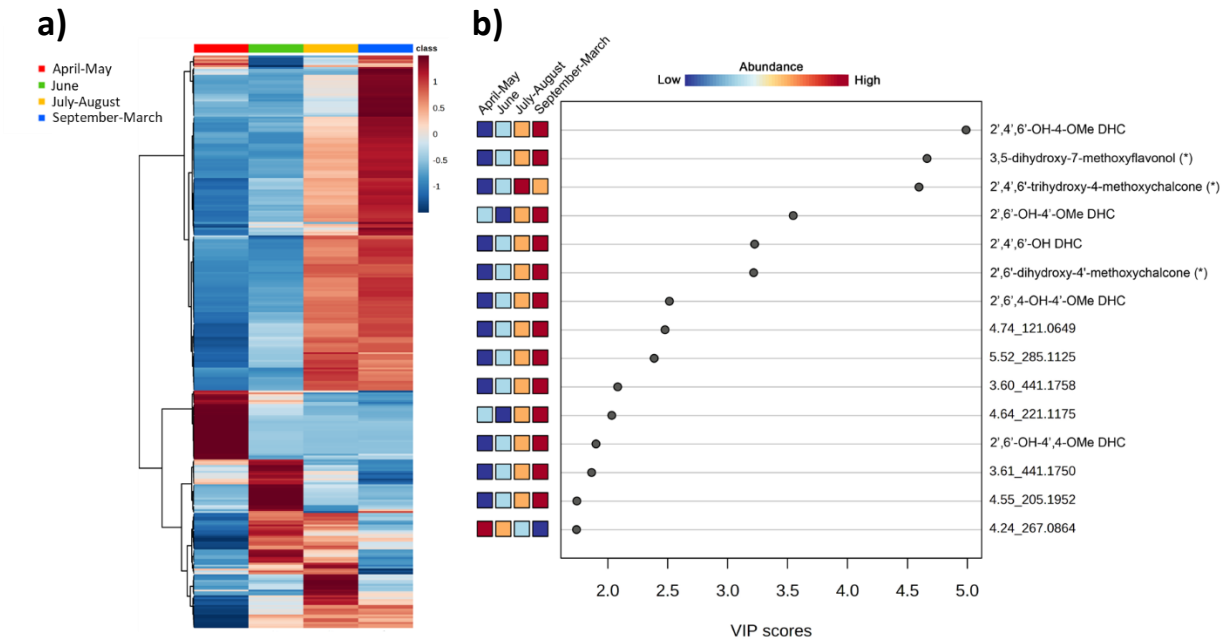

Figure 2.5. Metabolite distribution analysis of *P. trichocarpa* whole leaf bud extracts.
a) Hierarchical cluster heatmap of mass feature distribution representing the relative abundance of 298 mass features between the different sample groups. Sample groups are indicated by colour coding. b) Variable importance in projection (VIP) scores for detected mass features. A higher VIP score signifies a higher importance in component 1 of partial least-squares discriminant analysis (PLS-DA), shown in Fig 2.3b. The colour boxes indicate the relative abundance of a mass feature between the sample groups. When available, the mass features are annotated based on matching *m/z* of $[M+H]^+$ and retention time of analytical standards, including 2',4',6'-OH-4-OMe DHC (2',4',6'-trihydroxy-4-methoxydihydrochalcone), 2',6'-OH-4'-OMe DHC (2',6'-dihydroxy-4'-methoxydihydrochalcone), 2',4',6'-OH DHC (2',4',6'-trihydroxydihydrochalcone), 2',6',4-OH-4'-OMe DHC (asebogenin), and 2',6'-OH-4,4'-Me DHC (2',6'-dihydroxy-4,4'-dimethoxydihydrochalcone). Putatively identified mass features are indicated by (*). The naming includes retention time (RT) followed by the m/z for the unidentified mass features.

2.4.3 *P. trichocarpa* leaf bud surface extracts display large-scale seasonal shifts in metabolite profiles

We applied the same non-targeted metabolite analysis approach to analyzing leaf bud surface resin extracts. We detected 330 mass features above the noise threshold in the surface resin extracts. Hierarchical cluster analysis and PLS-DA analysis were conducted to analyze sample groups within the surface resin samples. Similarly to whole leaf buds, the surface resin samples were clustered into four groups. Notably, the sample groupings for surface resin samples comprised different months compared to the whole leaf buds. For the surface resin, the four distinguished groups were November-January, February-March, April and October, and May-August (Fig. 2.6a).

Interestingly, April and October, two non-consecutive time points, clustered together, setting them apart from the other sample groups, which predominantly consisted of consecutive sampling points. PLS-DA analysis confirmed the separation of the four different clades (Fig. 2.6b). According to the PLS-DA analysis, the first two components collectively explained 53 % of the variance in this data model. The loadings plot for the PLS-DA analysis is shown in Supplemental Figure S2.4b. The November-January group separated from the other sample groups, which suggested distinct differences in the surface resin metabolite profile. Overall, the clustering pattern of surface resin was distinctly different from the whole leaf buds.

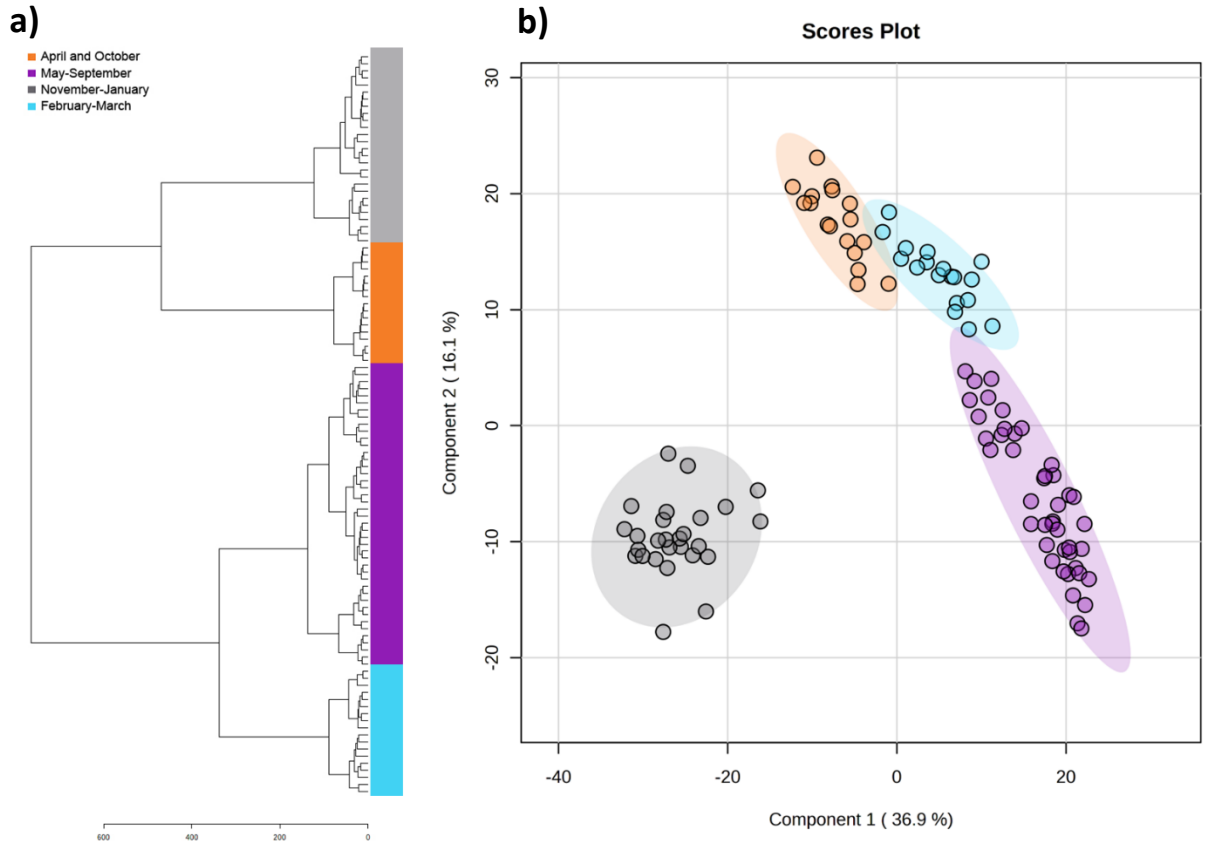

Figure 2.6. Non-targeted metabolomics analysis of *P. trichocarpa* leaf buds secreted surface resin extracts. a) Hierarchical cluster dendrogram and b) partial least-squares discriminate analysis (PLS-DA) scores plot of *P. trichocarpa* surface resin extract metabolites in positive ionization mode. Grouped samples are identified by colour coding and named based on their sampling months. Multivariate analysis was conducted using MetaboAnalyst 5.0 (Pang et al., 2021). Highlighting around the data points signifies the 95% confidence regions.

A qualitative distribution analysis of the 330 total detected mass features was conducted to investigate the mass feature distribution between the four defined sample groups (Fig. 2.7). Visualization of the mass feature intersections revealed that 121 mass features were shared between all sample groups. Interestingly, the highest diversity was found in the February-March group, with 306 detected mass features, accounting for 92.7 % of all detected mass features. Notably, the February-March group also consisted of the most unique mass features. The November-January group had the lowest diversity with 162 mass features. This suggests that between the dormancy in November-January and the release of dormancy in February-March, the metabolite composition of the surface resin shifts drastically. Of the 330 total mass features, only 144 are shared between the November-January and February-March groups. Similarly, the February-March and the April and October groups shared 203 mass features, demonstrating a shift of 127 mass features. In pairwise comparison, the February-March and May-September groups demonstrated the most common mass features, consistent with the PLS-DA analysis for these overlapping groups.

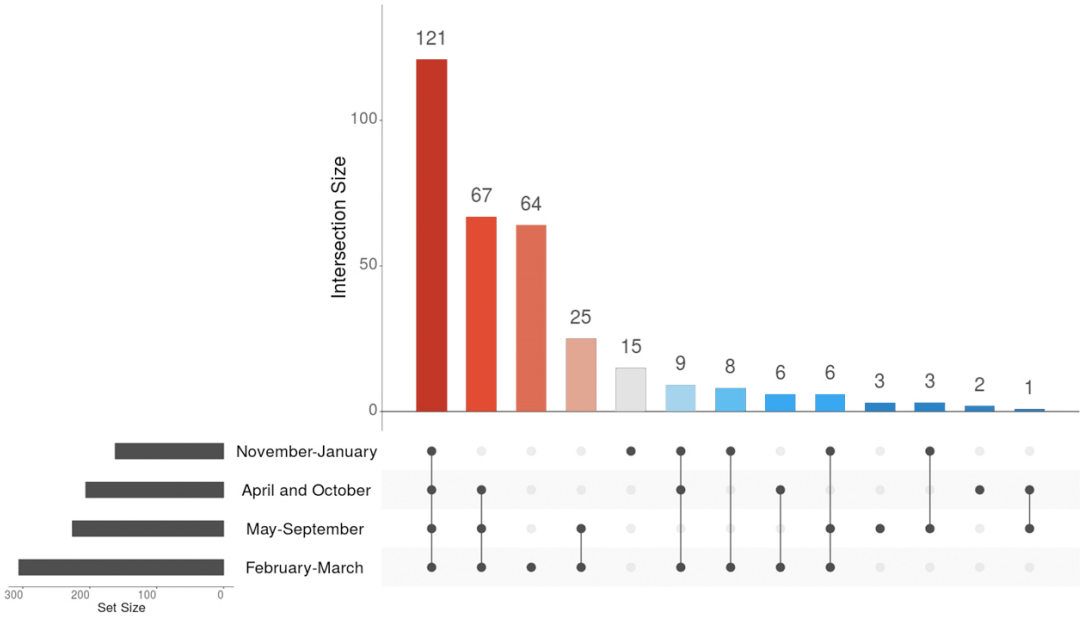

Figure 2.7. Non-targeted metabolomic differential analysis data of secreted surface resin extracts. UpSet plot of the metabolite intersection of 330 mass features detected above the noise threshold (peak height > 5e4) in each sample group. Set size refers to the total number of mass features detected in each sample group. Intersection size denotes the number of mass features shared by the sample groupings indicated by the connected dots.

Similar to the whole leaf bud analysis, quantitative distribution analysis of mass features across the four sample groups revealed substantial shifts in the metabolite profiles. Heatmap of mass feature abundance displayed large, characteristic clades of mass features for each sample group (Fig. 2.8a). Based on PLS-DA analysis, we identified mass features with the highest VIP scores on component 1 and component 2. Focusing on the top 15 mass features with the highest scores on component 1, we found that they were predominantly *O*-methylated flavonoids (Fig. 2.8b). Among them, a mass feature with an *m/z* of 301.1063 had the highest VIP score. Two other mass features with a similar *m/z*, 301.1064 and 301.1068, also showed high VIP scores. Together, the accurate masses of these mass features corresponded to a $[M+H]^+$ of $C_{17}H_{16}O_6$, consistent with 2',6'-dihydroxy-4',4-dimethoxychalcone, 5-hydroxy-7,4'-dimethoxyflavanone, and 5,7-dimethoxy-4'-hydroxyflavanone. Due to the similar accurate masses, the precise identity of these compounds could not be confirmed without analytical standards. However, 2',6'-dihydroxy-4',4-dimethoxychalcone and 5-hydroxy-7,4'-dimethoxyflavanone have been previously reported in poplar literature (Greenaway et al., 1991). The putative identification of these compounds was based on the predicted elution order based on the different *O*-methylation substitution patterns based on literature (Greenaway et al., 1991).

In addition to 2',6'-dihydroxy-4',4-dimethoxychalcone and 5-hydroxy-7,4'-dimethoxyflavanone, we identified 2',6'-dihydroxy-4'-methoxychalcone with high abundance in the November-January group, while putative 5,7-dimethoxy-4'-hydroxyflavanone had the highest abundance in the April and October group. Furthermore, unidentified mass features with *m/z* 277.1767, 310.3092, and 219.1738, along with a putative 3,5-dihydroxy-7-methoxyflavonol exhibited the highest VIP scores in the May-September group. The exact identity and the position of the *O*-methylation of the putative 3,5-dihydroxy-7-methoxyflavonol could not be verified without an analytical standard.

In total, we identified 75 mass features with a VIP score ≥ 1 (component 1), indicating their contribution to the differentiation between the surface resin sample groups (Supplemental Table S2.5). In addition to the described *O*-methylated flavonoids, we identified salicinoids, including salicortin and tremulacin, and putative cinnamic acid esters, including cinnamyl caffeate. Investigating the highest-scoring mass features contributing to component 2 revealed dihydrochalcones with high VIP scores (Supplemental Table S2.3b). These results suggest that

while methoxylated flavonoids played a significant role in separating the sample groups along components 1 and 2, dihydrochalcones were more influential in the differentiation of the sample groups along component 2.

Overall, both whole bud extracts and surface resin samples exhibited large-scale metabolomic shifts throughout the annual growth-dormancy cycle, displaying distinct seasonal patterns and variations in metabolite accumulation. Importantly, our findings highlighted differences in the seasonal metabolite patterns between the two sample types.

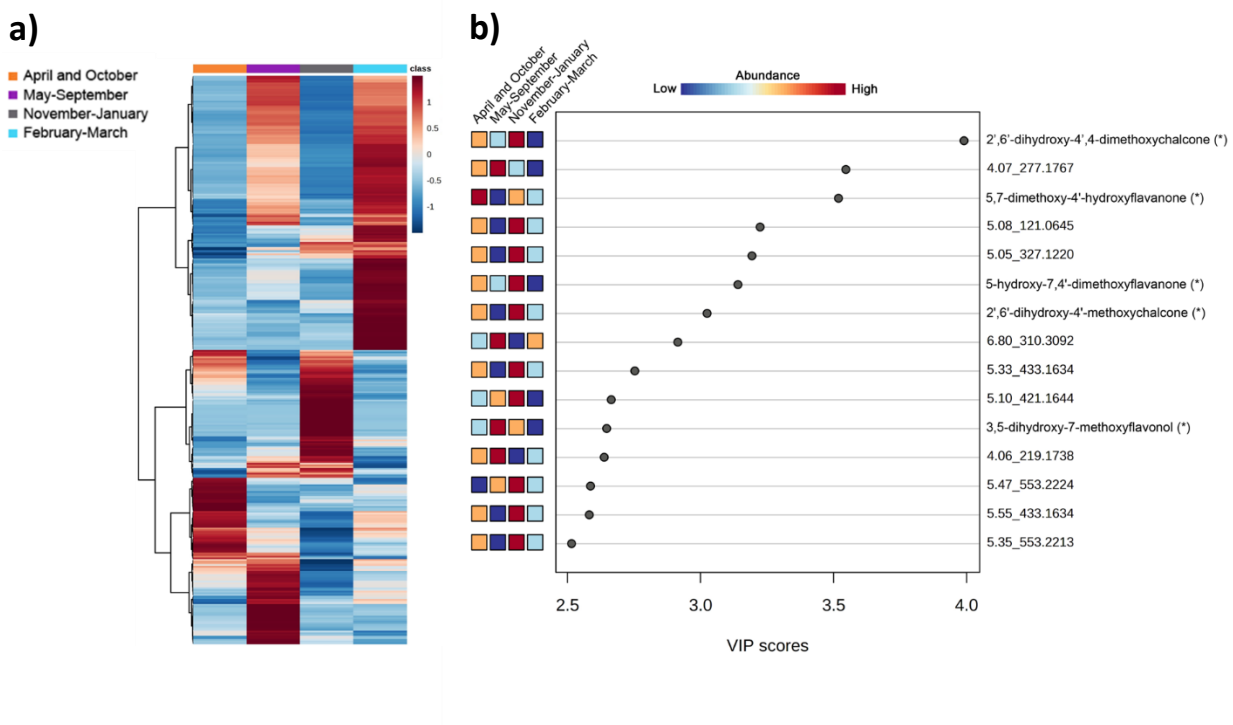

Figure 2.8. Metabolite distribution analysis of *P. trichocarpa* surface resin extracts.
a) Hierarchical cluster heatmap of mass feature distribution representing the relative abundance of 330 mass features between the different sample groups. Sample groups are indicated by colour coding. b) Variable importance in projection (VIP) scores for detected mass features. A higher VIP score signifies a higher importance on component 1 of partial least-squares discriminant analysis (PLS-DA) shown in Fig 2.6b. The colour boxes indicate the relative abundance of a mass feature between the sample groups. The mass features are annotated when available based on matching *m/z* of $[M+H]^+$. Putatively identified mass features are indicated by (*). The naming includes retention time (RT) and m/z for unidentified mass features.

2.5 Discussion

Analysis of *P. trichocarpa* leaf buds confirmed dihydrochalcones as some of the major phenolic components of leaf bud resin, aligning with previous literature (English et al., 1991). Our analysis demonstrated an accumulation of dihydrochalcones in the whole leaf buds during the active development of leaf buds in the summer. In contrast, the concentration of dihydrochalcones remains relatively constant in the overwintering dormant leaf buds until the bud break. The highest accumulation of dihydrochalcones in the surface resin occurred in April and October. Non-targeted metabolomic analysis of both whole leaf buds and surface resin unveiled substantial changes in the total metabolites over the growth-dormancy cycle, highlighting differences in the seasonal patterns between the two sample types.

Both sample sets displayed the importance of *O*-methylated dihydrochalcones and flavonoids for distinguishing different sample groups in the PLS-DA model. In addition to previously reported flavonoids, we found preliminary evidence of other *O*-methylated flavonoids not previously identified in the leaf bud resin of *P. trichocarpa*. Specifically, 2',6'-dihydroxy-4',4-dimethoxychalcone and 5-hydroxy-7,4'-dimethoxyflavanone have been previously reported in bud exudates of *P. sieboldii* (Greenaway et al., 1991), and 3,7-dihydroxy-5-methoxyflavonol in *P. balsamifera* (Greenaway and Whatley, 1990), but not *P. trichocarpa*.

Due to differences between the normalization of the whole leaf bud extract and the surface resin extracts, a direct relationship between the two data sets is difficult to establish. The whole leaf bud extract samples were normalized by the fresh weight of the extracted tissue, which does not account for the changes in the amount of leaf tissue. The amount of leaf tissue in the developing buds increases significantly during bud break (Curtis and Lersten, 1974). The water content in the leaf tissue is influenced by environmental factors (Silim et al., 2009), which likely influences the total water content in the whole leaf buds. These factors potentially dilute the dihydrochalcone concentration in samples with leaf tissue, including April.

In contrast, the surface resin samples were normalized by the dry weight of the extracted surface resin. The surface extracts likely included undetected surface tissue components, such as cuticular waxes (Isidorov and Vinogorova, 2003) on the surface of the extracted leaves and leaf

bud scales. At the lowest, the dihydrochalcones contributed less than 1.5 % to the dry extract weight in July, while at the highest in April, this proportion was over 17 %. The surface resin extracts collected during the summer contained a much higher proportion of leaf tissue than the samples collected in the fall, which may explain some of these differences. Between May and July, the small size of the developing leaf primordia necessitated the inclusion of the whole leaf nodes. Hence, the surface extracts collected during these time points include the residual resin on the surface of the flushed leaves.

2.5.1 Targeted metabolomic analysis of *P. trichocarpa* leaf bud extracts demonstrates seasonal accumulation and secretion of dihydrochalcones

Our analysis indicates that dihydrochalcone biosynthesis in *P. trichocarpa* occurs primarily in summer months during the early leaf bud development. The contribution of bud scales to the production of leaf bud resin, previously reported in *P. deltoides* (Curtis and Lersten, 1974), seems to be reflected in the increased synthesis of dihydrochalcones in *P. trichocarpa*, as the dihydrochalcone levels increase with the enlargement of leaf buds and the development of outer bud scales from May to August. This may be related to the increasing surface area of the secretory epidermis on the inner surface of the bud scales as the leaf buds grow. The sharp decline in total dihydrochalcone concentration observed in whole leaf buds in April may be due to the increasing proportion of leaf tissue in the samples during bud break, including greater water content and, presumably, a higher proportion of leaf-specific biosynthesis. A similar reduction in flavonoid content with increasing leaf size has been reported in *Betula* spp. (Valkama et al., 2004). Increasing leaf age and size led to a rapid decline in the concentrations of flavonoid aglycones due to a reduction in the density of the secretory trichomes on the leaf surface. This suggests that by weight, the production of surface exudates is proportionally highest at the early stages of birch leaf development. These results are consistent with our findings that the poplar resin components accumulated in the leaf buds during the active growth of the developing buds.

Seasonal accumulation patterns of dihydrochalcones in surface resin differ from those identified in the whole leaf bud extracts. The increasing abundance of dihydrochalcones in the

surface resin of the dormant buds between January and March, while buds are still largely closed, could indicate an increase in resin secretion to the bud surface due to environmental factors, such as change in the temperature or photoperiod. Environmental factors have been shown to mediate mechanisms related to the release of dormancy in poplar leaf buds (Conde et al., 2017), suggesting a potential connection between the release of dormancy and increased resin secretion. Additionally, increased resin secretion could be induced by expanding leaf tissue within the buds, generating internal pressure that mechanically pushes resin to the surface through crevices between bud scales. A pressure-based model for the secretion of lipophilic metabolites has been proposed (Paiva, 2016). This could explain the significant increase in dihydrochalcone content of the surface resin in April, which suggested increased availability of surface resin during the bud break. In addition to a potential increase in the resin secretion with increasing temperatures and longer photoperiod discussed earlier, this increase likely results from the extraction surface area as leaves emerge from the previously enclosed leaf buds.

Another major increase in dihydrochalcone concentration in surface resin occurred in October, two months after the cessation of dihydrochalcone accumulation in whole leaf buds. This disconnection between the accumulation and secretion suggests regulatory mechanisms controlling the resin secretion. The significant increase in dihydrochalcone levels in October relative to other components in the surface resin coincided with declining temperatures and shorter photoperiods in the fall, which have been shown to influence poplar leaf bud growth and bud scale development (Ruttink et al., 2007; Rohde et al., 2002). In addition, abiotic factors, such as water stress induced by dehydration and cold stress, are known to increase the accumulation of phenylpropanoids (Francini et al., 2019). This suggests a potential role of resin secretion in response to environmental acclimation. During acclimation, increased resin secretion may reduce transpiration and protect leaf buds from dehydration during winter (Pramsohler and Neuner, 2013).

The reason for the subsequent reduction in dihydrochalcone concentration after October is unclear. However, it coincides with leaf drop and could be due to increased accumulation of other components on the leaf buds, such as cuticular waxes and volatile sesquiterpenes. These types of components were not detected in our LC-MS analysis. The surface resin components may be volatilized during the seasons at different rates depending on temperature and

environmental conditions, which could lead to proportional changes in dihydrochalcones over the year, especially during the transitional stages in the fall and spring when the temperature and photoperiod change the most. Gas chromatography analysis of leaf bud contents seasonally could provide further insights.

2.5.2 Non-targeted metabolomic analysis of *P. trichocarpa* leaf bud extracts reveals large-scale shifts in the chemical composition

In our non-targeted analysis, both whole leaf bud extracts and surface resin samples formed distinct groups, generally representing consecutive sampling time points. Importantly, the groupings in the non-targeted analysis mirrored the accumulation patterns identified in the targeted analysis of dihydrochalcones. Generally, the samples displaying high dihydrochalcone content clustered separately from the samples with low concentrations. However, this general pattern did not directly match all sample groups, indicating that dihydrochalcone accumulation alone could not explain the sample groupings.

The sample groups identified in the analysis of whole leaf buds consisted of consecutive time points. The largest group was formed by dormant leaf buds harvested between September and March, which coincided with the samples displaying the highest dihydrochalcone content in the targeted analysis. Surprisingly, August, which aligns with the September-March group based on dihydrochalcone content, grouped together with July. These results suggest that August and July shared components beyond the dihydrochalcones. Additionally, the group formed by April and May samples clustered separately from June despite the similar dihydrochalcone concentrations.

In the analysis of the surface resin, the two non-consecutive time points displaying the highest dihydrochalcone content, April and October, clustered together. The clustering of the other groups followed similar patterns indicated by the dihydrochalcone content. May-September samples had the lowest dihydrochalcone concentration, while November-January and February-March samples, consisting of dormant buds, formed separate groups, consistent with the increasing dihydrochalcone concentration.

The consistency between the patterns identified between the targeted and non-targeted analyses implied the significance of dihydrochalcones in differentiating between the sample groups. The PLS-DA analysis of whole leaf buds consistently identified the high abundance of *O*-methylated dihydrochalcones in the overwintering dormant as one of the most significant changes in the total metabolite composition compared to other seasons. Interestingly, analysis of the surface resin revealed significant changes in other resin components beyond dihydrochalcones. In surface resin analysis, *O*-methylated flavonoids displayed a more pronounced impact on seasonal patterns than dihydrochalcones. Surface resin collected between November and January was distinguished from the other sample groups by the accumulation of *O*-methylated chalcones and flavanones.

At the late stages of the leaf bud development in the spring, several characteristic leaf compounds, including common salicinoids, became more prominent in whole leaf buds. However, the importance of salicinoids to the separation between the different sample clusters was much lower than that of the flavonoids in both whole leaf buds and surface resin samples. This suggests that salicinoids are likely residual components originating from the expansion of leaf tissue instead of metabolomic changes in the bud resin.

Together, these dynamic metabolite shifts indicate that the chemical composition of both whole leaf buds and the surface resin changes over the growing season. These changes detected in the metabolic profiles could be related to the age and developmental stage of the leaf buds. Phytochemical analysis of clonal poplars (*P. tremuloides*) has revealed age-related shifts in the quantities of condensed tannin and salicinoid concentrations in poplar leaves (Donaldson et al., 2006). A study on dormant *P. balsamifera* internodes demonstrated a decline in volatile defence compounds over the winter, with the defence compounds being barely detectable by early spring (Clausen et al., 2010). These findings support our model, suggesting that the groupings of the leaf bud samples correspond to different phenological stages of leaf bud development. These results suggest dynamic changes in the metabolite profiles as a part of the development cycle of poplar leaf buds.

In addition to metabolomics shifts related to developmental changes, the timing of the resin secretion and accumulation of different metabolites could be influenced by environmental

factors. The molecular mechanisms controlling the timing of the dormancy-growth cycle of poplar buds, as well as developmental shifts related to dormancy, are shown to be regulated by environmental conditions, such as photoperiod and temperature (Cooke et al., 2012; Conde et al., 2017). This implies that, by extension, the phenylpropanoid pathways related to resin synthesis may also be subject to similar regulation by environmental signals. Investigation of the environmental effects on leaf bud resin accumulation over multiple growing seasons could reveal how photoperiod and temperature changes influence the synthesis and secretion of leaf bud resin.

2.5.3 Hydrophobic flavonoids in whole leaf buds and surface resin show differences in their seasonal patterns

A critical observation is that the seasonal groups between the whole leaf buds and surface resin extracts did not align in the non-targeted and targeted analyses. The accumulation of dihydrochalcones and the clustering patterns between the sample groups in the non-targeted analysis differed, indicating different seasonal patterns in the secreted resin components and the total metabolites inside the buds. The overwintering dormant buds formed a single group of samples collected in the whole leaf bud analysis between September and March. In contrast, in the analysis of surface resin, the dormant buds were divided between the November-January and February-March groups. These results indicate that despite the total metabolite profile not changing significantly during dormancy, the metabolites secreted onto the surface are affected differently.

Despite different seasonal patterns in whole leaf bud and surface resin constituents, it is important to stress that we identified compounds possessing similar features with high importance in the multivariate model in both sample types. *O*-methylated flavonoids have greater importance in distinguishing between the different sample groups than the non-*O*-methylated versions. This result highlights the significance of biochemical modifications, such as methoxylation, as a part of the biosynthesis of leaf bud resin flavonoids. Especially in the surface resin, the conversion of water-soluble flavonoids into their hydrophobic counterparts by the methoxylation reactions could impact the physiological properties of the leaf bud resin, such as potentially enhancing the secretion of these compounds onto the leaf buds. However, the

mechanism of leaf bud resin secretion and whether it is influenced by internal pressure induced by the expansion of leaf tissues, physiological changes in the water potential due to dehydration, or other environmental effects have not yet been identified. The identification of different *O*-methoxylated flavonoids as major resin components provides multiple potential markers for tracking the secretion of poplar bud resin.

2.6 Conclusions

This study unveils the dynamic nature of metabolite accumulation within *P. trichocarpa* leaf bud resin extracts across different seasonal time points during the growth-dormancy cycle of leaf buds. Here, we highlight the seasonal patterns displayed by specialized metabolites in *P. trichocarpa* leaf bud resin extracts and how the patterns of other metabolites detected by the non-targeted analysis largely follow the patterns of dihydrochalcone accumulation. These results indicate that the accumulation of dihydrochalcones in the poplar buds is one of the most distinct seasonal changes in the chemistry of poplar buds over the growth-dormancy cycle. However, these chemical shifts are not limited to dihydrochalcones. In the secreted fraction of the bud resin, *O*-methylated chalcones and flavonoids are crucial contributors to the differentiation between developing and dormant buds.

Overall, *O*-methylated dihydrochalcones and flavonoids are among the most significant seasonally varied groups of compounds in poplar bud resin. The lack of alignment between the seasonal patterns observed in whole leaf buds and surface resin emphasizes the necessity to investigate the mechanisms of leaf bud resin biosynthesis and secretion and how they are potentially regulated by temperature and photoperiod. Identifying these key mechanisms could provide a deeper understanding of how various environmental factors influence the secretion of *O*-methylated flavonoids in leaf buds.

2.7 Acknowledgments

We thank Dr. David Overy, Samuel Shields, and Amanda Sproule from Agriculture and Agri-Food Canada for running the non-targeted UPLC-HRMS analysis and Dr. Ori Granot for the maintenance of the UPLC-MS system. Brad Binges for the upkeep and maintenance of the greenhouse and research compound facilities. The work in the Constabel laboratory is supported by the Natural Sciences and Engineering Research Council of Canada (NSERC).

2.8 Supplemental information

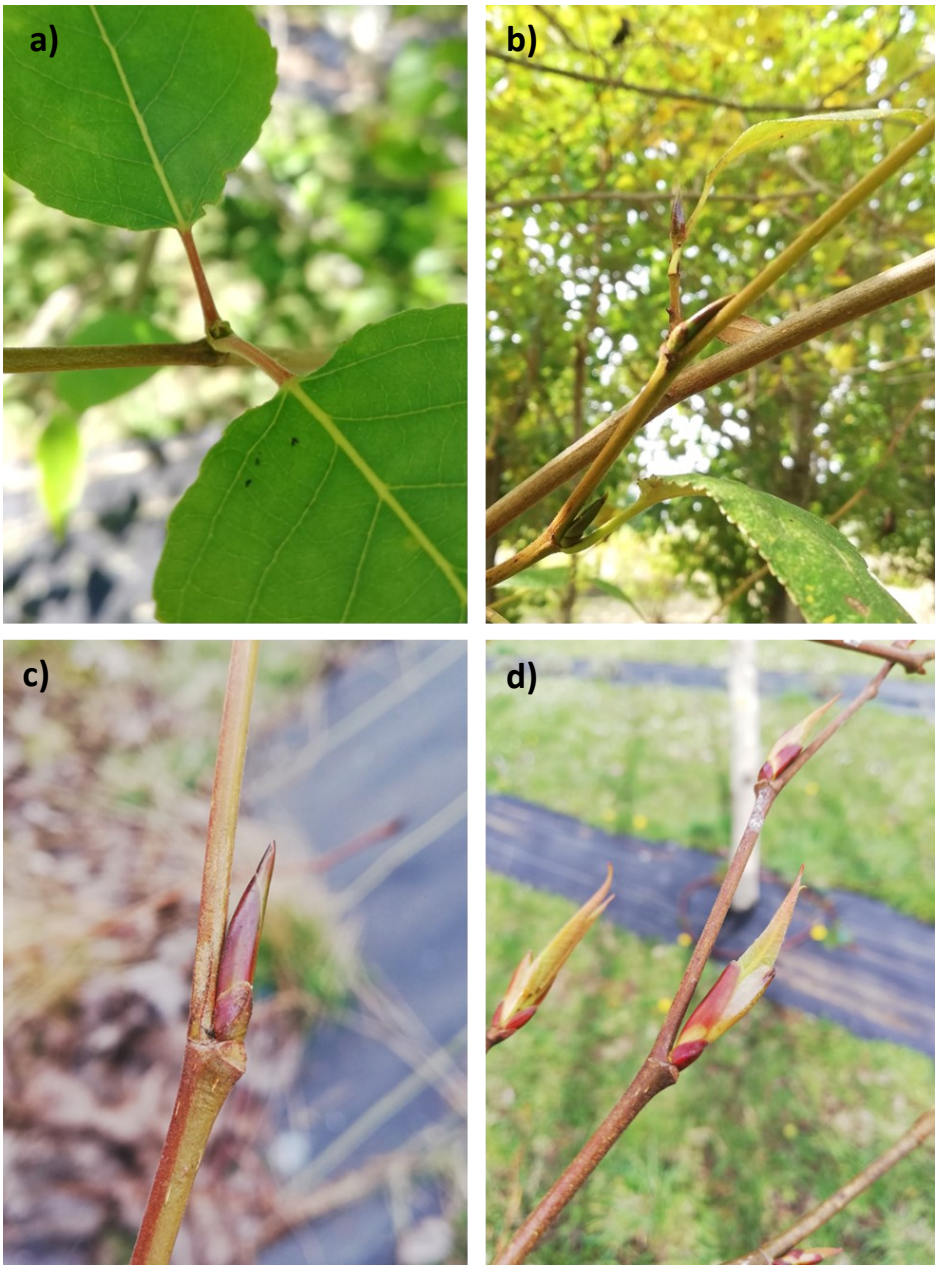

Supplemental Figure S2.1. Representative examples of lateral leaf buds of *P. trichocarpa* at different stages of the growth-dormancy cycle. a) Developing leaf buds collected in May, b) pre-dormant leaf buds in September, c) overwintering dormant leaf buds in January, and d) flushing leaf buds during bud break in April.

Supplemental Table S2.1. Detailed MZmine2 pre-processing parameters of the metabolomics data for the positive ionization data processing. Pre-processing steps included a) mass detection, b) ADAP chromatogram builder, c) chromatogram deconvolution, d) isotopic peak grouper, e) alignment, and f) gap filling parameters.

	Whole bud extracts	**Surface resin extracts**
a) Mass detection		
Mass detector	Exact mass	Exact mass
Noise level Threshold	2.00E+06	5.00E+04
b) ADAP Chromatogram Builder		
Min group size in # of scans	5	5
Group intensity threshold	2.00E+06	5.00E+04
Min highest intensity	6.00E+06	1.50E+05
m/z tolerance	5.0 ppm	5.0 ppm
c) Chromatogram deconvolution		
Method	Local minimum search	Local minimum search
Chromatographic threshold	95%	95%
Search minimum in RT range	0.05 min	0.05 min
Minimum relative height	30%	30%
Minimum absolute height	2.00E+06	3.00E+04
Min ratio of peak top/edge	1	1.5
Peak duration range	0.00-10.00 min	0.00-10.00 min
d) Isotopic Peak Grouper		
m/z tolerance	5.0 ppm	5.0 ppm
Retention time tolerance	0.5 min	0.5 min
Monotonic shape	Yes	Yes
Maximum charge	1	1
Representative isotope	Most intense	Most intense
e) Alignment		
Method	Join Aligner	Join Aligner
m/z tolerance	5.0 ppm	5.0 ppm
Weight for m/z	20	20
Weight for RT	10	10
Retention time tolerance	0.1 min	0.1 min
f) Gap filling		
Method	Peak Finder	Peak Finder
Intensity tolerance	5.0%	5.0%
m/z tolerance	5.0 ppm	5.0 ppm
Retention time tolerance	0.1 min	0.1 min

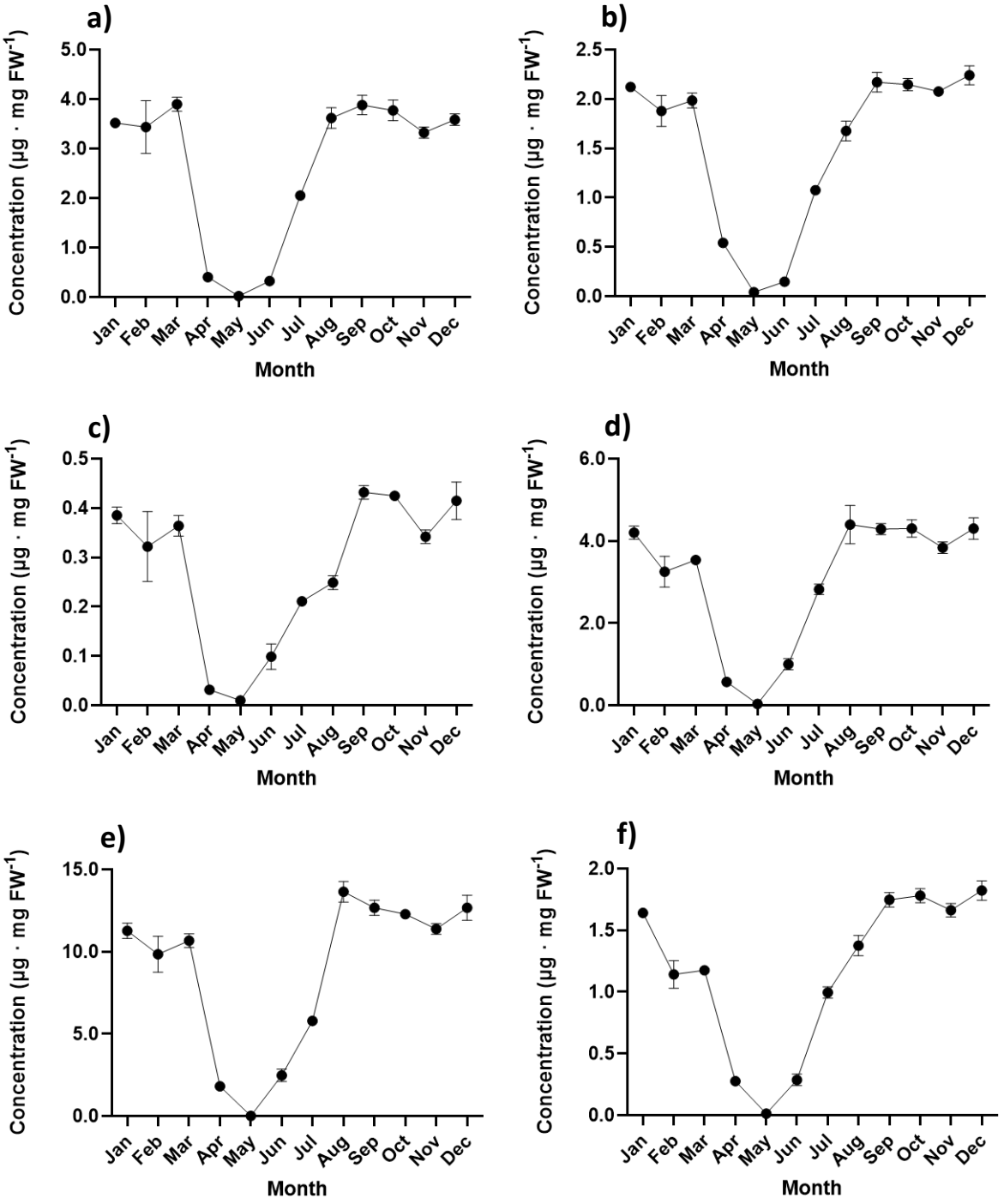

Supplemental Figure S2.2. Quantification of dihydrochalcones in *P. trichocarpa* whole bud extracts. a) 2',4',6'-OH DHC (2',4',6'-trihydroxydihydrochalcone), b) 2',6'-4'-OMe DHC (2',6'-dihydroxy-4'-methoxydihydrochalcone), c) 2',4',6',4-OH DHC (phloretin), d) 2',6',4-4'-OMe DHC (asebogenin), e) 2',4',6'-4-OMe DHC (2',4',6'-trihydroxy-4-methoxydihydrochalcone), and f) 2',6'-4,4'-OMe DHC (2',6'-dihydroxy-4,4'-dimethoxydihydrochalcone). Data points display the means ±SE (n = 3).

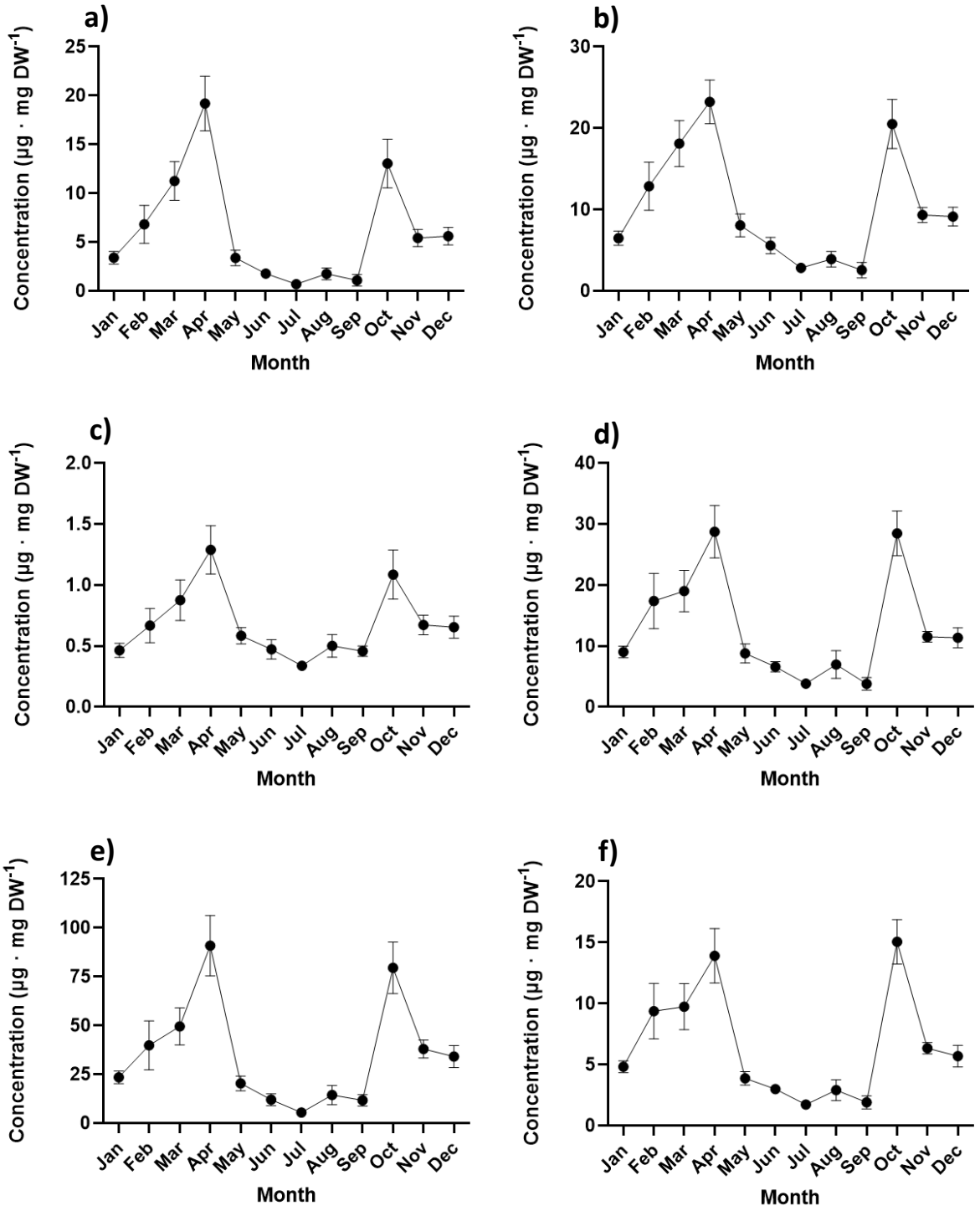

Supplemental Figure S2.3. Quantification of dihydrochalcones in *P. trichocarpa* leaf bud surface resin extracts. a) 2',4',6'-OH DHC (2',4',6'-trihydroxydihydrochalcone), b) 2',6'-4'-OMe DHC (2',6'-dihydroxy-4'-methoxydihydrochalcone), c) 2',4',6',4-OH DHC (phloretin), d) 2',6',4-4'-OMe DHC (asebogenin), e) 2',4',6'-4-OMe DHC (2',4',6'-trihydroxy-4-methoxydihydrochalcone), and f) 2',6'-4,4'-OMe DHC (2',6'-dihydroxy-4,4'-dimethoxydihydrochalcone). Data points display the means ±SE (n = 9).

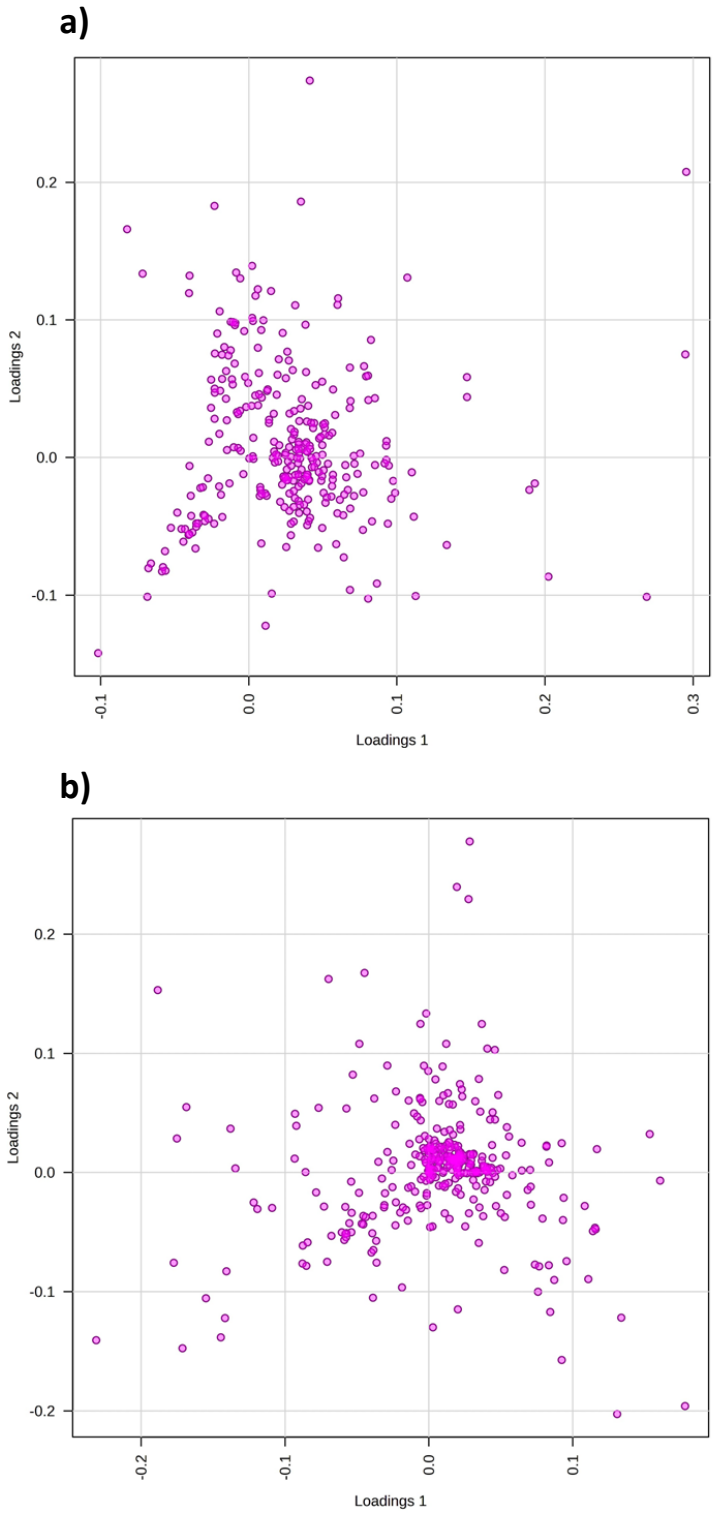

Supplemental Figure S2.4. Loadings plots of multivariate analysis of the leaf bud resin extracts. Loadings plots of the PLS-DA model for a) whole leaf buds (Fig. 2.3b) and b) surface resin (Fig. 2.6b).

Supplemental Table S2.2. A shortlist of the variable importance in projection (VIP) scores and loading values for mass features detected in whole leaf buds. Pseudomolecular ion annotations for the 15 mass features with the highest VIP scores based on PLS-DA analysis of whole leaf buds presented in Fig. 2.3b for a) component 1 and b) component 2. When available, the mass features are annotated based on matching *m/z* and retention time (RT) of analytical standards, including 2',4',6'-OH-4-OMe DHC (2',4',6'-trihydroxy-4-methoxydihydrochalcone), 2',6'-OH-4'-OMe DHC (2',6'-dihydroxy-4'-methoxydihydrochalcone), 2',4',6'-OH DHC (2',4',6'-trihydroxydihydrochalcone), 2',6',4-OH-4'-OMe DHC (asebogenin), and 2',6'-OH-4,4'-Me DHC (2',6'-dihydroxy-4,4'-dimethoxydihydrochalcone). Putatively identified mass features based on RT are indicated by (*). Component 1 explained 69.2 %, and component 2 explained 9.8 % of the variance in the PLS-DA data model.

a)

RT	*m/z*	Pseudomolecular Ion Annotation	VIP score	Loadings 1	Loadings 2
4.74	289.1070	2',4',6'-OH-4-OMe DHC $[M+H]^+$	4.99	0.29	0.07
4.80	285.0762	3,5-dihydroxy-7-methoxyflavonol $[M+H]^+$ (*)	4.66	0.27	-0.10
4.72	287.0915	2',4',6'-trihydroxy-4-methoxychalcone $[M+H]^+$ (*)	4.60	0.30	0.21
5.20	273.1123	2',6'-OH-4'-OMe DHC $[M+H]^+$	3.55	0.20	-0.09
4.79	259.0967	2',4',6'-OH DHC $[M+H]^+$	3.23	0.19	-0.02
5.16	271.0968	2',6'-dihydroxy-4'-methoxychalcone $[M+H]^+$ (*)	3.22	0.19	-0.02
4.67	289.1069	2',6',4-OH-4'-OMe DHC $[M+H]^+$	2.51	0.15	0.04
4.74	121.0649	Unknown	2.48	0.15	0.06
5.52	285.1125	Unknown	2.39	0.13	-0.06
3.60	441.1758	Unknown	2.08	0.11	-0.04
4.64	221.1175	Unknown	2.03	0.11	-0.10
5.14	303.1227	2',6'-OH-4,4'-Me DHC $[M+H]^+$	1.90	0.11	-0.01
3.61	441.1750	Unknown	1.86	0.09	-0.09
4.55	205.1952	Unknown	1.74	0.10	-0.03
4.24	267.0864	Unknown	1.74	-0.10	-0.14

b)

RT	*m/z*	Pseudomolecular Ion Annotation	VIP score	Loadings 1	Loadings 2
4.74	289.1070	2',4',6'-OH-4-OMe DHC $[M+H]^+$	4.95	0.29	0.07
4.80	285.0762	3,5-dihydroxy-7-methoxyflavonol $[M+H]^+$ (*)	4.63	0.27	-0.10
4.72	287.0915	2',4',6'-trihydroxy-4-methoxychalcone $[M+H]^+$ (*)	4.59	0.30	0.21
5.20	273.1123	2',6'-OH-4'-OMe DHC $[M+H]^+$	3.52	0.20	-0.09
4.79	259.0967	2',4',6'-OH DHC $[M+H]^+$	3.20	0.19	-0.02
5.16	271.0968	2',6'-dihydroxy-4'-methoxychalcone $[M+H]^+$ (*)	3.19	0.19	-0.02
4.67	289.1069	2',6',4-OH-4'-OMe DHC $[M+H]^+$	2.50	0.15	0.04
4.74	121.0649	Unknown	2.46	0.15	0.06
5.52	285.1125	Unknown	2.37	0.13	-0.06
3.60	441.1758	Unknown	2.07	0.11	-0.04
4.64	221.1175	Unknown	2.03	0.11	-0.10
5.14	303.1227	2',6'-OH-4,4'-Me DHC $[M+H]^+$	1.89	0.11	-0.01
3.61	441.1750	Unknown	1.87	0.09	-0.09
4.24	267.0864	Unknown	1.75	-0.10	-0.14
4.55	205.1952	Unknown	1.73	0.10	-0.03

Supplemental Table S2.3. A shortlist of the variable importance in projection (VIP) scores and loading values for mass features detected in surface resin extracts. Pseudomolecular ion annotations for the 15 mass features with the highest VIP scores based on PLS-DA analysis of surface resin presented in Fig. 2.6b for a) component 1 and b) component 2. When available, the mass features are annotated based on matching *m/z* and retention time (RT) of analytical standards, including 2',4',6'-OH-4-OMe DHC (2',4',6'-trihydroxy-4-methoxydihydrochalcone), 2',4',6'-OH DHC (2',4',6'-trihydroxydihydrochalcone), and 2',6'-OH-4'-OMe DHC (2',6'-dihydroxy-4'-methoxydihydrochalcone). Putatively identified mass features based on RT are indicated by (*). Component 1 explained 36.9 %, and component 2 explained 12.1 % of the variance in the PLS-DA data model.

a)

RT	*m/z*	Pseudomolecular Ion Annotation	VIP score	Loadings 1	Loadings 2
5.21	301.1063	2',6'-dihydroxy-4',4-dimethoxychalcone $[M+H]^+$ (*)	3.99	-0.23	-0.14
4.07	277.1767	Unknown	3.55	0.18	-0.20
5.03	301.1064	5,7-dimethoxy-4'-hydroxyflavanone $[M+H]^+$ (*)	3.52	-0.19	0.15
5.08	121.0645	Unknown	3.22	-0.18	-0.08
5.05	327.1220	Unknown	3.19	-0.18	0.03
5.40	301.1068	5-hydroxy-7,4'-dimethoxyflavanone $[M+H]^+$ (*)	3.14	-0.17	-0.15
5.09	271.0960	2',6'-dihydroxy-4'-methoxychalcone $[M+H]^+$ (*)	3.02	-0.17	0.05
6.80	310.3092	Unknown	2.91	0.16	-0.01
5.33	433.1634	Unknown	2.75	-0.15	-0.11
5.10	421.1644	Unknown	2.66	-0.14	-0.14
4.74	285.0751	3,5-dihydroxy-7-methoxyflavonol $[M+H]^+$ (*)	2.65	0.13	-0.20
4.06	219.1738	Unknown	2.64	0.13	-0.12
5.47	553.2224	Unknown	2.59	-0.14	-0.12
5.55	433.1634	Unknown	2.58	-0.14	-0.08
5.35	553.2213	Unknown	2.52	-0.14	0.04

b)

RT	*m/z*	Pseudomolecular Ion Annotation	VIP score	Loadings 1	Loadings 2
5.02	421.1636	Unknown	4.98	0.03	0.28
5.21	553.2202	Unknown	4.39	0.02	0.24
4.74	285.0751	3,5-dihydroxy-7-methoxyflavonol $[M+H]^+$ (*)	3.69	0.13	-0.20
4.07	277.1767	Unknown	3.56	0.18	-0.20
4.66	289.1063	2',4',6'-OH-4-OMe DHC	3.27	0.18	-0.20
4.73	259.0958	2',4',6'-OH DHC	2.83	-0.07	0.16
5.13	273.1115	2',6'-OH-4'-OMe DHC	2.80	-0.04	0.17
5.03	301.1064	5,7-dimethoxy-4'-hydroxyflavanone $[M+H]^+$ (*)	2.75	-0.19	0.15
5.40	301.1068	5-hydroxy-7,4'-dimethoxyflavanone $[M+H]^+$ (*)	2.74	-0.17	-0.15
4.60	123.0437	Unknown	2.65	0.09	-0.16
5.10	421.1644	Unknown	2.58	-0.14	-0.14
5.21	301.1063	2',6'-dihydroxy-4',4-dimethoxychalcone $[M+H]^+$ (*)	2.55	-0.23	-0.14
5.08	391.1535	Unknown	2.39	0.00	0.13
4.73	287.0906	2',4',6'-trihydroxy-4-methoxychalcone $[M+H]^+$ (*)	2.28	0.00	-0.13
5.47	553.2224	Unknown	2.274	-0.14	-0.12

Supplemental Table S2.4. Variable importance in projection (VIP) scores for mass features detected in whole leaf buds. Pseudomolecular ion annotations for mass features with VIP score ≥1 based on component 1 of PLS-DA analysis in whole leaf bud extracts. When available, the mass features are annotated based on matching *m/z* and retention time of analytical standards, including 2',4',6'-OH-4-OMe DHC (2',4',6'-trihydroxy-4-methoxydihydrochalcone), 2',6'-OH-4'-OMe DHC (2',6'-dihydroxy-4'-methoxydihydrochalcone), 2',4',6'-OH DHC (2',4',6'-trihydroxydihydrochalcone), 2',6',4-OH-4'-OMe DHC (asebogenin), and 2',6'-OH-4,4'-Me DHC (2',6'-dihydroxy-4,4'-dimethoxydihydrochalcone). Putatively identified mass features are indicated by (*).

RT	*m/z*	Pseudomolecular Ion Annotation	VIP score	Reference
4.74	289.1070	2',4',6'-OH-4-OMe DHC $[M+H]^+$	4.99	English et al., 1991
4.80	285.0762	3,7-dihydroxy-5-methoxyflavonol $[M+H]^+$ (*)	4.66	Greenaway et al., 1990
4.72	287.0915	2',4',6'-trihydroxy-4-methoxychalcone $[M+H]^+$ (*)	4.60	English et al., 1991
5.20	273.1123	2',6'-OH-4'-OMe DHC $[M+H]^+$	3.55	English et al., 1991
4.79	259.0967	2',4',6'-OH DHC $[M+H]^+$	3.23	English et al., 1991
5.16	271.0968	2',6'-dihydroxy-4'-methoxychalcone $[M+H]^+$ (*)	3.22	English et al., 1991
4.67	289.1069	2',6',4-OH-4'-OMe DHC $[M+H]^+$	2.51	English et al., 1991
4.74	121.0649	Unknown	2.48	
5.52	285.1125	Unknown	2.39	
3.60	441.1758	Unknown	2.08	
4.64	221.1175	Unknown	2.03	
5.14	303.1227	2',6'-OH-4,4'-Me DHC $[M+H]^+$	1.90	English et al., 1991
3.61	441.1750	Unknown	1.86	
4.55	205.1952	Unknown	1.74	
4.24	267.0864	Unknown	1.74	
3.60	325.0922	Unknown	1.71	
4.95	277.2165	Unknown	1.71	
4.56	123.1168	Unknown	1.70	
5.75	205.1953	Unknown	1.67	
4.70	235.1694	Unknown	1.66	
5.53	379.1546	Unknown	1.58	
4.86	301.0709	3,5,4'-trihydroxy-7-methoxyflavonol $[M+H]^+$ (*)	1.57	Greenaway et al. 1992
3.61	325.0917	Unknown	1.56	
5.52	506.1965	Unknown	1.54	
3.49	213.0910	Benzyl benzoate $[M+H]^+$ (*)	1.53	English et al., 1991
4.75	257.0811	2',4',6'-trihydroxychalcone $[M+H]^+$ (*)	1.53	Greenaway et al. 1992
5.40	403.1545	Unknown	1.52	
5.41	299.0917	Unknown	1.50	
3.50	442.1713	Salicortin $[M+H]^+$ (*)	1.43	Boeckler et al. 2011
5.43	283.0969	Unknown	1.41	
4.99	697.3748	Unknown	1.39	
4.56	135.1169	Unknown	1.37	
4.97	421.1653	Unknown	1.35	
5.01	299.0915	Unknown	1.31	

5.15	121.0649	Unknown	1.28	
3.61	163.0390	Unknown	1.28	
4.66	183.0652	Unknown	1.27	
4.95	295.2271	Unknown	1.27	
4.97	419.1492	Unknown	1.26	
5.43	405.1694	Unknown	1.24	
5.39	433.1650	Unknown	1.24	
5.08	419.1494	Unknown	1.24	
5.49	283.0969	Unknown	1.24	
3.55	479.0815	Quercetin 3-glucuronide $[M+H]^+$ (*)	1.23	Nissinen et al. 2007
5.85	491.2799	Unknown	1.22	
4.23	546.1970	Tremulacin $[M+NH_4]^+$ (*)	1.21	Boeckler et al. 2011
5.41	313.1072	Unknown	1.20	
5.19	553.2225	Unknown	1.17	
4.23	546.1978	Tremulacin $[M+NH_4]^+$ (*)	1.17	Boeckler et al. 2011
6.22	425.2326	Unknown	1.17	
5.43	311.1277	Unknown	1.16	
5.10	327.1231	Unknown	1.16	
5.16	391.1542	Unknown	1.15	
5.16	167.0340	Unknown	1.15	
5.16	417.1340	Unknown	1.12	
4.72	523.2694	Unknown	1.12	
2.98	135.0443	Unknown	1.08	
5.02	697.3744	Unknown	1.08	
3.60	181.0497	Caffeic acid $[M+H]^+$ (*)	1.06	Wang et al. 2017
4.95	335.2196	Unknown	1.05	
4.76	121.0650	Unknown	1.03	
3.54	303.0505	Quercetin 3-galactoside $[M+H]^+$ (*)	1.02	Nissinen et al. 2007
4.29	271.0604	Unknown	1.01	

Supplemental Table S2.5. Variable importance in projection (VIP) scores for detected mass features in surface resin. Pseudomolecular ion annotations for mass features with VIP score ≥1 based on component 1 of PLS-DA analysis in surface resin extracts. When available, the mass features are annotated based on matching *m/z* and retention time of analytical standards, including 2',4',6'-OH DHC (2',4',6'-trihydroxydihydrochalcone). Putatively identified mass features are indicated by (*).

RT	*m/z*	Pseudomolecular Ion Annotation	VIP score	Reference
5.21	301.1063	2',6'-dihydroxy-4',4-dimethoxychalcone $[M+H]^+$ (*)	3.99	Greenaway et al., 1991
4.07	277.1767	Unknown	3.55	
5.03	301.1064	5,7-dimethoxy-4'-hydroxyflavanone $[M+H]^+$ (*)	3.52	Greenaway et al., 1991
5.08	121.0645	Unknown	3.22	
5.05	327.1220	Unknown	3.19	
5.40	301.1068	5-hydroxy-7,4'-dimethoxyflavanone $[M+H]^+$ (*)	3.14	Greenaway et al., 1991
5.09	271.0960	2',6'-dihydroxy-4'-methoxychalcone $[M+H]^+$ (*)	3.02	English et al., 1991
6.80	310.3092	Unknown	2.91	
5.33	433.1634	Unknown	2.75	
5.10	421.1644	Unknown	2.66	
4.74	285.0751	3,5-dihydroxy-7-methoxyflavonol $[M+H]^+$ (*)	2.65	Greenaway et al., 1990
4.06	219.1738	Unknown	2.64	
5.47	553.2224	Unknown	2.59	
5.55	433.1634	Unknown	2.58	
5.35	553.2213	Unknown	2.52	
5.42	285.1115	Unknown	2.43	
6.06	280.2626	Unknown	2.43	
4.49	123.1165	Unknown	2.26	
4.49	205.1944	Unknown	2.26	
5.25	133.0645	Cinnamaldehyde $[M+H]^+$ (*)	2.23	-
4.49	135.1165	Unknown	2.23	
4.06	237.1843	Unknown	2.19	
4.60	183.0648	Unknown	2.10	
4.63	301.1063	5,7-dimethoxy-4'-hydroxyflavanone $[M+H]^+$ (*)	2.10	English et al., 1991
4.82	301.0701	3,5,4'-trihydroxy-7-methoxyflavonol $[M+H]^+$ (*)	2.02	Greenaway et al., 1992
4.60	123.0437	Benzoic acid $[M+H]^+$ (*)	1.99	English et al., 1991
5.03	203.1062	Unknown	1.89	
4.59	221.1165	Unknown	1.87	
5.92	254.2473	Unknown	1.81	
4.63	437.1583	Unknown	1.80	
5.10	297.1116	Cinnamyl-caffeate $[M+H]^+$ (*)	1.72	Greenaway et al., 1990
3.65	245.0800	Unknown	1.72	
4.01	301.1038	Unknown	1.70	
4.06	201.1633	Unknown	1.65	
4.90	335.2187	Unknown	1.64	
6.44	270.2783	Unknown	1.62	

4.65	287.0908	2’,6’,4-trihydroxy-4’-methoxychalcone $[M+H]^+$	1.62	English et al., 1991
5.53	211.0751	Unknown	1.61	
5.28	271.0961	2’,6’-dihydroxy-4’-methoxychalcone $[M+H]^+$ (*)	1.60	English et al., 1991
5.11	135.0437	Unknown	1.59	
5.43	299.0913	Unknown	1.58	
5.37	315.1223	Unknown	1.56	
4.49	149.1321	Unknown	1.55	
3.66	275.0905	Unknown	1.53	
4.91	327.1219	Unknown	1.49	
5.73	285.1116	Unknown	1.47	
4.06	159.1163	Unknown	1.46	
3.76	447.1618	Unknown	1.38	
6.13	268.2629	Unknown	1.38	
5.37	403.1532	Unknown	1.37	
3.46	442.1695	Salicortin $[M+NH_4]^+$ (*)	1.34	Boeckler et al. 2011
5.11	449.1587	Unknown	1.33	
5.11	167.0335	Unknown	1.32	
6.37	142.1222	Unknown	1.31	
5.80	228.2317	Unknown	1.29	
4.73	259.0958	2’,4’,6’-OH DHC $[M+H]^+$	1.20	English et al., 1991
6.55	270.2787	Unknown	1.19	
5.18	337.1039	Unknown	1.17	
6.37	226.2160	Unknown	1.16	
6.06	263.2361	Unknown	1.15	
3.72	447.1616	Unknown	1.14	
4.65	407.1483	Unknown	1.14	
6.37	212.2003	Unknown	1.11	
5.97	242.2470	Unknown	1.11	
4.83	319.0935	Cinnamyl caffeate $[M+Na]^+$ (*)	1.11	Greenaway et al. 1990
4.19	546.1959	Tremulacin $[M+NH_4]^+$ (*)	1.10	Boeckler et al. 2011
6.37	240.2316	Unknown	1.10	
5.29	417.1333	Unknown	1.08	
4.75	459.1412	Unknown	1.06	
6.88	467.3327	Unknown	1.06	
5.32	299.0910	Unknown	1.05	
5.42	283.0957	Unknown	1.05	
5.07	299.0911	Unknown	1.05	
5.74	315.1222	Unknown	1.01	
4.65	271.0959	2’,6’-dihydroxy-4’-methoxychalcone $[M+H]^+$ (*)	1.01	Greenaway et al. 1991

Chapter 3 - A novel *O*-methyltransferase specific for dihydrochalcones from *P. trichocarpa* and *P. balsamifera* leaf bud resin

3.1 Abstract

Production of secreted leaf bud resin is a key mechanism for poplar trees to protect their leaf buds against frost damage, dehydration during dormancy, and insect herbivory. Leaf bud resins of *P. trichocarpa* and *P. balsamifera* share similar metabolite profiles, consisting largely of singly or doubly *O*-methylated dihydrochalcones. The enzymatic reaction of *O*-methylation of dihydrochalcones has not been previously described in any plant species. In this study, we characterized a novel *O*-methyltransferase, PtDOMT1, capable of inducing *O*-methylation on dihydrochalcones using S-adenosyl-*L*-methionine as a methyl donor. Transcriptomics, differential gene expression, and enzymatic analyses identified PtDOMT1 as an *O*-methyltransferase, which can methylate 4- and 4'-positions of dihydrochalcones. These findings establish the terminal step for the biosynthesis of *O*-methylated dihydrochalcones and the first characterized step in the biosynthesis of leaf bud resin in poplar.

3.2 Introduction

Poplar trees, such as black cottonwood (*P. trichocarpa*) and balsam poplar (*P. balsamifera*), are known to secrete resinous exudate from their leaf buds. The synthesis of leaf bud resin is observed on the special secretary epidermis on the inner surface of bud scales (Curtis and Lersten, 1974). The biological function of leaf bud resin is to protect the leaf buds from frost during dormancy and young developing leaves from insect herbivory (Curtis and Lersten, 1974). Leaf bud resins from different poplar species contain diverse phenolic specialized metabolites (English et al., 1991, 1992; Greenaway et al., 1989a; Kuś et al., 2018). The chemical profiles of *P. trichocarpa* and *P. balsamifera* bud resins are specifically characterized by the abundance of *O*-methylated dihydrochalcone aglycones (English et al., 1991; Lavoie et al., 2013; Greenaway and Whatley, 1990). Despite a wealth of chemical knowledge, the biosynthesis of *O*-methylated dihydrochalcones has not been previously

investigated in poplar or any plant species. The abundance of *O*-methylated dihydrochalcones found in poplar leaf bud resins implies that a novel class of *O*-methyltransferases (OMTs) could play a key part in leaf bud resin biosynthesis.

Methyltransferases found in plants can act on hydroxyl groups of phenolic specialized metabolites and are responsible for catalyzing the methylation of these groups (Barakat et al., 2011). Methylation is a common substitution in phenolic specialized metabolites, and *O*-methylation has been reported in various phenylpropanoids, including flavonoids (Roje, 2006; Ibrahim et al., 1998). Flavonoid OMTs have been characterized from various plant species (Kim et al., 2010), including sweet basil (*Ocimum basilicum*) (Berim et al., 2012), wild tomato (*Solanum habrochaites*) (Schmidt et al., 2012, 2011), and peach (*Prunus percia*) (Cheng et al., 2014). To date, the only characterized OMT reported in poplar is identified from *P. deltoides* with the capacity to induce 7-*O*-methylation of flavones (Kim et al., 2006). OMTs have been shown to produce distinct substitution patterns on their substrates (Berim et al., 2012). This diversification in the substitution patterns originates from the regioselectivity of the OMT enzymes (Berim et al., 2012). Some OMTs are shown to be selective towards a single position on a very narrow selection of substrates, while others can produce multiple methylations on a broad spectrum of flavonoid substrates (Berim et al., 2012; Berim and Gang, 2016). This selectivity contributes to the accumulation and structural diversity of different specialized metabolites in plants (Cheng et al., 2014; Berim and Gang, 2016). The biosynthesis of dihydrochalcones, as well as their *O*-methylated modifications, are biologically significant features of *P. trichocarpa* and *P. balsamifera*, as these types of flavonoids are shown to be biologically active (Rivière, 2016). However, OMTs that act on dihydrochalcones have not been previously characterized in any plant species.

Here, we identify and characterize a novel OMT, which methylates dihydrochalcones characteristic of leaf bud resins of *P. trichocarpa* and balsam poplar *P. balsamifera*. We used transcriptomics to study large-scale gene expression patterns of leaf buds and phylogenetic analysis and enzyme assays to identify a dihydrochalcone-specific OMT. Our data indicate that this enzyme is responsible for the accumulation of methylated dihydrochalcones in *P. trichocarpa* and *P. balsamifera* leaf buds.

3.3 Materials and Methods

3.3.1 Sampling of *P. trichocarpa* and *P. balsamifera* lateral leaf buds

Poplar leaf bud samples of *P. trichocarpa* (Nisqually-1) were collected from the University of Victoria Research Compound. Lateral leaf buds of *P. trichocarpa* were collected monthly over 12 months as part of a study to examine seasonal patterns of PtDOMT1 expression. Leaf buds were collected from three adjacent clonal trees, which acted as biological replicates. Three replicate samples were gathered from each of the biological replicates. In addition, to study differences in the accumulation of dihydrochalcones in and expression of PtDOMT1 in different leaf bud tissues, leaf bud scales and the enclosed embryonic leaf tissues were manually separated from samples collected in April during bud break.

To examine leaf bud development and leaf bud resin accumulation in a controlled setting, dormant cuttings of female *P. trichocarpa* (Nisqually-1) and *P. balsamifera* (LOV-5) were induced to flush in a growth chamber. Dormant cuttings of *P. balsamifera* were acquired from Dr. Raju Soolanayakanahally (Agriculture and Agri-Food Canada, AAFC) in Saskatoon, Canada. The dormant poplar cuttings, harvested in February, were 30 cm long on average and stored at 4°C in the dark before being placed in a growth chamber. The dormant twigs were placed in water in controlled light (16 hours of light) and temperature conditions (22°C). Leaf buds were collected every other day over 12 days (Supplemental Figure S3.1). For each time point, three replicates of *P. balsamifera* and two replicates of *P. trichocarpa* leaf buds were collected from one individual cutting to prevent wound-induced effects during the time course. All samples were frozen immediately in liquid nitrogen, ground in liquid nitrogen, and stored at -80°C prior to extraction.

3.3.2 Targeted metabolite analysis by UPLC-MS

Poplar leaf bud samples were extracted as described in Chapter 2 (section 2.3.4). The samples were analyzed using a Waters Acquity UPLC System coupled to an Acquity PDA eLambda Detector and an Acquity QDa single quadrupole mass spectrometer (Waters, Milford, MA, USA). The column used for separation was Acquity BEH C18 (2.1 mm, 50 mm, 1.7 µm). The UPLC-MS parameters were described in Chapter 2 (section 2.3.5). The UPLC-MS data were processed using TargetLynx (Version 4.2). Analytical standards used are described in Chapter 2 (section 2.3.1)

3.3.3 RNA extraction and RT-qPCR analysis

Total RNA was extracted from the lateral leaf buds as described by Muoki et al. (2012). Extracted RNA was treated with RQ1 DNase (Promega, Madison, WI, USA) to remove genomic DNA. ProtoScript® II Reverse Transcriptase kit (New England BioLabs) was used for first-strand cDNA synthesis.

RT-qPCR analysis was performed in a total volume of 15 µL reactions using Luna® Universal qPCR Master Mix (New England BioLabs), using a protocol adapted and scaled down from the manufacturer. Each reaction contained 1 µL of 1:10 diluted cDNA template. PtDOMT1 transcript abundance was measured using forward primer 5'-ATGTTGTAGCAACAGCACCA-3' and reverse primer 5'–TCATCGGTCCAATCATGCAA–3' (Supplemental Table S3.3). Primer annealing efficiency was optimized using a dilution series of cDNA templates prior to quantitative analysis. The primer efficiency of PtDOMT1 was 95.75 % (R^2 = 0.9936) at 58°C temperature, yielding 121 bp amplicon. PtDOMT1 transcript abundance was normalized using the geometric mean of ubiquitin (UBQ10; Potri.014G115100) and actin (ACT; Potri.001G309500) as housekeeping genes. Samples without cDNA templates were used as negative controls.

3.3.4 RNA-seq analysis

Total RNA was purified from lateral leaf buds of *P. trichocarpa* and *P. balsamifera* cuttings induced to flush in a growth chamber were used for RNA extraction. Samples collected at day 0 (D0), day 4 (D4), and day 10 (D10) were selected to represent dormant, pre-bud break, and bud break phases of the lateral leaf buds, respectively. Three biological replicates of *P. balsamifera* and two biological replicates of *P. trichocarpa* were used to prepare RNA-seq libraries as previously described (Ma et al., 2018). A total of 15 RNA libraries were pooled together and sequenced on one HiSeq lane using the Illumina NextSeq 550 platform by the University of British Columbia Sequencing and Bioinformatics Consortium (Vancouver, BC, Canada).

The sequence alignment of the raw RNA-seq data was performed using HiSAT2 (Kim et al., 2019), and Cufflinks (Trapnell et al., 2012) was used for transcript assembly. The *P. trichocarpa* v4.1 genome was used as a reference genome sequence (Goodstein et al., 2012, http://phytozome.jgi.doe.gov). Differential expression analysis was conducted using DESeq2 package (Love et al., 2014) in R (version 4.3.1). Annotated *P. trichocarpa* v4.1 reference transcriptome (http://phytozome.jgi.doe.gov) was used for gene annotations.

3.3.5 Phylogenetic analysis

Sequences for the characterized genes were acquired from the NCBI database (https://www.ncbi.nlm.nih.gov/protein/). Multiple gene alignments were performed in Mega11 (v 11.0.13) using the ClustalW algorithm. Phylogenetic analysis was performed using the maximum-likelihood statistical method and the Jones-Taylor-Thorton (JTT) model with 1000 bootstrapping replicates. The graphical presentation of the phylogenetic tree was generated using FigTree (v 1.4). Names, accession numbers, and plant species of the characterized OMTs used in the phylogenetic analysis were as follows: ShMOMT1 (ADZ76433, *Solanum habrochaites*), ShMOMT2 (ADZ76434, *Solanum habrochaites*), ShMOMT3 (AGK26768, *Solanum habrochaites*), CrOMT2 (Q8GSN1, *Catharanthus roseus*), PkHOMT1 (Q43046, *Populus sieboldii* × *Populus grandidentata*), ObEOMT1 (Q93WU2, *Ocimum basilicum*),

ObCVOMT1 (Q93WU3, *Ocimum basilicum*), ObFOMT1 (AFU50295, *Ocimum basilicum*), ObFOMT2 (AFU50296, *Ocimum basilicum*), ObFOMT3 (AFU50297, *Ocimum basilicum*), ObFOMT4 (AFU50298, *Ocimum basilicum*), ObFOMT5 (AFU50299, *Ocimum basilicum*), ObFOMT6 (AFU50300, *Ocimum basilicum*), MsIOMT8 (O24529, *Medicago sativa*), MsIOMT6 (O22308, *Medicago sativa*), MsIOMT9 (O22309, *Medicago sativa*), MsCOMT (AAB46623, *Medicago sativa*), SlAOMT (NP_001289828, *Solanum lycopersicon*), HlOMT2 (B0ZB56, *Humulus lupulus*), and NtCOMT2 (AAL91506, *Nicotiana tabacum*).

3.3.6 Recombinant protein expression and purification

The coding sequences of candidate genes, including the recombinant Potri.013G136300, Potri.019G102900, and Potri.013G122400 expression vectors, were synthesized by Twist Bioscience (South San Francisco, CA, USA). The vector construct included N-terminal His-tagged expression vector pET-28a(+), containing XhoI and BamHI restriction sites and *E. coli* codon-optimized insert sequences. The recombinant vector was transferred into electrocompetent *E. coli* (BL21 DE3) via electroporation, and the transformed colonies were selected on LB plates containing 50 µg/mL kanamycin. The plates were incubated overnight at 37°C. A single colony was transferred into a liquid starter culture containing 6 mL LB media and 50 µg/mL kanamycin. The liquid culture was incubated at 37°C and 250 rpm until OD_{600} reached 0.4–0.6. For protein induction, 4 mL of the liquid culture was transferred into 100 mL of fresh LB media with 1 mM IPTG. The induction culture was incubated for 24h at 20°C and 250 rpm, after which the culture was centrifuged at 4000 rpm and 4°C for 20 mins to harvest the cells. The supernatant was discarded, and the pellet was used for protein purification.

The bacterial pellet was resuspended in 4 mL of lysis buffer (50 mM NaH_2PO_4, 300 mM NaCl, 10 mM imidazole, pH 8) and incubated on ice for 20 min. The pellet was lysed on ice using a sonicator rod, and the lysate was centrifuged for 20 mins at 4°C and 15000 rpm to collect the lysate supernatant. The supernatant was mixed with 1 mL Ni-NTA agarose (Qiagen, Hilden, Germany), stabilized in lysis buffer, and loaded into a column. Flow-through of the column was collected, and the column was washed twice with 2.5 mL of wash buffer (50 mM NaH_2PO_4, 300 mM NaCl, 20 mM imidazole, pH 8). The protein fraction was eluted by washing the column four

times with 0.5 mL of elution buffer (50 mM NaH_2PO_4, 300 mM NaCl, 100 mM imidazole, pH 8). The collected fractions were pooled and desalted using a centrifugal concentrator column (30 kDa, Sigma-Aldrich) and exchange buffer (50 mM Tris/HCl, 10% glycerol, 1 mM DTT, pH 7.5). The concentration of the purified protein was determined using Pierce™ BCA Protein Assay kit (ThermoFisher) against a BSA standard curve.

The purity and molecular weight of the recombinant proteins were confirmed by electrophoresis. A 1 µg sample of the purified protein was separated using sodium dodecyl sulphate-polyacrylamide electrophoresis (SDS-PAGE) on a 12% acrylamide mini gel. Coomassie staining was used to confirm the molecular size of the purified product, and Western blot was used to confirm the His-tagged protein. A 0.2-µm polyvinylidene difluoride (PVDF) membrane (Bio-Rad) was used for Western blotting. The membrane was blocked with 3% BSA/TTBS for 1 h and incubated with His-tag mouse mAb (1:5000; Cell Signaling Technology) for 1 h. A DAB substrate kit (Bio Basic) visualized His-tagged recombinant proteins.

3.3.7 Biochemical characterization

The standard assays were conducted using a reaction mixture containing 5 µg of purified recombinant protein, 0.10 mM of the acceptor substrate, 0.50 mM of S-adenosyl-*L*-methionine (SAM) (Sigma-Aldrich), and 1 mM dithiothreitol (DTT) in 0.1 M phosphate buffer (pH 7.5), with a total reaction volume of 200 µL. The reactions were incubated for 20 min at 30°C. To stop the reactions, 20 µL of 6 N HCl was added, and the samples were centrifuged for 5 min at 15000 rpm at 4°C. The resulting supernatant was used for UPLC-MS analysis. The reaction temperature, pH, and incubation time were optimized to ensure that the reaction velocity remained linear during the kinetic measurements. Controls for the enzyme activity assays included boiled enzyme preparations as a negative control and previously characterized flavonoid OMT recombinant proteins ObFOMT1, ObFOMT3, and ObFOMT5 (Berim et al., 2012).

The enzyme reaction linearity was investigated by measuring the reaction product in 5-minute intervals for 30 mins at pH 7.5 and 30°C. For determining the pH optimum of the enzyme

reactions, the pH range from 3 to 5 was covered using 0.1 M citrate-phosphate buffer, pH 5 to 8 using 0.1 M phosphate buffer, and pH 8.6 to 10 using 0.1 M glycine-NaOH buffer. The optimal pH was determined by measuring the product concentration after 20 min incubation at 30°C. Incubation temperature was tested in 5°C intervals in the 10–50°C range. The substrate for reaction condition optimization was 2',4',6'-OH DHC. The reaction buffer was preconditioned at tested temperatures for 10 min before the addition of the recombinant protein.

The kinetic properties for each substrate were determined at the optimal pH (7.5) at 30°C with saturating concentrations of methyl donor and varying concentrations of the methyl acceptor (5 to 300 μM). All kinetic parameters were measured through three separate recombinant protein preparations. The reaction products were analyzed on UPLC-MS using optimized SIR methods, as mentioned above, and the peak areas were used to determine the product concentration using standard curves. The product concentration was used to calculate the Michaelis-Menten kinetic parameters using nonlinear regression analysis in GraphPad Prism (Version 8.4.3).

3.3.8 Statistical analysis

Statistical analysis of the chemical data was done by using two-way ANOVA and Tukey's post hoc HSD using GraphPad Prism (Version 8.4.3). Similarly, the calculation of the Michaelis-Menten kinetic parameters was performed using nonlinear regression analysis.

3.4. Results

3.4.1 Dihydrochalcone composition of *P. trichocarpa* and *P. balsamifera* lateral leaf buds

We used targeted UPLC-MS methods to analyze the chemical composition and quantify dihydrochalcones in *P. trichocarpa* and *P. balsamifera* whole leaf buds. Dormant lateral leaf buds on short twigs were induced to flush for four days in a growth chamber, and the whole buds were harvested and extracted. The concentrations of detected dihydrochalcones, normalized by

fresh weight, were generally higher in *P. balsamifera* leaf buds compared to *P. trichocarpa* (Fig. 3.1a).

Of the *O*-methylated dihydrochalcones, only 2',6',4-OH-4'-OMe DHC did not significantly differ in abundance between the studied species. Both poplar species displayed similar relative abundances of the other dihydrochalcones. Both species showed a higher prevalence of the *O*-methylated dihydrochalcones compared to the non-methylated dihydrochalcones; 2',6'-OH-4'-OMe DHC was present at the highest concentration, while the doubly methoxylated 2',6'-OH-4,4'-OMe DHC was present at lower concentration in both species. The non-methylated 2',4',6',4-OH DHC was detected at the lowest concentration in both sample types.

In addition to the whole leaf bud extracts, we analyzed the abundance of dihydrochalcones separately in leaf bud scales and embryonic leaf tissue dissected from the *P. trichocarpa* leaf buds. *P. trichocarpa* only was used for this analysis due to the availability of leaf buds. We separated bud scales from leaf tissues of leaf buds harvested in April during bud break, and in August when the leaf buds are fully intact. The UPLC analysis showed that the leaf tissue had a nearly two-fold higher dihydrochalcone concentration than leaf bud scales in April per fresh weight (Fig. 3.1b). Similarly, samples collected in August showed a higher accumulation of dihydrochalcones in the embryonic leaf tissue. However, the difference between the two tissues was smaller than in the April samples (Fig. 3.1c).

Overall, dihydrochalcones were found in both poplar species, but *P. balsamifera* leaf bud extracts showed a significantly higher abundance of dihydrochalcones compared to *P. trichocarpa* leaf bud extracts. Additionally, our analysis indicated that dihydrochalcones are accumulated primarily on the embryonic leaves.

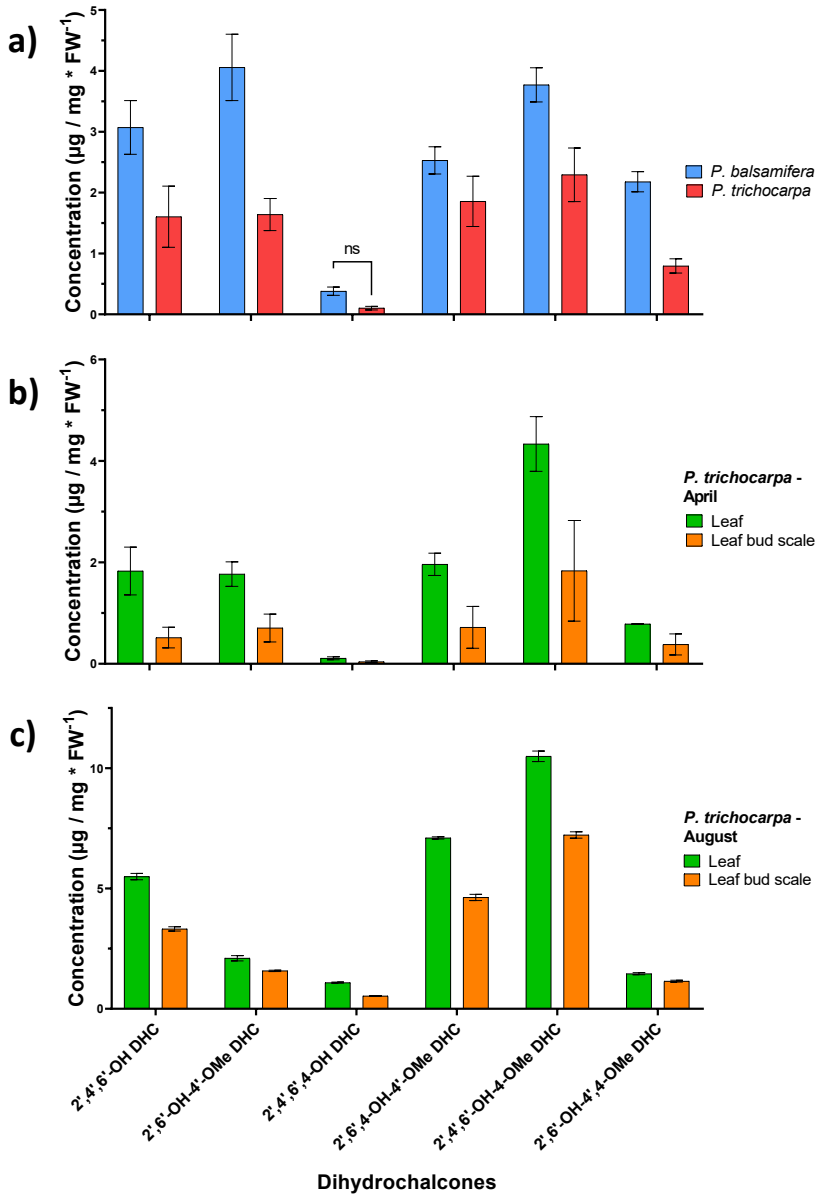

Figure 3.1. Analysis of dihydrochalcones in *P. trichocarpa* and *P. balsamifera* lateral leaf buds. Dihydrochalcones in methanolic extracts of *P. trichocarpa* and *P. balsamifera* were quantified by UPLC-MS and normalized by the fresh weight of the extracted tissue. a) Whole leaf buds of *P. trichocarpa* and *P. balsamifera. P. trichocarpa* leaf bud scales and embryonic leaves collected in b) April and c) August. The data represent the means ±SE (n = 3). Statistical analyses were done by multiple t-tests ($P < 0.05$). All pairwise comparisons were statistically significant unless indicated by ns (non-significant). Indicated abbreviations are as follows; 2',4',6'-OH DHC (2',4',6'-trihydroxydihydrochalcone), 2',6'-OH-4'-OMe DHC (2',6'-dihydroxy-4'-methoxydihydrochalcone), 2',4',6'-OH-4-OMe DHC (2',4',6'-trihydroxy-4-methoxydihydrochalcone), and 2',6'-OH-4,4'-OMe DHC (2',6'-dihydroxy-4',4-dimethoxydihydrochalcone).

3.4.2 Transcriptomic analysis and identification of candidate genes in *P. trichocarpa* and *P. balsamifera* lateral leaf buds

Next, we generated transcriptomes for *P. trichocarpa* and *P. balsamifera* leaf buds by RNA-seq in order to identify candidates for dihydrochalcone-specific OMTs. A total of 33582 and 33404 unique transcripts were identified and annotated for *P. trichocarpa* and *P. balsamifera*, respectively. Based on gene annotation using the *P. trichocarpa* genome (version 4.1), we identified a total of 36 OMTs expressed in the leaf bud samples across both species, including 13 OMTs unique to *P. trichocarpa* and 14 OMTs unique to *P. balsamifera* (Supplemental Table S3.1). Nine candidate OMTs expressed in both *P. trichocarpa* and *P. balsamifera* were identified. Phylogenetic analysis of the nine common candidate genes together with previously characterized OMTs (Fig. 3.2) suggested a putative substrate class for the candidate genes. Based on this analysis, Potri.013G136300, Potri.013G143800, and Potri.019G102900 were assigned to a clade with HlOMT2, an OMT capable of acting on chalcones, which we considered a structurally relevant group of flavonoids. Alignment of the Potri.013G136300 peptide sequence with Potri.013G143800 indicated that these two genes shared a very high similarity (99.44 %). This suggested that they likely are recently duplicated paralogs. However, Potri.013G136300 displayed higher expression in both poplar species and was selected to represent this paralogue pair in further analysis. Alignment of HlOMT2 with Potri.013G136300 and Potri.019G102900 showed 51.97 % and 57.10 % similarity, respectively.

Further selection and analysis of the putative candidate genes were performed using gene expression patterns of known phenylpropanoid and flavonoid pathway genes within both *P. trichocarpa* and *P. balsamifera* datasets. PAL1 and PAL3 were selected as markers for the phenylpropanoid pathway, and CHS1-5 were selected as marker genes for the flavonoid-related gene expression patterns. The corresponding differential expression patterns for the marker and candidate genes are displayed as log2 fold change between initial sampling and after four and ten days of bud flush induction in the growth chamber (Table 3.1, Supplemental Table S3.2). Genes with log2 fold changes > 2 were considered to have increased expression in the pairwise comparisons. We observed an increase in expression levels of PAL3 in the leaf buds of both species after four days of incubation in the growth chamber. CHS2, CHS3 and CHS5 showed an increase in the expression levels in *P. trichocarpa*, while in *P. balsamifera,* only CHS1 showed

an increase. Only two candidate OMTs, Potri.013G136300 and Potri.013G143800, displayed a significant increase in their expression, reflecting the trend displayed by the marker genes. No phenylpropanoid and flavonoid-related marker genes displayed increased expression after ten days of flushing induction. In contrast, Potri.013G136300 and Potri.013G143800 were still highly expressed after ten days.

Based on phylogenetic and expression pattern analysis, we designated Potri.013G136300 as the primary candidate for OMTs associated with leaf bud resin dihydrochalcones. In parallel, we selected two additional candidate genes expressed in both studied species, Potri.019G102900 and Potri.013G122400, for further biochemical characterization. Potri.019G102900 was selected based on phylogenetic analysis and its grouping within the same clade as Potri.013G136300. Alignment of Potri.019G102900 and Potri.013G136300 revealed 66.86 % peptide sequence identity. Potri.013G122400 was selected due to its distinct phylogenetic distance from the other candidate genes, as well as its closeness to ObEOMT1 and ObVCOMT1, which utilize eugenol substrate, a phenolic non-flavonoid. Alignment of Potri.013G122400 and Potri.013G136300 displayed 34.75 % identity.

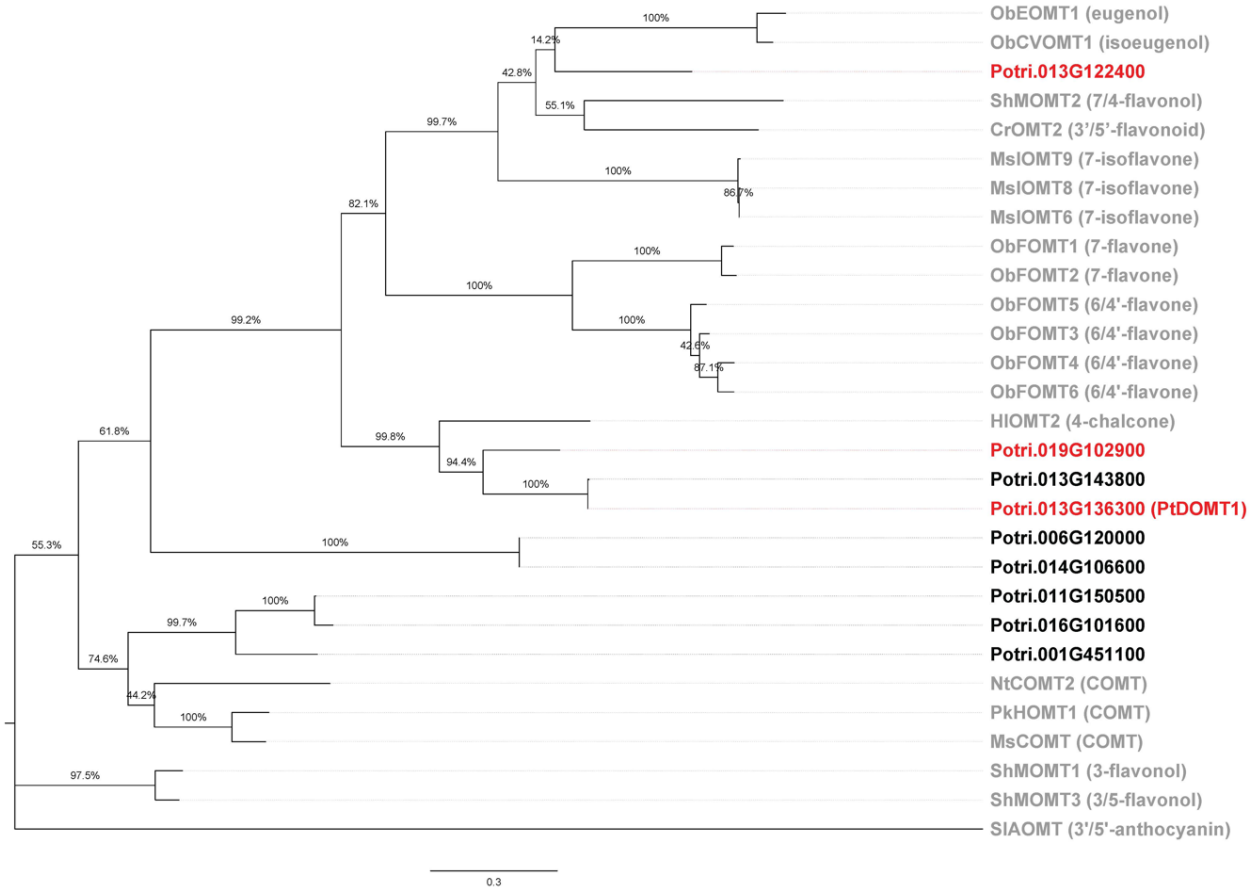

Figure 3.2. Phylogenetic analysis of *O*-methyltransferases expressed in *P. trichocarpa* and *P. balsamifera* lateral leaf buds. Maximum-likelihood phylogenetic tree of poplar *O*-methyltransferases expressed in both *P. trichocarpa* and *P. balsamifera* leaf buds. Poplar genes are indicated in black, and other previously functionally characterized *O*-methyltransferases are indicated in gray. Bootstrap support (1000) is shown as a percentage for each branch. Characterized genes have been annotated with their substrate specificity and possible regioselectivity. COMT, caffeic acid 3-*O*-methyltransferase. Candidate genes selected for protein expression and biochemical characterization are highlighted in red.

Table 3.1. Expression analysis of known phenylpropanoid and flavonoid genes and candidate OMTs identified by RNA-seq analysis of *P. trichocarpa* and *P. balsamifera* lateral leaf buds. Values display log2 fold change between the initial sampling (D0) and samples collected after four days (D4) of bud flush induction. Positive fold change indicates an increase in expression levels. Genes highlighted in red were selected for protein expression and biochemical characterization. Potri.013G136300 was designated PtDOMT1 based on subsequent biochemical analysis.

		P. trichocarpa		*P. balsamifera*	
Potri number	**Gene name**	Log2 Fold change	q-value	Log2 Fold change	q-value
Potri.006G126800	PAL1	1.55	7.5E-07	1.28	7.7E-02
Potri.016G091100	PAL3	2.08	6.7E-06	2.28	9.8E-03
Potri.014G145100	CHS1	1.29	1.6E-01	2.68	2.3E-03
Potri.001G051500	CHS2	2.49	1.5E-01	-	-
Potri.001G051600	CHS3	2.72	1.4E-01	0.30	8.0E-01
Potri.003G176900	CHS5	3.70	6.7E-07	0.69	4.3E-01
Potri.006G120000		-0.12	8.8E-01	-0.26	3.8E-01
Potri.001G451100		-1.37	6.2E-02	-0.69	4.0E-01
Potri.011G150500		0.59	7.6E-01	-2.29	9.3E-03
Potri.013G122400		**4.27**	**7.3E-27**	**2.23**	**6.6E-05**
Potri.013G136300	**PtDOMT1**	**8.46**	**1.5E-05**	**6.91**	**2.1E-05**
Potri.013G143800		7.09	8.8E-04	6.69	4.9E-06
Potri.014G106600		-0.86	3.8E-01	0.75	4.2E-01
Potri.016G101600		-0.76	7.2E-01	-2.15	2.1E-02
Potri.019G102900		**0.52**	**9.1E-01**	**-1.43**	**2.2E-01**

3.4.3 Biochemical characterization of candidate OMTs

To analyze the biochemical characteristics of the candidate genes, we expressed recombinant Potri.013G136300, Potri.019G102900, and Potri.013G122400 in electrocompetent *E. coli* using a N-terminal His-tagged protein expression vector. The recombinant proteins were purified by affinity chromatography using a Ni-NTA column. SDS-PAGE analysis of the purified product with Coomassie staining and Western blot confirmed the expected product sizes and the presence of the 6x-His-tag (Fig. 3.3, Supplemental Figure S3.4).

The OMT activities of the candidate genes were tested using SAM as the methyl donor (Supplemental Figure S3.5). Initially, we tested potential substrates with the candidate gene products using relevant dihydrochalcones as substrates. Of the three candidates, only Potri.013G136300 yielded products with any of the substrates tested (Fig. 3.4). Analysis of the reaction products indicated that Potri.013G136300 produced *O*-methylated products with several dihydrochalcone aglycones that have one or more unoccupied hydroxyl groups at either 4 (4-OH) or 4’ (4’-OH) positions. The highest relative activity was observed with 2’,4’,6’-OH DHC, which yielded 2’,6’-OH-4’-OMe DHC as the reaction product. Assays with 2’,4’,6’-OH-4-OMe DHC and 2’,6’,4-OH-4’-OMe DHC converted both substrates into 2’,6’-OH-4,4’-OMe DHC. Reaction with 2’,4’,6’,4-OH DHC yielded two primary *O*-methylated products, 2’,4’,6’-OH-4-OMe DHC and 2’,6’,4-OH-4’-OMe DHC, as well as a secondary product, 2’,6’-OH-4,4’-OMe DHC. The secondary product was likely a product of further *O*-methylation of 2’,6’,4-OH-4’-OMe DHC and 2’,4’,6’-OH-4-OMe DHC. Notably, reactions with 2’,6’-OH-4’-OMe and 2’,6’-OH-4,4’-OMe as substrates yielded no products.

We also tested 14 other phenolic substrates, including flavonoids and benzoic acid esters, which yielded no significant products when incubated with Potri.013G136300 (Supplemental Table S3.4). Based on the results, we concluded that Potri.013G136300 is a dihydrochalcone-specific OMT, which exhibits regioselectivity toward two possible sites for the *O*-methylation reaction. Therefore, we designated Potri.013G136300 as *P. trichocarpa* dihydrochalcone OMT 1 (PtDOMT1).

To obtain additional information into the biochemical properties of PtDOMT1, the reaction conditions, including pH, temperature, and incubation time, were optimized (Fig. 3.5). The optimal temperature for the enzyme reaction was observed at 30-35°C, followed by a steep decline at 40°C (Fig. 3.5a). The highest activity was observed at pH 7.5 (Fig. 3.5b). A linear range of the enzyme reaction was observed to be 10–25 min (Fig. 3.5c). Therefore, the optimized reaction conditions were 30°C, pH 7.5, and 20 min incubation time.

Using the optimized reaction conditions, we measured the Michaelis-Menten kinetic parameters of PtDOMT1 (Fig. 3.6). Of the tested substrates, 2',4',6'-OH DHC had the lowest K_m value (25.1 μM) and the highest turnover rate of the four tested dihydrochalcone substrates. Kinetic parameters for the two primary reaction products of 2',4',6',4-OH DHC were calculated separately. Of these two reaction products, 2',6',4-OH-4'-OMe DHC had the lower K_m value (31.0 μM) compared to 2',4',6'-OH-4-OMe DHC (64.0 μM). In the reactions using 2',6',4-OH-4'-OMe DHC and 2',4',6'-OH-4-OMe DHC as the reaction substrates, 2',4',6'-OH-4-OMe DHC achieved a lower K_m value (57.0 μM) compared to asebogenin (59.1 μM).

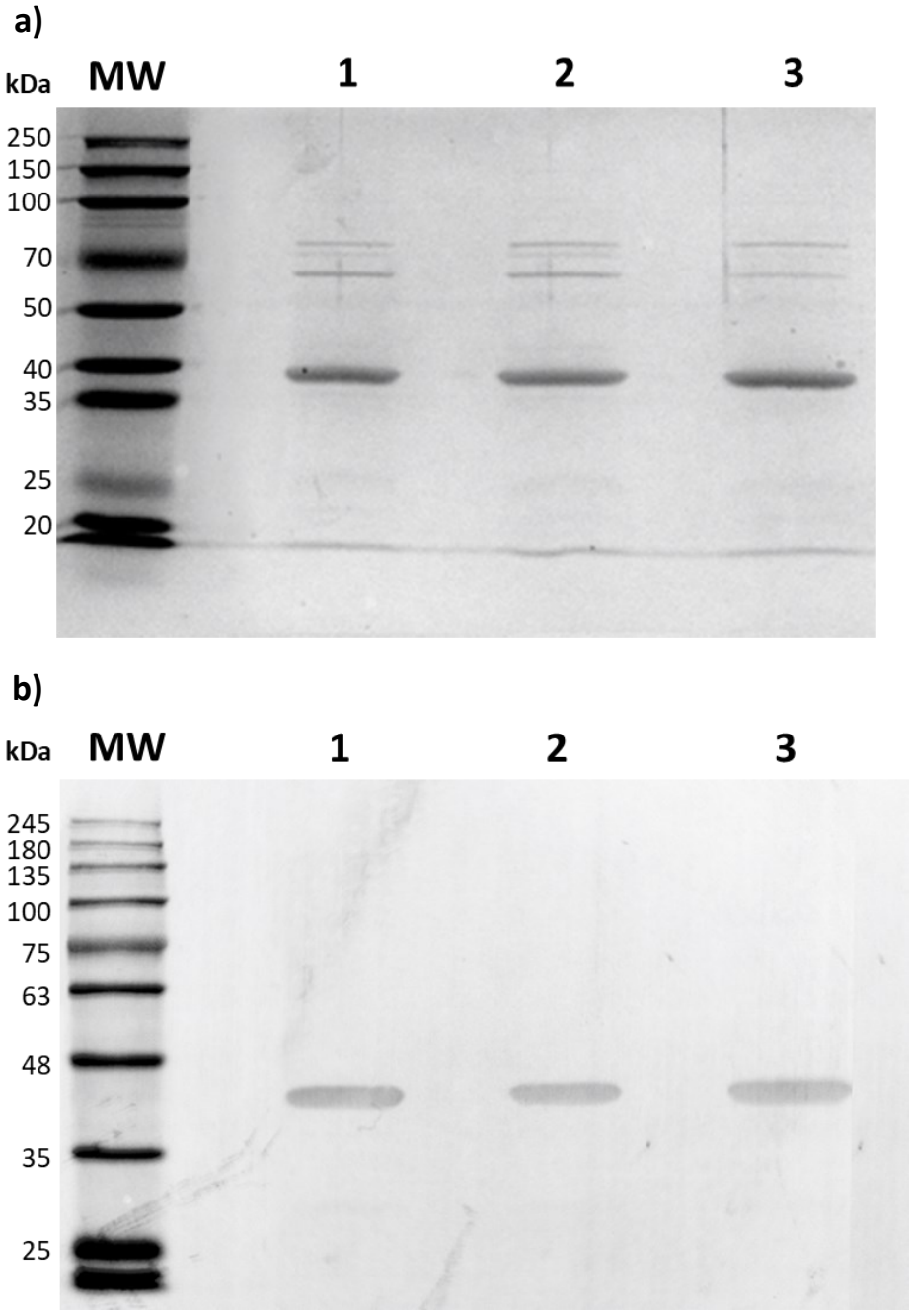

Figure 3.3. Analysis of the purified recombinant PtDOMT1. SDS-PAGE analysis of the purified recombinant proteins using a) Coomassie staining and b) Western blotting. Lanes 1-3 were loaded with individually purified protein preparations of recombinant Potri.013G136300 (39.6 kDa). The MW lane represents the molecular weight ladder.

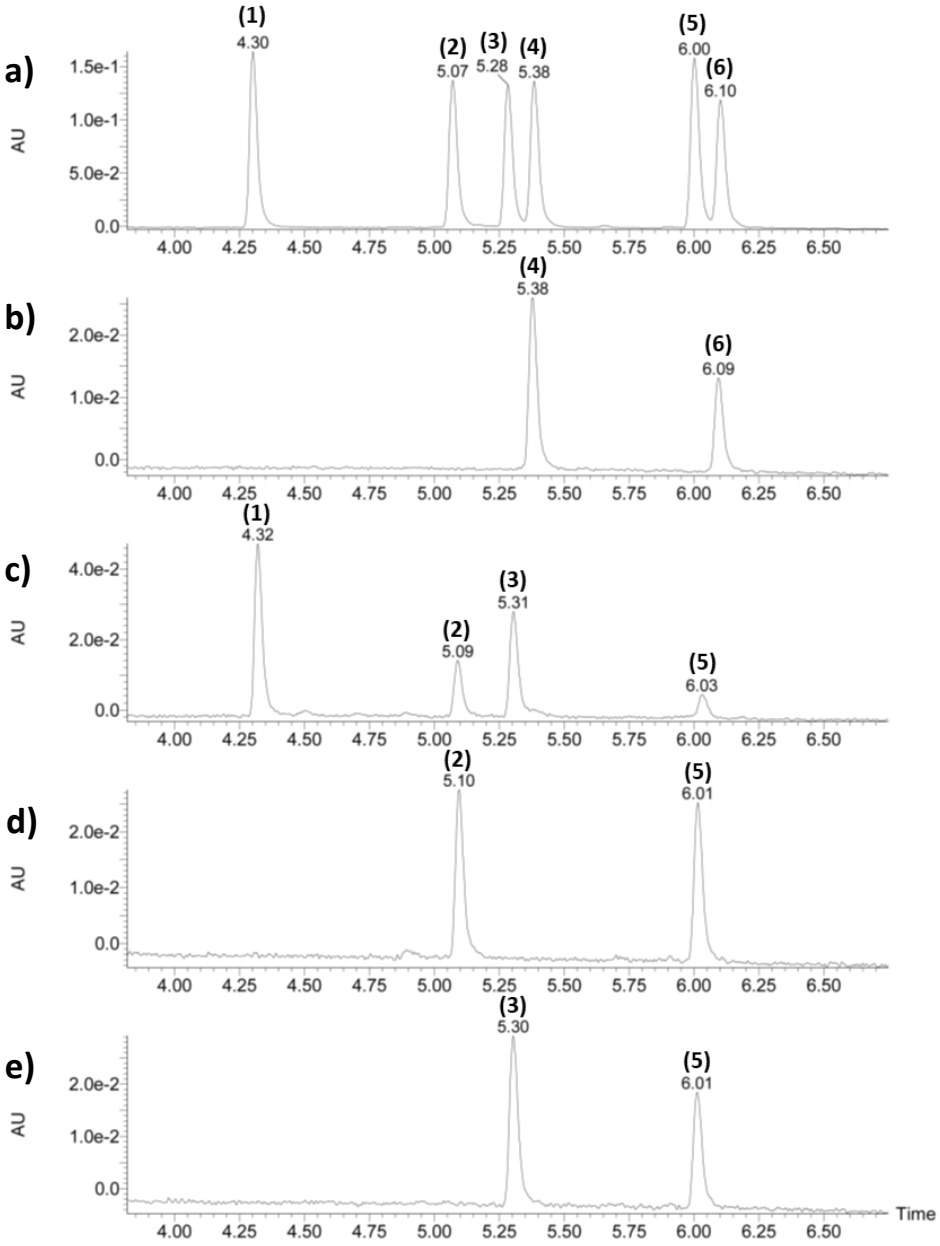

[1-6] Peaks identities in order of elution are (1) 2',4',6',4-OH DHC (phloretin), (2) 2',4',6'-OH DHC (2',4',6'-trihydroxydihydrochalcone), (3) 2',6',4-OH-4'-OMe DHC (asebogenin), (4) 2',4',6'-OH-4-OMe DHC (2',4',6'-trihydroxy-4-methoxydihydrochalcone), (5) 2',6'-OH-4,4'-OMe DHC (2',6'-dihydroxy-4',4-dimethoxydihydrochalcone), and (6) 2',6'-OH-4'-OMe DHC (2',6'-dihydroxy-4'-methoxydihydrochalcone).

Figure 3.4. Enzyme assays of PtDOMT1 with dihydrochalcone substrates. Enzyme assay products of PtDOMT1 with dihydrochalcones were analyzed using UPLC-DAD at 280 nm. Analysed samples included a) analytical standard mix containing the six tested dihydrochalcones (1-6), enzyme reaction with b) 2',4',6'-OH DHC (2',4',6'-trihydroxydihydrochalcone), c) 2',4',6',4-OH DHC (phloretin), d) 2',6',4-OH-4'-OMe DHC (asebogenin), and e) 2',4',6'-OH-4-OMe DHC (2',4',6'-trihydroxy-4-methoxydihydrochalcone).

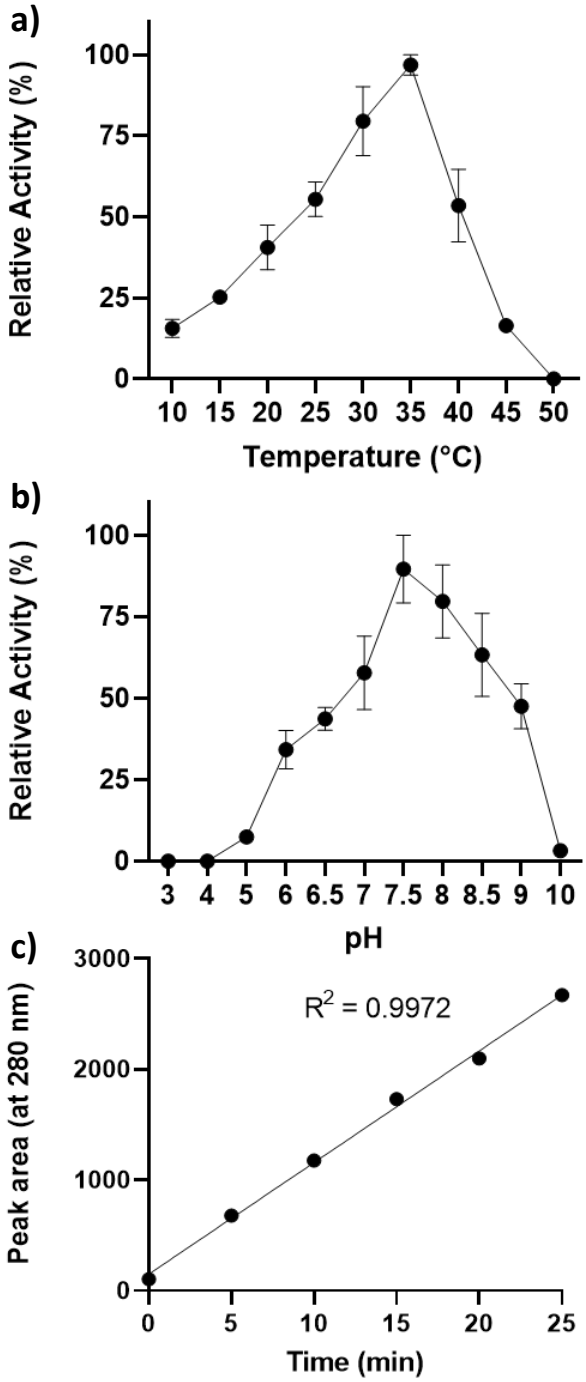

Figure 3.5. Determination of optimal enzyme reaction conditions for PtDOMT1. The optimal enzyme assay conditions for PtDOMT1 were determined by UPLC-DAD at 280 nm using 2',4',6'-OH DHC (2',4',6'-trihydroxydihydrochalcone) as a substrate. Optimized conditions included a) pH, b) temperature, and c) linearity of enzyme reaction over time. Relative activities were calculated based on the peak area of the reaction product. The data represent the means of independent PtDOMT1 recombinant protein preparations (n = 3), and error bars represent ±SE.

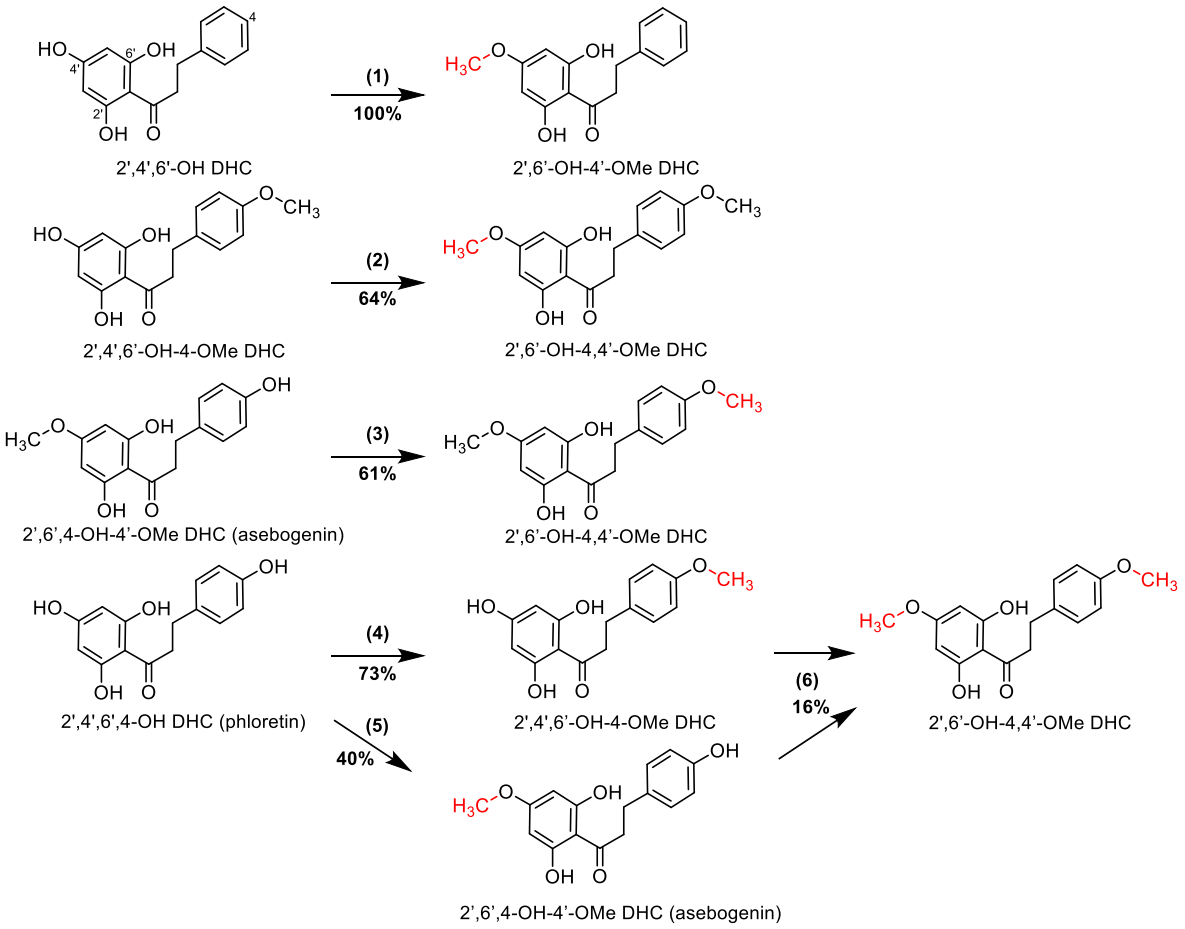

Substrate[1]	Reaction	Product[2]	Relative activity	K_m (µM)	V_{max} (pkat mg^{-1})	V_{max}/K_m
2',4',6'-OH DHC	**(1)**	2',6'-OH-4'-OMe DHC	100 %	25.1 ± 2.1	11.7 ± 0.4	0.47
2',4',6'-OH-4-OMe DHC	**(2)**	2',6'-OH-4,4'-OMe DHC	64 %	57.0 ± 3.4	7.6 ± 0.2	0.13
2',6',4-OH-4'-OMe DHC	**(3)**	2',6'-OH-4,4'-OMe DHC	61 %	59.1 ± 4.1	7.7 ± 0.3	0.13
2',4',6',4-OH DHC	**(4)**	2',4',6'-OH-4-OMe DHC	73 %	64.0 ± 3.3	9.8 ± 0.2	0.15
	(5)	2',6',4-OH-4'-OMe DHC	40 %	31.0 ± 1.4	5.2 ± 0.2	0.17
	(6)	2',6'-OH-4,4'-OMe DHC	16 %	-	-	-

[1,2] 2',4',6'-OH DHC (2',4',6'-trihydroxydihydrochalcone), 2',6'-OH-4'-OMe DHC (2',6'-dihydroxy-4'-methoxydihydrochalcone), 2',4',6'-OH-4-OMe DHC (2',4',6'-trihydroxy-4-methoxydihydrochalcone), 2',6',4-OH-4'-OMe DHC (asebogenin), 2',4',6',4-OH DHC (phloretin), and 2',6'-OH-4,4'-OMe DHC (2',6'-dihydroxy-4',4-dimethoxydihydrochalcone).

Figure 3.6. Relative activity and Michaelis-Menten kinetic parameters for PtDOMT1 with different dihydrochalcone substrates. The top panel shows reactions carried out by PtDOMT1 and the relative activity under standard conditions. Enzyme reaction with phloretin yielded two primary products, 2',4',6'-OH-4-OMe DHC and asebogenin, and a secondary product, 2',6'-OH-4,4'-OMe DHC. Michaelis-Menten kinetic parameters were computed using nonlinear regression analysis based on the concentration of enzyme reaction products under standard conditions, as described in materials and methods. Kinetic parameters of phloretin are indicated separately for these primary products. The data represent the means (±SE) of independent PtDOMT1 recombinant protein preparations (n = 3).

3.4.4. Expression analysis of PtDOMT1 in *P. trichocarpa* lateral leaf buds

We analyzed the expression of PtDOMT1 in *P. trichocarpa* leaf buds harvested monthly over one year (Fig. 3.7a). Relative PtDOMT1 transcript levels were analyzed using RT-qPCR. PtDOMT1 displayed an increasing trend in relative expression in the whole leaf buds from June to August, followed by a drastic drop in September. PtDOMT1 did not show significant expression in dormant leaf buds between October and May.

Additionally, we analyzed PtDOMT1 expression by RT-qPCR separately in bud scales and embryonic leaves in the lateral leaf buds collected in April (Fig. 3.7b) and August (Fig. 3.7c). Corresponding to the analysis of the whole buds, the expression of PtDOMT1 was significantly higher in August samples compared to April. PtDOMT1 was expressed in both tissue types. However, the transcript levels of PtDOMT1 were almost two-fold higher in the leaf bud scales compared to inner embryonic leaves in April and similarly nearly six-fold higher in August samples.

From these results, we concluded that the biosynthesis of *O*-methylated dihydrochalcones in poplar leaf buds occurs largely in the summer. This biosynthetic process of modifying dihydrochalcones is primarily localized in the leaf bud scales, though the embryonic leaves also possess this capacity.

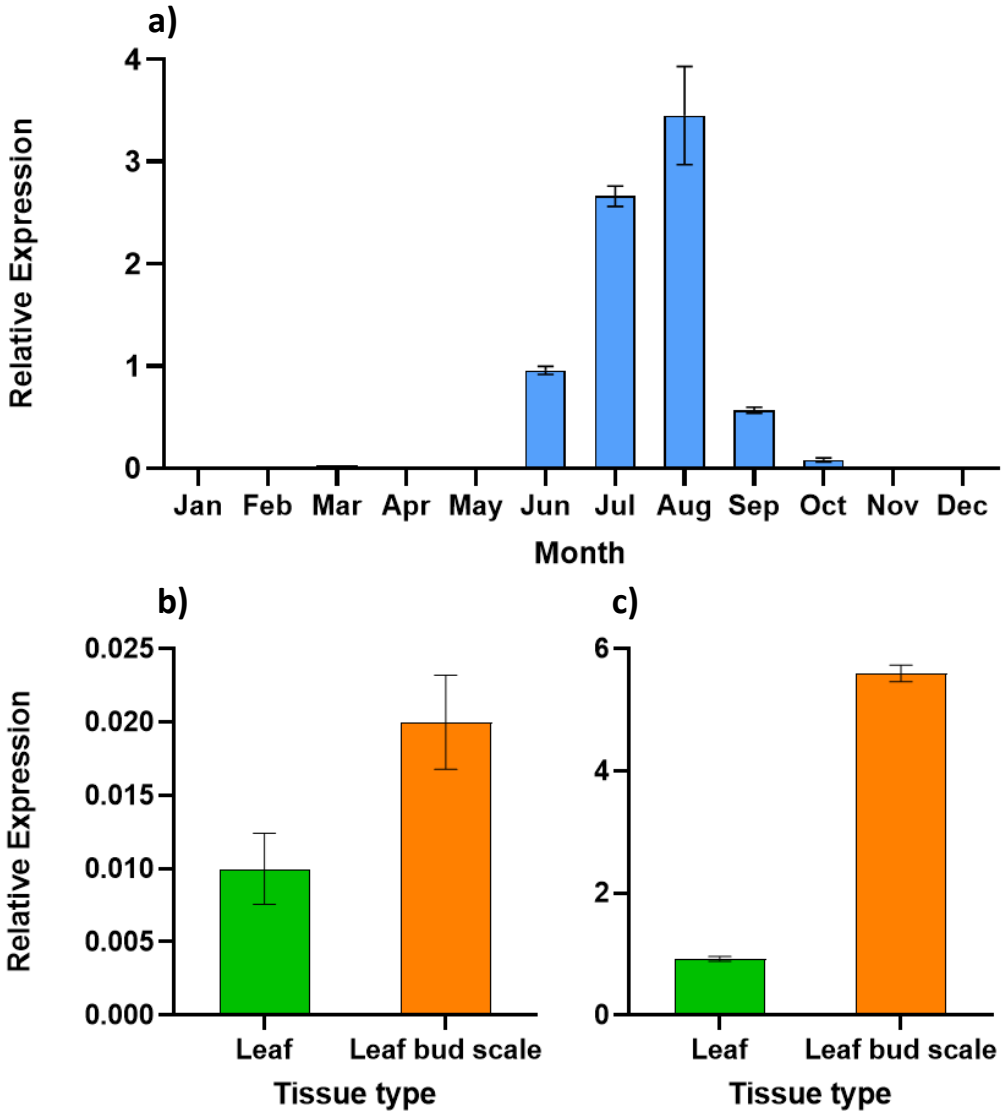

Figure 3.7. Expression of PtDOMT1 in *P. trichocarpa* lateral leaf buds across seasons and different bud tissues. The expression of PtDOMT1 was analyzed using RT-qPCR, as described in materials and methods. The relative expression was measured in a) whole leaf buds over the annual dormancy-growth cycle. Leaf bud scales and embryonic leaves were collected in b) April and c) August. The data represent the means ±SE (n = 3).

3.5. Discussion

Chemical analysis of *P. trichocarpa* and *P. balsamifera* confirmed the presence of dihydrochalcones, and specifically, the abundance of *O*-methylated dihydrochalcones, which account for the majority of the dihydrochalcones in both studied species. Our analysis aligns with previous GC-MS studies of *P. trichocarpa* and *P. balsamifera* bud exudates (Greenaway et al., 1992a; English et al., 1991) despite the fundamental methodological differences in the utilized analytical methods. Dihydrochalcones were found to accumulate in the embryonic leaves in higher concentrations compared to the leaf bud scales.

Biochemical characterization of PtDOMT1 demonstrated its substrate-specificity towards dihydrochalcones and its regioselectivity. Gene expression analysis of PtDOMT1 identified its primary localization in the leaf bud scales and demonstrated its seasonal expression patterns over the annual growth-dormancy cycle.

3.5.1. PtDOMT1 is a regioselective dihydrochalcone OMT in *P. trichocarpa* and *P. balsamifera* lateral leaf buds

A phylogenetic analysis of PtDOMT1 indicated it was located in a distinct cluster with an HlOMT2 previously characterized in hop (*Humulus lupulus*). HlOMT2 induces *O*-methylation of a chalcone as a substrate (Nagel et al., 2008). This result suggested substrate specificity of PtDOMT1 outside of the general flavonoids. The biochemical characterization of PtDOMT1 demonstrated its specific affinity towards dihydrochalcones but not to any tested flavonoids, chalcones, and phenolic glycosides. PtDOMT1 was regioselective and capable of methylating two different positions of dihydrochalcones. Analysis of the relative activity of PtDOMT1 indicated that in a non-competitive reaction, PtDOMT1 has a higher affinity towards the available 4’-OH position present in 2’,4’,6’-OH DHC and 2’,4’,6’-OH-4-OMe DHC. Comparison of the kinetic parameters of 2’,4’,6’-OH DHC, 2’,4’,6’-OH-4-OMe DHC, and 2’,6’,4-OH-4’-OMe DHC verified the same order of affinity indicated by the analysis of relative activity. However, the formation of the two primary products and a secondary product with 2’,4’,6’,4-OH DHC substrate implies that the secondary enzyme reaction with the intermediate

products is competitive. In a competitive scenario, the enzyme reaction was more prone to induce *O*-methylation in the 4-OH position using 2',6',4-OH-4'-OMe DHC as an intermediate substrate. In an assay where enzyme reaction was incubated for 24 h using 2',4',6',4-OH DHC substrate, both primary products were ultimately converted into 2',6'-OH-4,4'-OMe DHC (data not shown). These activities demonstrated that PtDOMT1 is involved in the synthesis of all *O*-methylated dihydrochalcones detected in *P. trichocarpa* and *P. balsamifera*, indicating its key role in the biosynthesis of leaf bud resin.

Regioselective OMTs with a similar capability to produce two subsequent methoxylations in different positions of aromatic rings of flavonoid structures have been previously reported in *Ocimum basilicum* (Berim et al., 2012). For example, ObFOMT3, ObFOMT4, ObFOMT5, and ObFOMT6 have been shown to carry out 6- and 4'-*O*-methylations of flavones. While these OMTs can act on both positions, they display a higher affinity towards one of them. Subtle changes in specific amino acid residues determine this regioselectivity (Berim et al., 2012). Consequently, the relative activity toward the subsequent substrate is reduced after the initial reaction where the preferred position is occupied. PtDOMT1 displayed similar behaviour with the phloretin substrate after the initial methoxylation. Identification of the amino acid residues involved in defining the regioselectivity of PtDOMT1 could enable the identification or design of proteins with specific regioselectivity towards dihydrochalcones.

3.5.2. Expression PtDOMT1 displays seasonal and tissue-specific patterns

The dormancy-growth cycle in poplar leaf buds is regulated by environmental signals, such as temperature and photoperiod (Conde et al., 2017; Ruttink et al., 2007; Rohde et al., 2007). In our experiment, the expression pattern analysis of general phenylpropanoid and flavonoid-related genes demonstrated a temporary increase in their expression in response to breaking dormancy in leaf buds during induced bud break in the growth chamber. PtDOMT1 displayed a similar initial increase. However, the expression level of PtDOMT1 remained elevated for a longer time than the compared PAL and CHS genes in *P. trichocarpa*, indicating that the phenylpropanoid pathway does not directly regulate PtDOMT1. Interestingly, in *P.*

balsamifera, the expression of PtDOMT1 diminished after ten days, following the pattern displayed by the marker genes.

Analysis of PtDOMT1 gene expression in *P. trichocarpa* leaf buds collected over one year of the growth-dormancy cycle confirmed that PtDOMT1 was subject to seasonal patterns. However, the qPCR analysis of outdoor samples did not display a similar increase in the expression levels of PtDOMT1 during the bud break, in contrast with the growth chamber samples, which exhibited an increase in gene expression as the buds were released from dormancy. This major difference in the gene expression pattern could result from the differences in the photoperiod between the growth chamber and outdoor, as well as temperature. Expression of PtDOMT1 was highest in developing leaf buds in summer, and the expression levels fell drastically toward the fall and induction of dormancy of the leaf buds. Given the impact of temperature observed on the relative activity of recombinant PtDOMT1, lowering temperatures in the fall may impact its expression during dormancy, as indicated by the lowering of PtDOMT1 expression in September and October. The shortening of photoperiod in fall and winter has previously been shown to affect bud development (Rohde et al., 2002), which could be the leading reason why PtDOMT1 displayed very low expression during the winter and early spring. The timing of the increase in the expression of PtDOMT1 in the leaf buds from June to August aligns with the development of newly formed leaf buds, increasing with the age of the leaf buds. These two trends are seemingly related to the development of the leaf buds and could indicate that the regulation of PtDOMT1 could be related to the leaf bud development.

A comparison of the abundance of dihydrochalcones on *P. trichocarpa* inner leaves and leaf bud scales indicated that dihydrochalcones are present in both tissue types. This localization may support the previous observations by Curtis and Lersten (1974), who described resin synthesis both in leaf bud scales and glandular trichomes of young leaves in *P. deltoides*. However, the relative expression of PtDOMT1 was much higher in leaf bud scales than in the inner embryonic leaves, which suggests that the methoxylation of dihydrochalcones likely occurs primarily in the secretory epidermis on the leaf bud scales. This is supported by the relative expression of PtDOMT1 being much higher in August, when the embryonic leaves are much smaller, compared to April when the leaves are flushing. Based on chemical analysis, however, the resin accumulates on the inner leaves at higher concentrations than the leaf bud scales. This

suggests that while the resin fills the inner space of the leaf buds, the resin is secreted from the bud scales onto the embryonic leaves. This supports the postulated function of leaf bud resin as the primary protection of embryonic leaf tissues (Curtis and Lersten, 1974). The seasonality of the synthesis of methoxylated dihydrochalcones suggests that the leaf bud resin is produced during the active growth and development of leaf buds, specifically the bud scales.

3.6 Conclusions

In summary, our work demonstrated the identification of a novel *O*-methyltransferase in *P. trichocarpa* and *P. balsamifera.* PtDOMT1 induces *O*-methylation of 4-OH and 4'-OH sites as a part of the downstream of dihydrochalcone and leaf bud resin biosynthesis. This is the first study to demonstrate the biochemical and kinetic characterization of a poplar leaf bud resin biosynthesis-related gene. Our results show that PtDOMT1 has narrow substrate-specificity, playing a crucial role in the *O*-methylation of dihydrochalcone aglycones found in poplar leaf bud resin. We also demonstrated the gene expression of PtDOMT1 in poplar leaf buds is subject to seasonal patterns. Expression of PtDOMT1 and, by extension, synthesis of leaf bud resin, may be regulated by bud development or environmental factors, such as temperature or photoperiod.

Identification of PtDOMT1 establishes the first characterized step in elucidating the biochemical pathways of poplar leaf bud resin synthesis. PtDOMT1 can be used as a marker gene for further investigation and identification of specific genes related to leaf bud resin synthesis. One such gene of interest includes double bond reductase (DBR) involved in the reduction of *p*-courmaroyl-CoA into *p*-dihydrocourmaroyl-CoA, which acts as an up-stream branching-off point for the formation of dihydrochalcones from the general phenylpropanoid pathway (Ibdah et al., 2014). Furthermore, PtDOMT1 expression analysis in poplars grown in different conditions can identify how the accumulation of leaf bud resin synthesis responds to and is impacted by biotic stress, such as insect herbivory, or abiotic stress, such as increasing temperature due to climate change.

3.7 Acknowledgments

We thank Dr. Anna Berim for providing *Ocimum basilicum* flavonoid *O*-methyltransferase plasmids and support with enzyme assays. Dr. Raju Soolanayakanahally and Chris Stefner for providing *P. balsamifera* cuttings. Brad Binges for the upkeep and maintenance of the greenhouse and research compound facilities. Dr. Ori Granot for the maintenance of the UPLC-MS system, and Dr. Dawei Ma for preparing RNA-seq libraries. Work in the Constabel laboratory is supported by the Natural Sciences and Engineering Research Council of Canada (NSERC).

3.8 Supplemental information

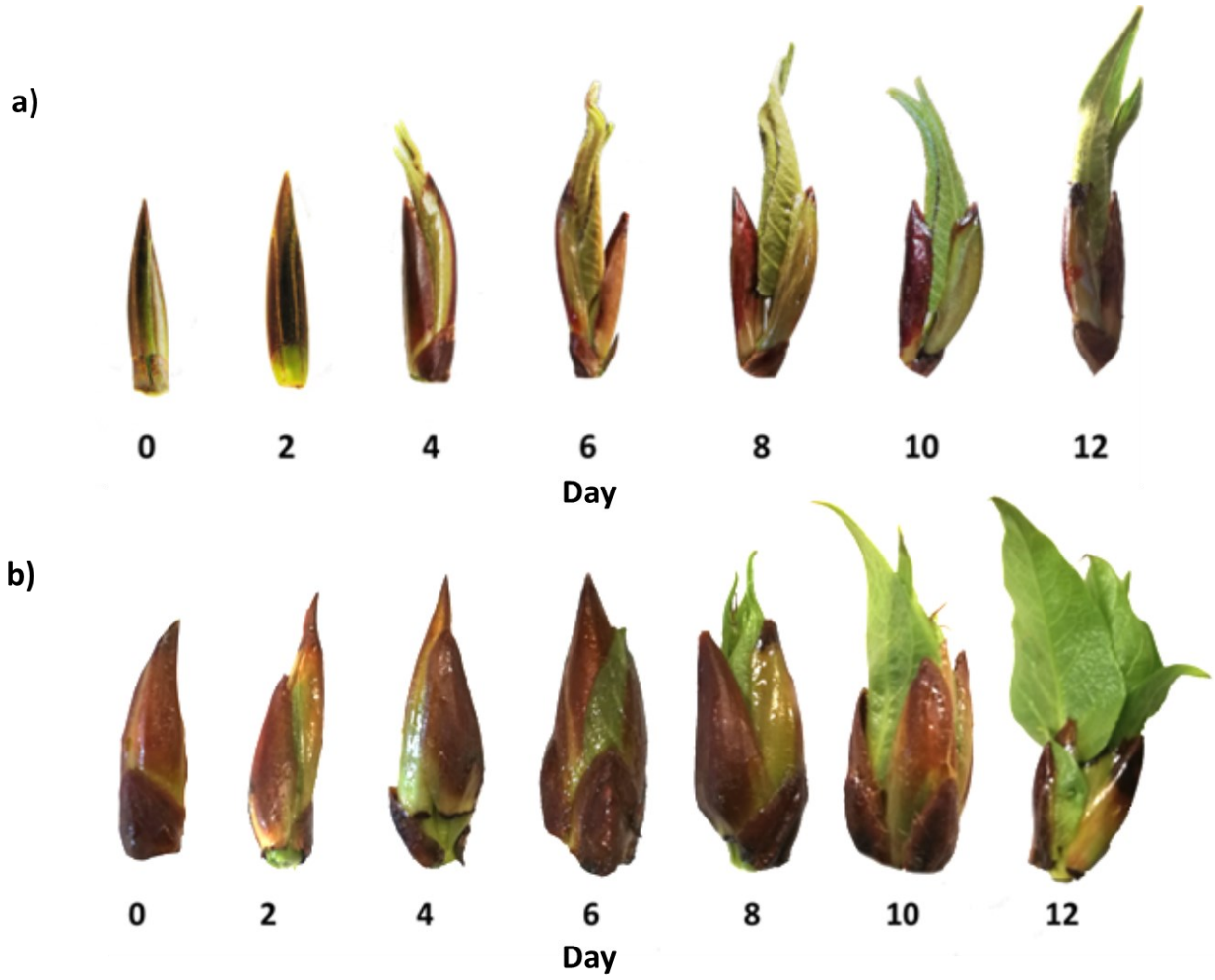

Supplemental Figure S3.1. Time series of *P. trichocarpa* and *P. balsamifera* lateral leaf buds. Lateral leaf buds of days a) *P. trichocarpa* and b) *P. balsamifera* were induced to flush in a growth chamber over a total of 12 days. Leaf buds were collected every other day. The presented leaf buds are collected from individual cuttings at each time point.

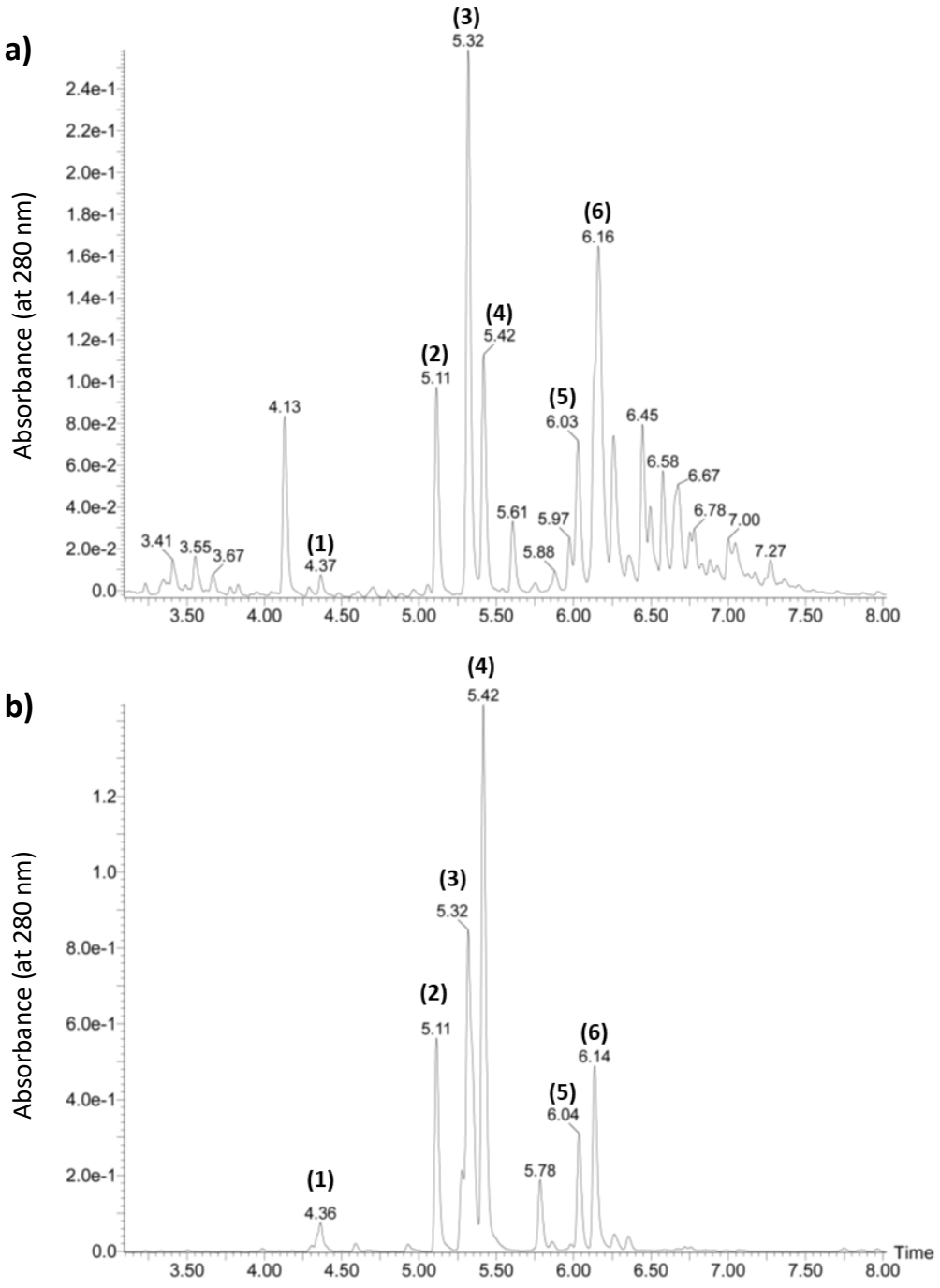

Supplemental Figure S3.2. UPLC-DAD analysis of *P. trichocarpa* and *P. balsamifera*. UV-chromatograms of methanolic extracts of a) *P. trichocarpa* and b) *P. balsamifera* lateral leaf buds. Leaf buds were induced to flush for four days in a growth chamber and analyzed by UPLC-DAD at 280 nm. Identified peaks are as follows: (1) 2',4',6',4-OH DHC (phloretin), (2) 2',4',6'-OH DHC (2',4',6'-trihydroxydihydrochalcone), (3) 2',6',4-OH-4'-OMe DHC (asebogenin), (4) 2',4',6'-OH-4-OMe DHC (2',4',6'-trihydroxy-4-methoxydihydrochalcone), (5) 2',6'-OH-4,4'-OMe DHC (2',6'-dihydroxy-4',4-dimethoxydihydrochalcone), and (6) 2',6'-OH-4'-OMe DHC (2',6'-dihydroxy-4'-methoxydihydrochalcone).

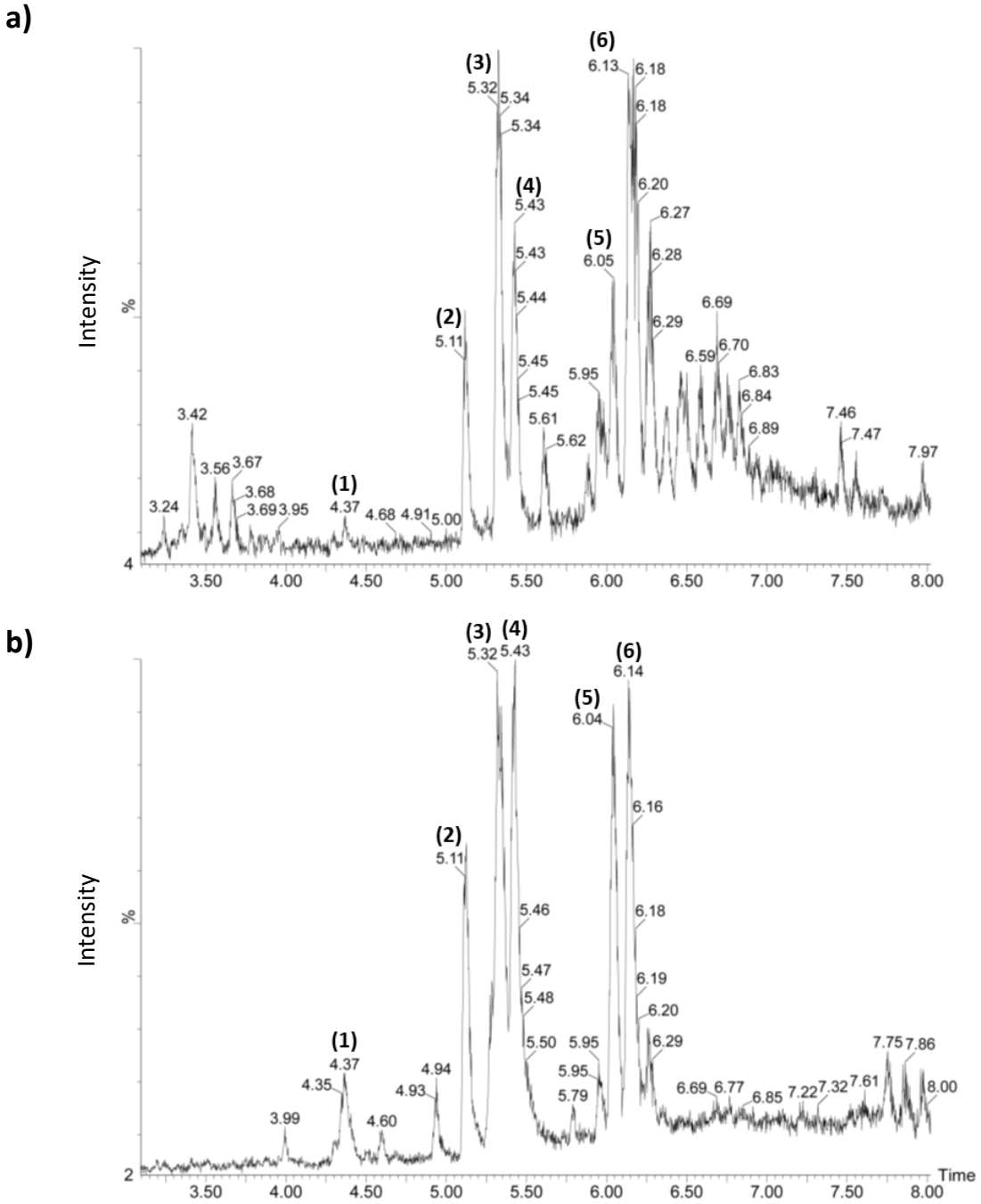

Supplemental Figure S3.3. UPLC-MS analysis of *P. trichocarpa* and *P. balsamifera* leaf buds. Total ion chromatograms of methanolic extracts of a) *P. trichocarpa* and b) *P. balsamifera* lateral leaf buds. Leaf buds were induced to flush for four days in a growth chamber and analyzed by UPLC-MS. Identified peaks are as follows: (1) 2',4',6',4-OH DHC (phloretin), (2) 2',4',6'-OH DHC (2',4',6'-trihydroxydihydrochalcone), (3) 2',6',4-OH-4'-OMe DHC (asebogenin), (4) 2',4',6'-OH-4-OMe DHC (2',4',6'-trihydroxy-4-methoxydihydrochalcone), (5) 2',6'-OH-4,4'-OMe DHC (2',6'-dihydroxy-4',4-dimethoxydihydrochalcone), and (6) 2',6'-OH-4'-OMe DHC (2',6'-dihydroxy-4'-methoxydihydrochalcone).

Supplemental Table S3.1. *O*-methyltransferases expressed in the lateral leaf buds of *P. trichocarpa* and *P. balsamifera*. Putative *O*-methyltransferases were identified in an RNA-sequencing data set based on gene annotations of *P. trichocarpa* genome (v4.1).

Potri number	Gene name	*P. trichocarpa*	*P. balsamifera*
Potri.004G050400		x	
Potri.004G050500		x	
Potri.009G139700		x	
Potri.011G059500		x	
Potri.011G059600		x	
Potri.012G006400		x	
Potri.013G120800		x	
Potri.013G121300		x	
Potri.013G121400		x	
Potri.013G122000		x	
Potri.014G106500		x	
Potri.015G003100		x	
Potri.019G093100		x	
Potri.019G102900		x	x
Potri.001G451100		x	x
Potri.006G120000		x	x
Potri.011G150500		x	x
Potri.013G122400		x	x
Potri.013G136300	PtDOMT1	x	x
Potri.013G143800		x	x
Potri.014G106600		x	x
Potri.016G101600		x	x
Potri.002G076766			x
Potri.002G180600			x
Potri.002G180700			x
Potri.002G183600			x
Potri.008G136600			x
Potri.009G139800			x
Potri.013G017210			x
Potri.013G121800			x
Potri.013G121900			x
Potri.013G122100			x
Potri.014G098800			x
Potri.018G070300			x
Potri.019G093000			x
Potri.019G093200			x

Supplemental Table S3.2. Expression analysis of known flavonoid genes and candidate OMTs identified by RNA-seq analysis of *P. trichocarpa* and *P. balsamifera* lateral leaf buds. Values display log2 Fold change between the initial sampling (D0) and samples collected after ten days (D10) of bud flush induction. Positive fold change indicates an increase in expression levels. Bolded genes were selected for protein expression and biochemical characterization. Potri.013G136300 was designated PtDOMT1 based on subsequent biochemical analysis.

		P. trichocarpa		*P. balsamifera*	
Potri number	**Gene name**	Log2 Fold change	q-value	Log2 Fold change	q-value
Potri.006G126800	PAL1	1.34	9.1E-06	-0.45	6.1E-01
Potri.016G091100	PAL3	2.51	3.3E-09	-0.82	4.4E-01
Potri.014G145100	CHS1	-0.29	7.3E-01	-0.49	6.7E-01
Potri.001G051500	CHS2	0.19	9.1E-01	-	-
Potri.001G051600	CHS3	1.46	3.3E-01	-1.39	1.7E-01
Potri.003G176900	CHS5	1.48	6.1E-02	-1.73	3.3E-02
Potri.006G120000		0.10	7.8E-01	-0.36	2.1E-01
Potri.001G451100		-3.55	1.7E-11	-0.27	7.9E-01
Potri.011G150500		1.35	1.0E-01	-1.11	2.7E-01
Potri.013G122400		**5.46**	**5.0E-45**	**0.36**	**3.5E-01**
Potri.013G136300	**PtDOMT1**	**4.81**	**1.6E-02**	**0.11**	**9.7E-01**
Potri.013G143800		3.97	6.3E-02	-2.16	3.8E-01
Potri.014G106600		-3.21	1.1E-09	2.00	2.0E-02
Potri.016G101600		-4.37	8.0E-02	-0.79	4.7E-01
Potri.019G102900		**1.32**	**3.8E-01**	**0.88**	**5.2E-01**

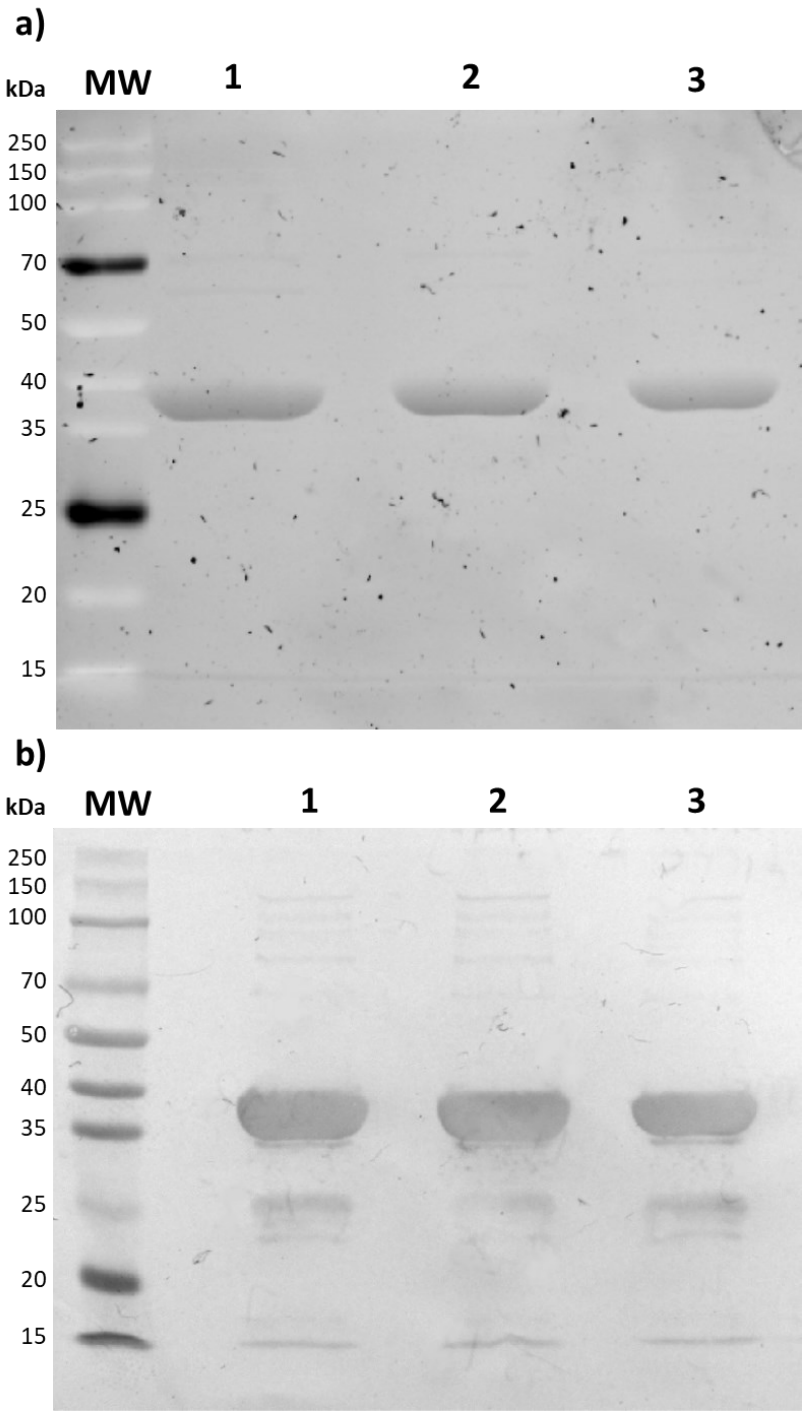

Supplemental Figure S3.4. Analysis of purified recombinant proteins. SDS-PAGE analysis of purified recombinant proteins by a) Coomassie staining and b) Western blotting. Lanes 1-3 were loaded with purified protein preparations of recombinant Potri.013G136300 (39.61 kDa), Potri.019G102900 (38.68 kDa), and Potri.013G122400 (40.49 kDa), respectively. MW represents the molecular weight ladder.

Supplemental Table S3.3. qPCR primer list. Forward and reverse primers were used for the expression analysis of PtDOMT1. Actin and UBQ10 were used as housekeeping genes for the qPCR analysis. Tm indicates melting temperature.

Gene	Potri number	Forward	Reverse	Tm	Amplicon (bp)
PtDOMT1	Potri.013G136300	ATGTTGTAGCAACAGCACCA	TCATCGGTCCAATCATGCAA	58	121
Actin	Potri.001G309500	CCCATTGAGCACGGTATTGT	TACGACCACTGGCATACAGG	56	235
UBQ10	Potri.014G115100	ACCAAGCCCAAGAAGATCAAGCA	CCAGCACCGCACTCAGCA	64	131

Supplemental Table S3.4. Relative activity of PtDOMT1 with different phenolic substrates. Relative activities of PtDOMT1 with different phenolic substrates tested using standard reaction conditions described in materials and methods. Relative activities were calculated based on the concentration of enzyme reaction products measured on UPLC-DAD at 280 nm. Indicated abbreviations are as follows; 2’,4’,6’-OH DHC (2’,4’,6’-trihydroxydihydrochalcone), 2’,6’-OH-4’-OMe DHC (2’,6’-dihydroxy-4’-methoxydihydrochalcone), 2’,4’,6’-OH-4-OMe DHC (2’,4’,6’-trihydroxy-4-methoxydihydrochalcone), 2’,6’,4-OH-4’-OMe DHC (asebogenin), 2’,4’,6’,4-OH DHC (phloretin), and 2’,6’-OH-4,4’-OMe DHC (2’,6’-dihydroxy-4’,4-dimethoxydihydrochalcone).

Substrate	Product	Relative activity
2',4',6’-OH DHC	2',6’-OH-4’-OMe DHC	100 %
2',4’,6’,4-OH DHC *	2',4',6’-OH-4-OMe DHC	73 %
2',4’,6’,4-OH DHC *	2’,6’,4-OH-4’-OMe DHC	40 %
2',4’,6’,4-OH DHC *	2',6’-OH-4,4’-OMe DHC	16 %
2',4',6’-OH-4-OMe DHC	2',6’-OH-4,4’-OMe DHC	64 %
2’,6’,4-OH-4’-OMe DHC	2',6’-OH-4,4’-OMe DHC	61 %
2',6’-OH-4’-OMe DHC	-	-
2',6’-OH-4,4’-OMe DHC	-	-
Naringenin chalcone	Unknown	Trace
Pinocembrin chalcone	-	-
Galangin	Unknown	Trace
Chrysin	-	-
Pinobanksin	-	-
Pinocembrin	-	-
Apigenin	-	-
Kaempferol	-	-
Catechin	-	-
Benzyl 2,5-dihydroxybenzoate	-	-
3-hydroxybenzyl benzoate	-	-
2,5-dihydroxybenzyl benzoate	-	-
2,6-dihydroxybenzyl benzoate	-	-
Salicyl gentisate	-	-

* Enzyme reaction with 2’,4’,6’,4-OH DHC yielded two primary products, 2’,4’,6’-OH-4-OMe DHC and 2’,6’,4-OH-4’-OMe DHC, and a secondary product, 2’,6’-OH-4,4’-OMe DHC. The relative activity of 2’,4’,6’,4-OH DHC is indicated separately for these products. Relative activities were calculated based on the concentration of enzyme reaction products.

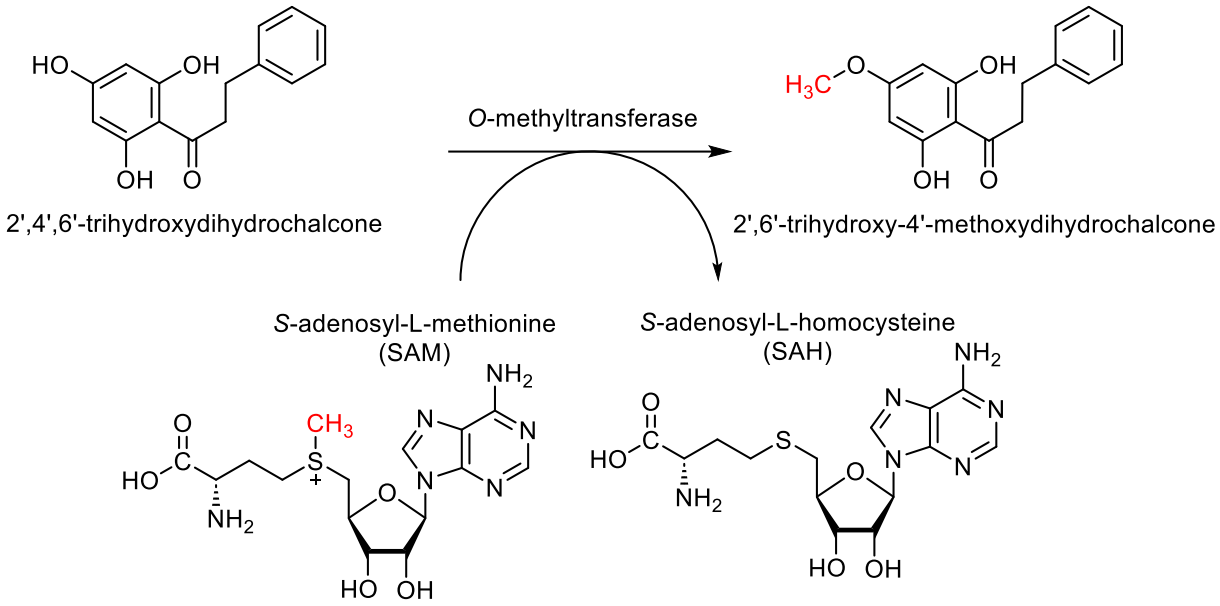

Supplemental Figure S3.5. The general reaction of S-adenosyl-*L*-methionine with a dihydrochalcone substrate. S-adenosyl-*L*-methionine was used as the methyl donor for the enzyme reactions with dihydrochalcones, yielding methoxylated dihydrochalcones.

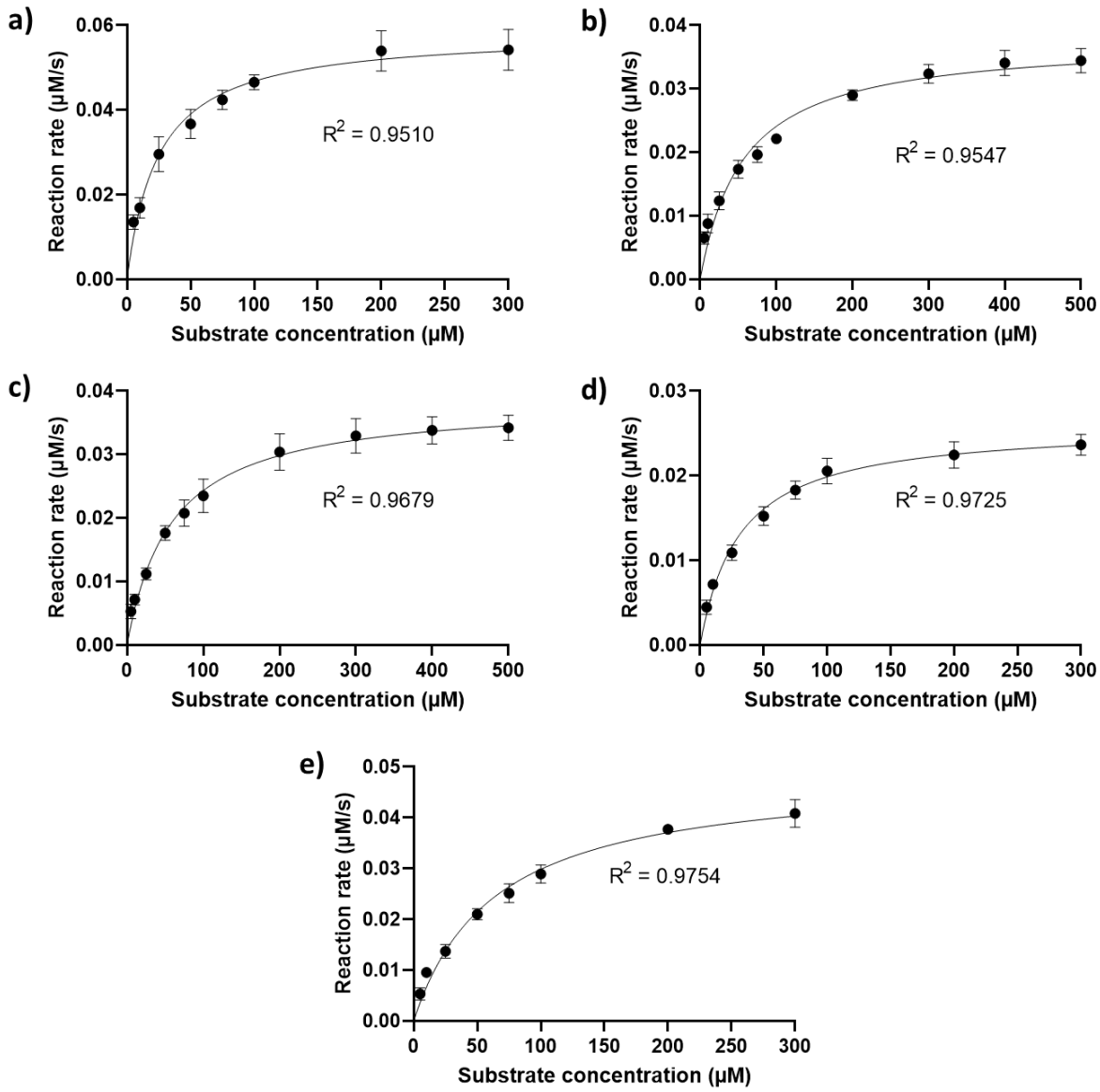

Supplemental Figure S3.6. Kinetic curves of PtDOMT1 reaction with dihydrochalcone substrates. Reactions depicted as follows: a) 2',4',6'-OH DHC (2',4',6'-trihydroxydihydrochalcone), b) 2',4',6'-OH-4-OMe DHC (2',4',6'-trihydroxy-4-methoxydihydrochalcone), c) 2',6',4-OH-4'-OMe DHC (asebogenin), d) 2',4',6',4-OH DHC (phloretin) to 2',6',4-OH-4'-OMe DHC, and e) 2',4',6',4-OH DHC to 2',4',6'-OH-4-OMe DHC. These data were used for nonlinear regression analysis to determine Michaelis-Menten kinetic parameters for each substrate. The data represent the means (±SE) of independent PtDOMT1 recombinant protein preparations (n = 3).

Chapter 4 – A novel poplar BAHD-type acyltransferase synthesizes acylated dihydroflavonols found in bud resin of *P. deltoides*

4.1 Abstract

Poplar trees produce flavonoid-rich bud resin to protect their developing buds from abiotic stress and herbivory. Studies of *Populus deltoides* leaf bud resin have identified dihydroflavonols and corresponding acylated dihydroflavonols as some of the characteristic bioactive resin components associated with antimicrobial effects, which could be important for honey bees (*Apis mellifera*). To date, the enzymes responsible for the acylation of flavonoid aglycones have not been elucidated in any plant species. This research aimed to identify candidate genes encoding BAHD-type acyltransferases that can catalyze *O*-acylation on dihydroflavonols. Using transcriptomics, differential gene expression analysis, and enzymatic assays, we identified PdDAT1, a BAHD-type acyltransferase with the capacity to acylate pinobanksin using acetyl-CoA, butyryl-CoA, and propionyl-CoA as acyl donors. This activity defines the final step in the synthesis of acylated dihydroflavonols and represents the first characterized step of bud resin biosynthesis in *Populus deltoides*.

4.2 Introduction

Poplar trees have evolved diverse defence mechanisms against external and internal sources of stress. They produce a wide range of specialized metabolites, including condensed tannins, hydroxycinnamate esters, and salicinoids as defence compounds in response to biotic and abiotic stress (Tsai et al., 2006; Philippe and Bohlmann, 2007; Constabel and Lindroth, 2010). In addition, many poplars produce flavonoid-rich bud resins. These resins prevent dehydration and freezing of the leaf buds during overwintering dormancy and protect young leaves from insect herbivory (Curtis and Lersten, 1974). Based on microscopic analysis of *P. deltoides*, the synthesis of poplar bud resin is believed to occur in bud scales of developing leaf buds (Curtis and Lersten, 1974). However, the localization of bud resin biosynthesis has not been analyzed using molecular methods.

The chemical composition of poplar bud resin varies significantly among *Populus* species, and distinct resin components are characteristic of different poplar species (English et al., 1992, 1991; Greenaway et al., 1991). The *Aigeiros* family of poplars, which includes eastern cottonwood (*P. deltoides*), western cottonwood (*P. fremontii*), and black poplar (*P. nigra*), produce resins with characteristic *O*-acylated dihydroflavonols such as pinobanksin-3-acetate, pinobanksin-3-propanoate, and pinobanksin-3-butanoate (Fig. 4.1) (English et al., 1992; Kuś et al., 2018). These *O*-acylated pinobanksin derivatives are rare but have been identified in plant species such as *Eremophila alternifolia* (Biva et al., 2016) and *Pinus armandii* (Fang et al., 1988). Despite extensive chemical knowledge, the biosynthesis of these resin compounds has not been explored, although the core enzymes for flavonoid biosynthesis in poplar are well known (Tsai et al., 2006). Investigating the biosynthesis of these biologically active flavonoids is an opportunity to improve our understanding of the biochemistry and chemical ecology of poplar bud resin.

Resin from native poplar species has been widely used in traditional medicine in North America (Moerman, 1998; Ghisalberti, 1979; Uprety et al., 2012). The major components in the poplar resin include hydrophobic phenylpropanoids, benzenoids, and several classes of flavonoid aglycones (English et al., 1991; Greenaway and Whatley, 1990; English et al., 1992; Kuś et al., 2018; Isidorov and Vinogorova, 2003). In addition to human medicine, the resin compounds are found in propolis produced by honey bees (*Apis mellifera*) using poplar resins. For honey bees, propolis offers antimicrobial protection against bee pathogens causing common bee diseases, such as American foulbrood (*Paenibacillus larvae*) and chalkbrood disease (*Ascosphaera apis*) (Simone-Finstrom et al., 2017; Wilson et al., 2015; Simone-Finstrom and Spivak, 2010; Wilson et al., 2017). The unique acylated dihydroflavonols found in poplar resin, in particular, *O*-acylated pinobanksin derivatives, were discovered to be associated with the significant biological activities of propolis (Wilson et al., 2017). These biological activities highlight the pharmacological, ecological, and economic importance of poplar resins since honey bee pollination significantly contributes to global agriculture (Gallai et al., 2009; Johnson, 2010).

The acylation of specialized metabolites is carried out by acyltransferases (AT). There are several distinct types of ATs in plants (Bontpart et al., 2015; D'Auria, 2006; Kruse et al., 2022). ATs that use CoA thioesters as donor molecules for acylation reactions of plant

metabolites belong to the BAHD-type ATs (Kruse et al., 2022; Wang et al., 2022; D'Auria, 2006; Tuominen et al., 2011). The BAHD family is a large group of ATs capable of utilizing various CoA thioesters to acylate a wide range of metabolites, including terpenoids and flavonoids (Dudareva et al., 1998; Fujiwara et al., 1998; St-Pierre et al., 1998; Yang et al., 1997). The BAHD enzymes are typically located in the cytosol of plant cells (Bontpart et al., 2015). They are classified into phylogenetic clades based on the types of substrates they use, including alcohols, terpenoids, flavonoids, and alkaloids (Kruse et al., 2022). Several BAHD-ATs acting on flavonoids, such as anthocyanins, have been identified (Kruse et al., 2022; Wang et al., 2022; D'Auria, 2006; Tuominen et al., 2011). However, these ATs commonly use glycosylated flavonoids as their substrate, inducing acylation on the C6-OH or C3-OH position on glycoside moiety. Acylated flavonoid aglycones are much less common, and the corresponding enzymes have not been characterized.

In this study, we use a combination of analytical chemistry and transcriptomics to identify a BAHD-type AT, PdDAT1, capable of acylation of dihydroflavonols characteristic of bud resin of *P. deltoides* using several acyl-CoAs. The chemical analysis of the accumulation of acylated dihydroflavonols and the expression analysis of PdDAT1 suggest that *P. deltoides* bud resin synthesis is largely localized in the bud scales of leaf and flower buds and embryonic leaves.

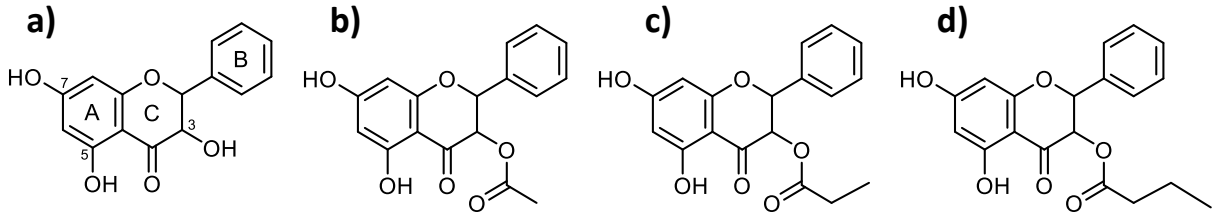

Figure 4.1. Structures of pinobanksin and its acylated derivatives found in *P. deltoides* bud resin. a) Pinobanksin, b) pinobanksin-3-acetate, c) pinobanksin-3-propionate, and d) pinobanksin-3-butyrate.

4.3 Materials and Methods

4.3.1 Sampling of *P. deltoides* lateral leaf buds

Dormant cuttings of female *P. deltoides* (9573) were acquired from Dr. Raju Soolanayakanahally, Agriculture and Agri-Food Canada (AAFC), Saskatoon, Canada. The dormant poplar cuttings were harvested in February and were 30 cm long on average. The cuttings were kept dormant by storing them at 4°C in the dark prior to being placed in a growth chamber. To induce flushing, the dormant twigs were placed in water in controlled light (16 hours of light) and temperature conditions (22°C). Lateral leaf buds were collected every other day over 12 days. For each time point, we harvested 10 buds from three individual cuttings as replicates to prevent wound-induced effects during the time course. For tissue-specific analyses, leaf and flower buds were manually separated into leaves, leaf bud scales, flower bud scales, and flowers. All samples were frozen immediately in liquid nitrogen and ground in liquid nitrogen using mortar and pestle. Samples were stored at -80°C prior to analyses.

4.3.2 UPLC-MS analysis of dihydroflavonols

The samples were extracted as described in Chapter 2 (section 2.3.4). Targeted analysis of *P. deltoides* embryonic leaves, leaf bud scales, flower bud scales, and flowers was conducted as described in Chapter 2 (section 2.3.5). The samples were analyzed using a Waters Acquity UPLC System coupled to an Acquity PDA eLambda Detector and an Acquity QDa single quadrupole mass spectrometer (Waters, Milford, MA, USA). Acquity BEH C18 column (2.1 mm, 50 mm, 1.7 µm) was used to separate the analytes. The UPLC-MS parameters were described in Chapter 2 (section 2.3.5). The MS data were recorded in negative mode, and compound-specific data were extracted from the total ion current (TIC) based on *m/z* values of corresponding molecular ions $[M+H]^-$. The UV data were observed at 280 nm. The UPLC data were processed using TargetLynx (Version 4.2). The analytical standard for pinobanksin was acquired from Toronto Research Chemicals (Toronto, Canada).

4.3.3 RNA-seq analysis of bud development and tissues

Total RNA was extracted from the *P. deltoides* lateral leaf bud tissues as described by Muoki et al. (2012). Whole leaf buds collected at day 0 (D0), day 2 (D2), day 4 (D4), and day 10 (D10) of induced bud flushing were selected for RNA-seq analysis of whole leaf buds (Supplemental Figure S4.1). These time points represented the most visible changes in the morphology of the leaf buds. The D0 samples represented dormant leaf buds. On D2, we observed small amounts of bud resin on the surface of the leaf buds. D4 marked the first time point with partially open leaf buds and visible leaf tissue. D10 represented the time point where the leaves were flushed with the bud scales still attached.

Additionally, leaf buds and flower buds collected on D4 (Supplemental Figure S4.2) were separated into leaves, leaf bud scales, flowers and flower bud scales for comparative analysis between the tissues. Three biological replicates of *P. deltoides* RNA-seq libraries of each sample were prepared. RNA-seq libraries of the whole leaf buds were prepared as previously described by Ma et al. (2018). RNA-seq library preparations of the different *P. deltoides* leaf and flower bud tissues were done by the University of British Columbia Sequencing and Bioinformatics Consortium (Vancouver, BC, Canada). For each RNA-seq set, 12 RNA libraries were pooled together and sequenced on one HiSeq lane using the Illumina NextSeq 550 platform by the University of British Columbia Sequencing and Bioinformatics Consortium.

Raw RNA-seq data was aligned using HiSAT2 (Kim et al., 2019), and transcript assembly was conducted using Cufflinks (Trapnell et al., 2012). The *P. deltoides* v2.1 genome was used as a reference genome sequence (Goodstein et al., 2012, http://phytozome.jgi.doe.gov). DESeq2 package (Love et al., 2014) was used to analyze differential expression in R (version 4.3.1). Gene annotations of *P. deltoides* v2.1 reference transcriptome were obtained from (http://phytozome.jgi.doe.gov).

4.3.4 Phylogenetic analysis

Sequences for the characterized genes were acquired from the NCBI database (https://www.ncbi.nlm.nih.gov/protein/). Names, accession numbers, and plant species of the characterized genes included in the phylogenetic analysis were AtCHAT (AF500201.1, *Arabidopsis thaliana*), CbBEAT (AF043464, *Clarkia breweri*), CmAAT1 (CAA94432.1, *Cucumis melo*), CmAAT3 (AY859053, *Cucumis melo*), CmAAT4 (AY859054, *Cucumis melo*), FaAAT (AF193789, *Fragaria ananassa*), FvVAAT (AX025504, *Fragaria vesca*), LeAAT1 (LC520138, *Lithospermum erythrorhizon*), LeSAT1 (LC520137, *Lithospermum erythrorhizon*), MdAAT1 (AY707098, *Malus domestica*), MsAAT (AX025506, *Musa sapientum*), ObCAAT1 (MN031888, *Ocimum basilicum*), PaxCFAT (DQ767969.1, *Petunia axillaris*), PhBPBT (AY611496, *Petunia x hybrida*), PtBEBT (KP228019.1, *Populus trichocarpa*), PtSABT (KP228018.1, *Populus trichocarpa*), RhAAT1 (AY850287, *Rosa hybrida*), and SlAAT (KM975322.1, *Solanum lycopersicum*). Mega11 (v 11.0.13) was used to conduct multiple gene alignments using the ClustalW algorithm. Phylogenetic analysis was performed using the maximum-likelihood statistical method and the Jones-Taylor-Thorton (JTT) model with 1000 bootstraps. The graphical presentation of the phylogenetic tree was generated and edited using FigTree (v 1.4).

4.3.5 Recombinant protein expression and purification

Expression vectors with the coding sequences of Podel.13G080100 and Podel.14G175800 were synthesized by Twist Bioscience (South San Francisco, CA, USA). The expression vector constructs consist of N-terminal His-tagged expression vector pET-28a(+), XhoI and BamHI restriction sites, and *E. coli* codon-optimized insert sequences of the candidate genes. The recombinant vector was transferred into electrocompetent *E. coli* (BL21 DE3) via electroporation for recombinant protein expression. The recombinant protein expression and purification were conducted as described in Chapter 3 (section 3.3.6). A DAB substrate kit (ThermoFisher) visualized His-tagged recombinant proteins.

4.3.6 Biochemical characterization

The preliminary enzyme assays were conducted using a reaction mixture containing 5 µg of purified recombinant protein, 0.20 mM of the acceptor substrate, 0.75 mM of acyl donor (acetyl-CoA, propionyl-CoA or butyryl-CoA; Sigma-Aldrich), and 1 mM (DTT) in 0.1 M Tris-HCl (pH 7.5), with a total reaction volume of 200 µL. The reaction mixtures were incubated for 60 min at 30°C. The reactions were stopped by adding 20 µL of 6 N HCl, and the samples were centrifuged for 5 min at 15000 rpm and 4°C. The resulting supernatant was used for UPLC-MS analysis. Boiled enzyme preparations were used as negative controls for enzyme activity.

4.3.7 Statistical analysis

Statistical analyses were done using two-way ANOVA and Tukey's post hoc HSD in GraphPad Prism 8.4.3.

4.4. Results

4.4.1 Dihydroflavonol composition of *P. deltoides* lateral buds

We used targeted UPLC-MS to analyze the dihydroflavonols composition of *P. deltoides* leaf and flower buds. The buds were manually dissected into leaves, leaf bud scales, flower bud scales, and flowers. We identified the previously reported dihydroflavonols (English et al., 1992) in leaf and flower bud scales and embryonic leaves (Supplemental Figure S4.3). In flowers, only pinobanksin and pinobanksin-3-acetate were detected.

In addition to masses corresponding to pinobanksin-3-acetate (*m/z* 313), pinobanksin-3-propionate (*m/z* 327), and pinobanksin-3-butyrate (*m/z* 341), we also detected a series of other compounds tentatively identified as acylated dihydroflavonols in embryonic leaves and both types of bud scales based on molecular mass (Supplemental Figure S4.4). These included pinobanksin-3-pentanoate (*m/z* 355), pinobanksin-3-hexanoate (*m/z* 369), pinobanksin-3-

heptanoate (*m/z* 383), pinobanksin-3-octanoate (*m/z* 397), pinobanksin-3-decanoate (*m/z* 425), and pinobanksin-3-dodecanoate (*m/z* 453). Pinobanksin-3-pentanoate, pinobanksin-3-hexanoate, and pinobanksin-3-octanoate have been previously described in poplar resin literature (English et al., 1992; Wilson et al., 2017). However, pinobanksin-3-heptanoate, pinobanksin-3-decanoate, and pinobanksin-3-dodecanoate have not been previously identified as poplar resin components.

We conducted relative quantification of the four most abundant dihydroflavonols (Fig. 4.2). In leaf and flower bud tissues, pinobanksin-3-acetate was consistently the most prevalent dihydroflavonol, followed by pinobanksin. There were no significant differences in the abundance between pinobanksin-3-butyrate and pinobanksin-3-propionate in any studied tissues. Overall, the dihydroflavonol composition was similar in all tissues except the flowers. Flower bud scales had the highest abundance of dihydroflavonols per fresh weight, while flowers had the lowest.

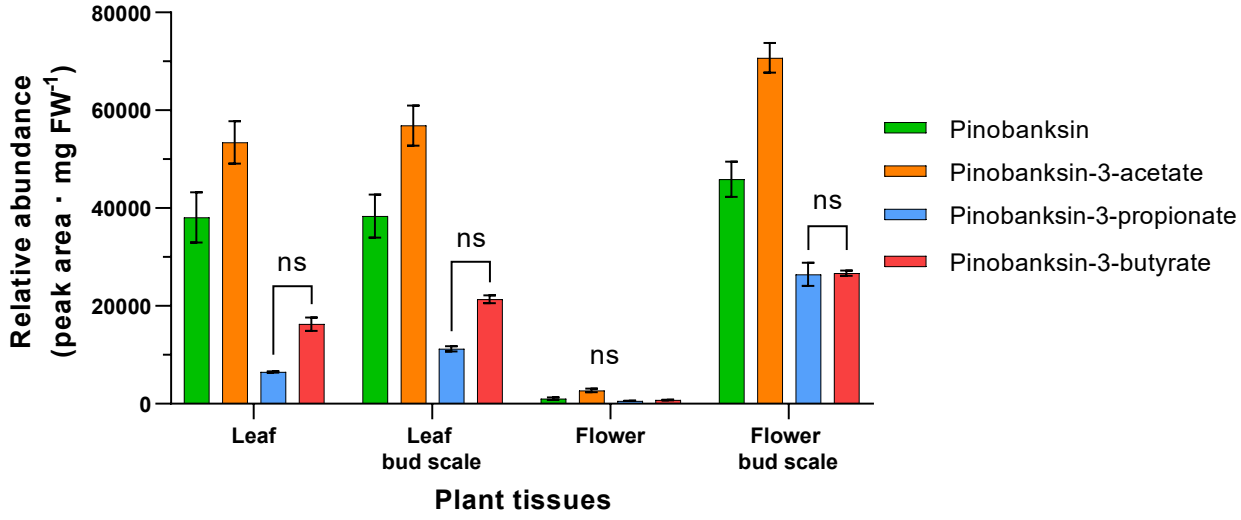

Figure 4.2. UPLC-MS analysis of common dihydroflavonols *P. deltoides* leaf buds and flower buds. The relative quantities of dihydroflavonols in methanolic extracts of *P. deltoides* embryonic leaves, leaf bud scales, flowers, and flower bud scales were quantified based on the peak areas of molecular ions $[M+H]^-$ detected on negative ionization mode. The samples were normalized by the fresh weight of the extracted tissue. The bars show the means ±SE (n = 3). Statistical analysis was done by multiple t-tests ($P < 0.05$). All pairwise comparisons within the sample tissues were statistically significant unless indicated by ns (non-significant).

4.4.2 Transcriptomic analysis of acyltransferases in *P. deltoides* buds

We generated transcriptomes for two sets of *P. deltoides* buds to identify candidate genes for dihydroflavonols-specific ATs. One data set consisted of the different tissues of leaf and flower buds to analyze and compare tissue-specific expression. In this data set, 42694 unique transcripts were detected in the data set of the different bud tissues. Based on the gene annotations of the *P. deltoides* genome (version 2.1), we identified 40 putative ATs annotated as HXXXD-type acyltransferase family proteins (Table 4.1), a common annotation for BAHD-type ATs. The other sample set included a time series of *P. deltoides* leaf buds induced to flush in a growth chamber to study changes in gene expression during the transition from dormancy to bud break. In the time series analysis of the whole leaf buds, we detected 32341 unique transcripts and 33 putative BAHD-ATs.

We first identified *P. deltoides* orthologs of chalcone synthases (CHS) based on sequence similarity of corresponding genes in *P. trichocarpa* (Tsai et al., 2006) based on gene annotations and BLAST search. These genes were used as markers for flavonoid gene expression patterns. We identified orthologs for five of the six CHSs reported in *P. trichocarpa* (Tsai et al., 2006). The identified CHS orthologs included Podel.14G152900, Podel.14G153100, Podel.01G055900, Podel.01G055700 and Podel.03G190100,

We next conducted a comparative tissue-specific expression analysis of the 40 identified BAHD-ATs between the four studies of bud tissues. For the differential analysis, we used the normalized counts to set a threshold of ≥100 reads to filter low-abundance transcripts. Based on the expression analysis, we identified many of these genes expressed simultaneously in the multiple tissues (Fig. 4.3). Seven genes were common between all four tissues. The intersecting genes, indicating the presence of these genes in the different tissues, were visualized.

Table 4.1. List of BAHD-type acyltransferases identified in *P. deltoides* leaf and flower bud tissues by RNA-seq. Relative expression levels of BAHD acyltransferases in different bud tissues expressed as normalized counts. The genes highlighted were selected as top candidates for bud resin-related BAHD-ATs.

	Normalized counts			
Podel number	**Leaf**	**Flower**	**Leaf bud scale**	**Flower bud scale**
Podel.01G136300	89.3	6.0	304.5	38.1
Podel.01G345800	0.6	250.0	17.5	200.0
Podel.01G419600	1461.2	900.1	127.3	132.8
Podel.01G472700	299.6	350.4	45.3	39.6
Podel.03G059600	130.9	431.0	56.4	76.4
Podel.03G085500	1247.0	440.7	349.2	119.0
Podel.04G057400	143.1	333.6	42.8	52.7
Podel.04G106400	226.6	83.3	80.9	54.2
Podel.04G113200	385.2	245.9	42.0	25.3
Podel.05G004700	265.2	116.1	176.3	288.0
Podel.05G026200	491.9	303.5	42.4	26.2
Podel.05G056600	441.9	329.3	137.7	99.2
Podel.05G245400	412.8	172.1	42.0	36.1
Podel.06G010900	21.5	92.5	1206.7	5311.6
Podel.06G034600	1433.2	843.9	96.3	83.5
Podel.06G106300	239.5	632.3	355.7	263.1
Podel.08G041500	2144.8	2476.9	351.1	192.7
Podel.08G041700	10.7	5178.8	50.2	33.1
Podel.08G079900	1765.0	463.1	7016.5	1921.4
Podel.08G208300	12.9	25.2	175.0	229.7
Podel.10G048100	2.2	425.7	29.7	197.2
Podel.10G050300	88.2	97.1	3235.4	8015.6
Podel.11G125600	208.1	61.6	289.0	45.6
Podel.12G066000	245.0	1023.0	229.9	44.2
Podel.12G153100	525.8	808.8	152.1	57.3
Podel.13G080000	**511.8**	**6.9**	**1331.5**	**170.2**
Podel.13G080100	**1217.2**	**10.1**	**1632.3**	**155.5**
Podel.13G080200	461.9	2043.2	48.7	42.1
Podel.14G175800	**2698.3**	**0.8**	**5313.0**	**720.6**
Podel.15G123100	512.0	5.4	411.7	31.8
Podel.15G149500	898.1	632.9	234.2	87.5
Podel.16G118200	274.4	199.5	1180.4	311.0
Podel.17G010200	4.4	28.4	112.5	503.1
Podel.19G001400	406.6	422.4	48.0	36.9
Podel.19G001500	218.5	710.5	226.0	60.1
Podel.19G001700	1219.1	1443.8	109.4	81.8
Podel.19G046000	53.5	619.7	160.8	36.1
Podel.19G125100	369.5	377.4	102.4	48.4
Podel.T047800	619.3	551.2	50.1	41.5
Podel.T048200	206.8	217.3	25.5	20.5

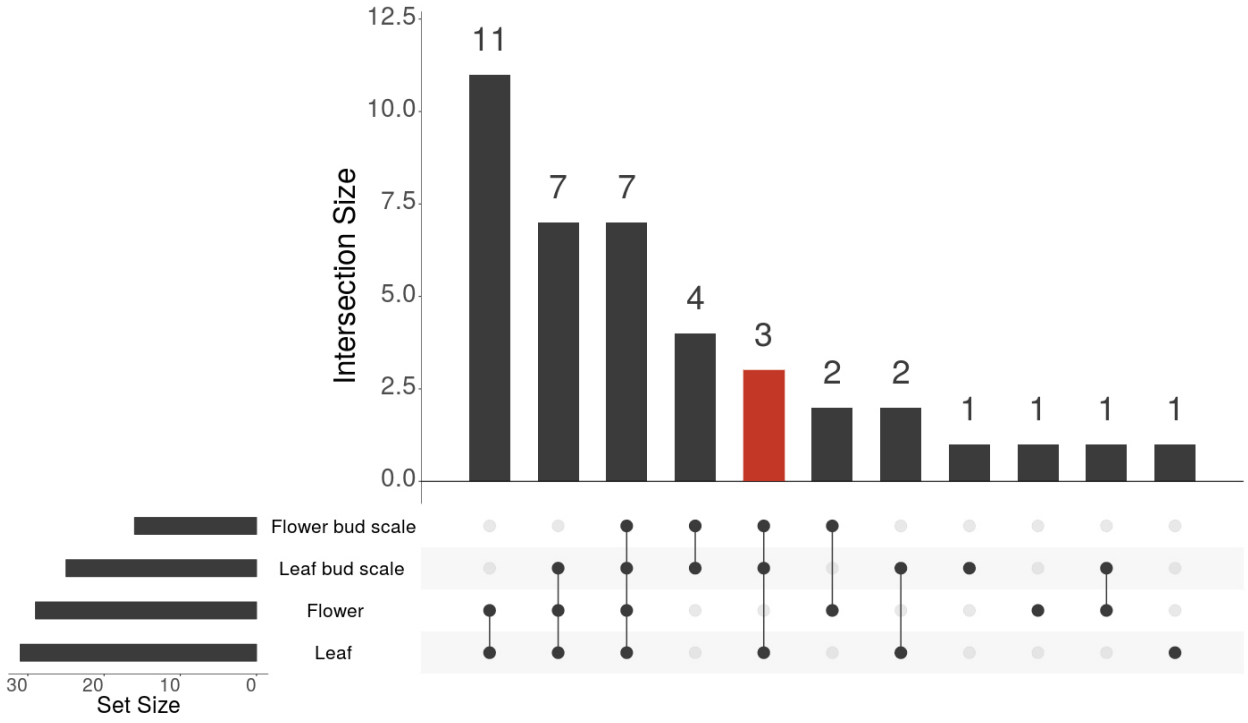

Figure 4.3. Differential analysis of the acyltransferases in *P. deltoides* leaf bud and flower bud tissues. UpSet plot of the intersection of 40 transcripts annotated as BAHD-type acyltransferases found in embryonic leaves, leaf bud scales, flowers, and flower bud scales. Set size refers to the number of genes detected in each tissue type. Intersection size denotes the number of genes shared by the sample groupings indicated by the connected dots. The red highlight indicates a group with an intersection between leaf, leaf bud scales, and flower bud scales.

We used the tissue-specific accumulation pattern of dihydroflavonols to predict the expression patterns of ATs, which act on dihydroflavonols to identify candidate genes. The localization of the dihydroflavonols in leaf and flower buds suggested that dihydroflavonols-related ATs should be highly expressed in embryonic leaves, leaf bud scales, and flower bud scales but not in flowers. Out of the total 40 ATs, 11 candidates were not expressed in the flowers but were expressed in other tissues (Table 4.2a). Notably, out of the 11 shortlisted candidates, only three genes, Podel.13G080000, Podel.13G080100, and Podel.14G175800, were expressed in leaves, leaf bud scales, and flower bud scales, matching the accumulation of dihydroflavonols. Of the marker flavonoid genes, Podel.03G190100 was the only gene matching this expression pattern.

In parallel with the tissue-specific analysis, we conducted a differential expression analysis of 11 shortlisted candidates in whole leaf buds induced to flush in a growth chamber (Table 4.2b). Out of the candidate genes, Podel.13G080000, Podel.13G080100, and Podel.14G175800 were among the genes with the highest increase in their expression levels over the time course. All three candidates showed a similarly high increase in their expression after four and ten days of induced flushing. Of the flavonoid marker genes, Podel.03G190100 was the only one showing a considerable increase in expression levels.

From these results, we concluded that Podel.13G080000, Podel.13G080100, and Podel.14G175800 match the predicted tissue-specific expression pattern. Their expression increases as the buds are induced to flush, matching the expression patterns of a flavonoid marker gene, Podel.03G190100, which suggests that Podel.13G080000, Podel.13G080100, and Podel.14G175800 may be connected to the flavonoid pathway.

Table 4.2. Expression analysis of shortlisted BAHD-type acyltransferases in *P. deltoides* buds tissues identified by RNA-seq. Expression analysis of BAHD-type acyltransferases with low expression in flowers. a) Normalized read counts for the CHS-related marker genes and BAHD-type acyltransferases in all four sample tissues and b) log2 fold change between the initial sampling and samples collected after four or ten days of incubation (D10). Positive fold change indicates an increase in expression and genes with log2 fold change > 2 and q-values (< 5e-02) were considered to have increased expression levels. Genes highlighted in red are expressed in leaves, leaf bud scales, and flower bud scales.

a)

		Normalized counts			
Podel number	**Gene name**	**Leaf**	**Flower**	**Leaf bud scale**	**Flower bud scale**
Podel.14G152900	CHS	111.0	1061.7	33.7	72.1
Podel.14G153100	CHS	467.0	4039.9	148.6	366.1
Podel.01G055900	CHS	3.2	600.4	6.5	38.2
Podel.01G055700	CHS	10.0	679.9	6.2	32.7
Podel.03G190100	CHS	313.9	40.8	890.3	112.6
Podel.10G050300		88.2	97.1	3235.4	8015.6
Podel.01G136300		89.3	6.0	304.5	38.1
Podel.04G106400		226.6	83.3	80.9	54.2
Podel.06G010900		21.5	92.5	1206.7	5311.6
Podel.08G208300		12.9	25.2	175.0	229.7
Podel.11G125600		208.1	61.6	289.0	45.6
Podel.13G080000		**511.8**	**6.9**	**1331.5**	**170.2**
Podel.13G080100	**PdDAT1**	**1217.2**	**10.1**	**1632.3**	**155.5**
Podel.14G175800		**2698.3**	**0.8**	**5313.0**	**720.6**
Podel.15G123100		512.0	5.4	411.7	31.8
Podel.17G010200		4.4	28.4	112.5	503.1

b)

		Day 0 to Day 4		**Day 0 to Day 10**	
Podel number	**Gene name**	Log2 Fold change	q-value	Log2 Fold change	q-value
Podel.14G152900	CHS	0.62	3.4E-01	-0.17	7.78E-01
Podel.14G153100	CHS	-0.34	5.9E-01	0.08	8.89E-01
Podel.01G055900	CHS	1.84	3.3E-03	2.39	1.09E-05
Podel.01G055700	CHS	1.31	8.9E-03	2.01	2.59E-06
Podel.03G190100	CHS	7.40	2.0E-07	6.59	1.27E-03
Podel.10G050300		-3.59	1.2E-59	-2.85	1.7E-38
Podel.01G136300		-0.41	4.2E-01	-1.25	9.6E-03
Podel.04G106400		3.39	7.1E-09	3.75	1.3E-10
Podel.06G010900		1.09	9.0E-02	-0.24	7.5E-01
Podel.08G208300		-0.32	4.1E-01	0.10	8.1E-01
Podel.11G125600		4.13	1.8E-10	2.21	1.1E-03
Podel.13G080000		**8.30**	**4.0E-06**	**7.23**	**6.7E-05**
Podel.13G080100	**PdDAT1**	**11.85**	**1.6E-08**	**10.19**	**1.4E-06**
Podel.14G175800		**12.35**	**4.4E-07**	**10.72**	**1.4E-05**
Podel.15G123100		10.72	2.4E-07	7.88	1.9E-04
Podel.17G010200		3.27	6.8E-03	0.32	8.3E-01

In order to further study the 11 candidate ATs expressed in all bud tissues except the flowers, we conducted a phylogenetic analysis with previously characterized BAHD-ATs (Fig. 4.4). The reference genes were selected based on their ability to utilize acyl-CoA substrates as donors for acylation of aromatic and aliphatic alcohols. The phylogenetic analysis of the primary candidates revealed that Podel.13G080000 and Podel.13G080100 clustered together. The closest characterized genes clustering close to Podel.13G080000 and Podel.13G080100 were PtBEBT and PtSABT, previously characterized in *Populus trichocarpa* (Chedgy et al., 2015). Both of these enzymes catalyze reactions between acetyl-CoA or benzoyl-CoA and 3-hexen-1-ol, 5-hexanol and 1-octanol to produce the volatile compounds, including 3-hexenyl-, 5-hexanyl- and 1-octyl acetate, and respective benzoates.

Alignment of Podel.13G080000 and Podel.13G080100 revealed 97.74 % peptide sequence identity. However, based on RNA-seq data, Podel.13G080100 had the higher overall expression in buds. Therefore, Podel.13G080100 was selected as the primary candidate between the two genes. In contrast to Podel.13G080100, Podel.14G175800 did not group directly adjacent to any previously characterized BAHD-ATs. The closest related clade of reference genes included MsAAT from *Musa sapientum* (Beekwilder et al., 2004), which uses aliphatic alcohols, including 1-octanol, with acetyl-CoA to form 1-octyl acetate.

Overall, based on the expression of the candidate BAHD-ATs in embryonic leaves, leaf bud scales, and flower bud scales, together with phylogenetic analysis indicating their potential use of acyl-CoA donors and aromatic alcohol acceptors, we selected Podel.13G080100 and Podel.14G175800 for recombinant protein expression and biochemical characterization.

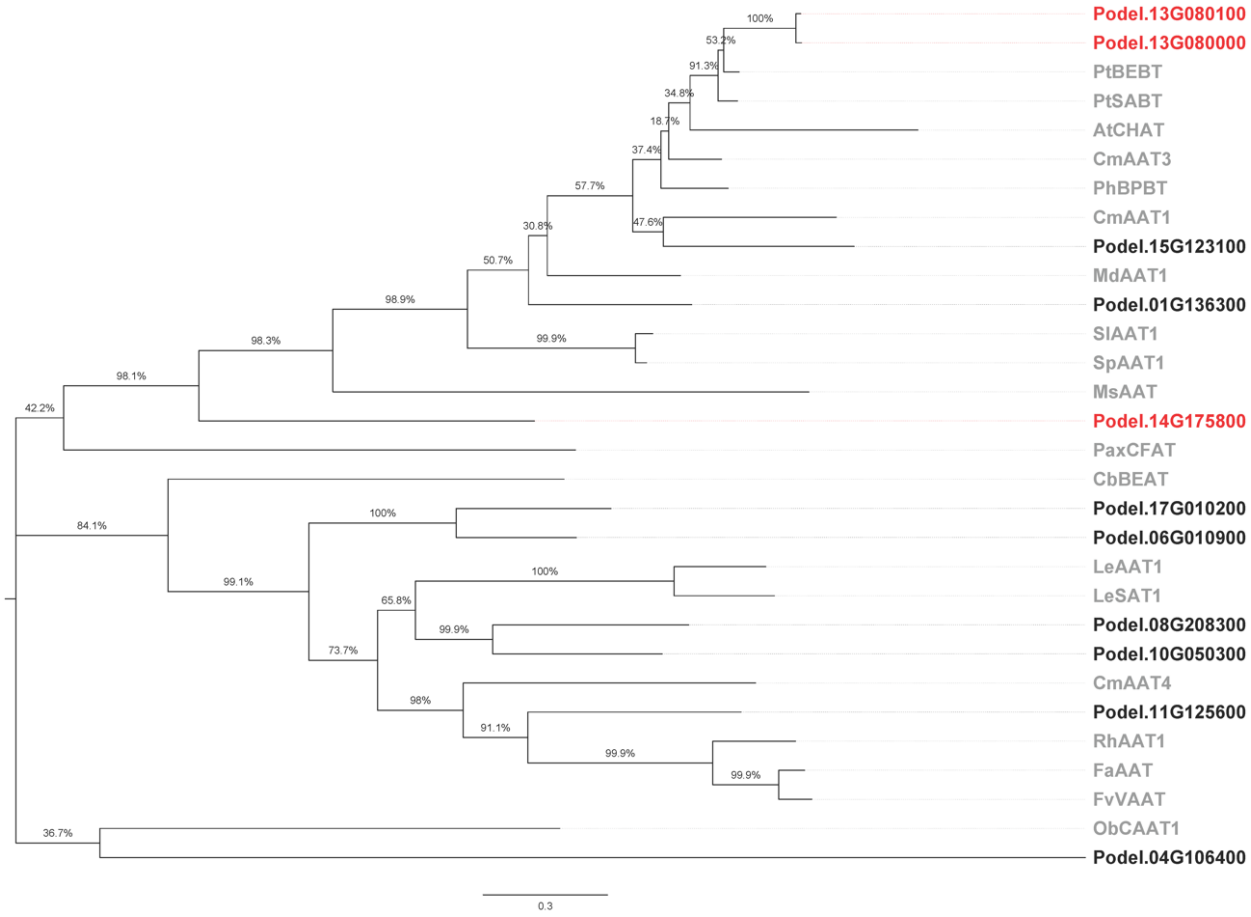

Figure 4.4. Phylogenetic analysis of BAHD-type acyltransferases and candidate genes. Maximum-likelihood phylogenetic tree of previously characterized BAHD-type acyltransferases from diverse plant species with the ATs expressed in *P. deltoides* embryonic leaves, leaf bud scales, and flower bud scales but not in flowers. Previously functionally characterized BAHD-Ats are shown in gray. Bootstrap support (1000) is shown as a percentage for each branch. Genes highlighted in red were the primary candidates expressed in leaves, leaf bud scales, and flower bud scales.

4.4.3 Biochemical assessment of candidate genes

The candidate genes were expressed as recombinant proteins to test if they encode BAHD-ATs with the predicted activity towards pinobanksin. The expression vectors with *E. coli* codon-optimized insert sequences of the candidate genes, including the recombinant Podel.13G080100 and Podel.14G175800, and an N-terminal His-tag, were synthesized. We expressed the recombinant Podel.13G080100 and Podel.14G175800 in *E. coli*. Subsequently, we purified the recombinant proteins through affinity chromatography utilizing a Ni-NTA column. The purified molecular weight of the purified products and the presence of the 6x-His-tag on the expressed recombinant protein were assessed through SDS-PAGE analysis with Coomassie staining and Western blotting (Fig. 4.5). These analyses confirmed the expected product size for both recombinant proteins and the presence of the 6x-His-tag.

We next tested the predicted enzyme activities of the purified recombinant proteins using acetyl-CoA, propionyl-CoA, and butyryl-CoA as the acyl donor and pinobanksin as the acyl acceptor. Analysis of the reaction products indicated that Podel.13G080100 recombinant protein produced *O*-acylated products with pinobanksin and all three acyl donors (Fig. 4.6, Supplemental Figure S4.5). The highest relative activity of Podel.13G080100 between the different acyl donors was found with acetyl-CoA (Supplemental Table S4.1). By contrast, the Podel.14G175800 recombinant protein did not yield any detectable reaction products in our enzyme assays. In addition to pinobanksin, Podel.13G080100 was tested with a flavonol substrate. However, there was no detectable reaction product using galangin, the flavonol most similar to pinobanksin.

These results indicate that Podel.13G080100 encodes a BAHD-type AT capable of acylation of pinobanksin using acetyl-CoA, butyryl-CoA, and propionyl-CoA as acyl donors. Therefore, we designated Podel.13G080100 as *P. deltoides* dihydroflavonol acyltransferase 1 (PdDAT1).

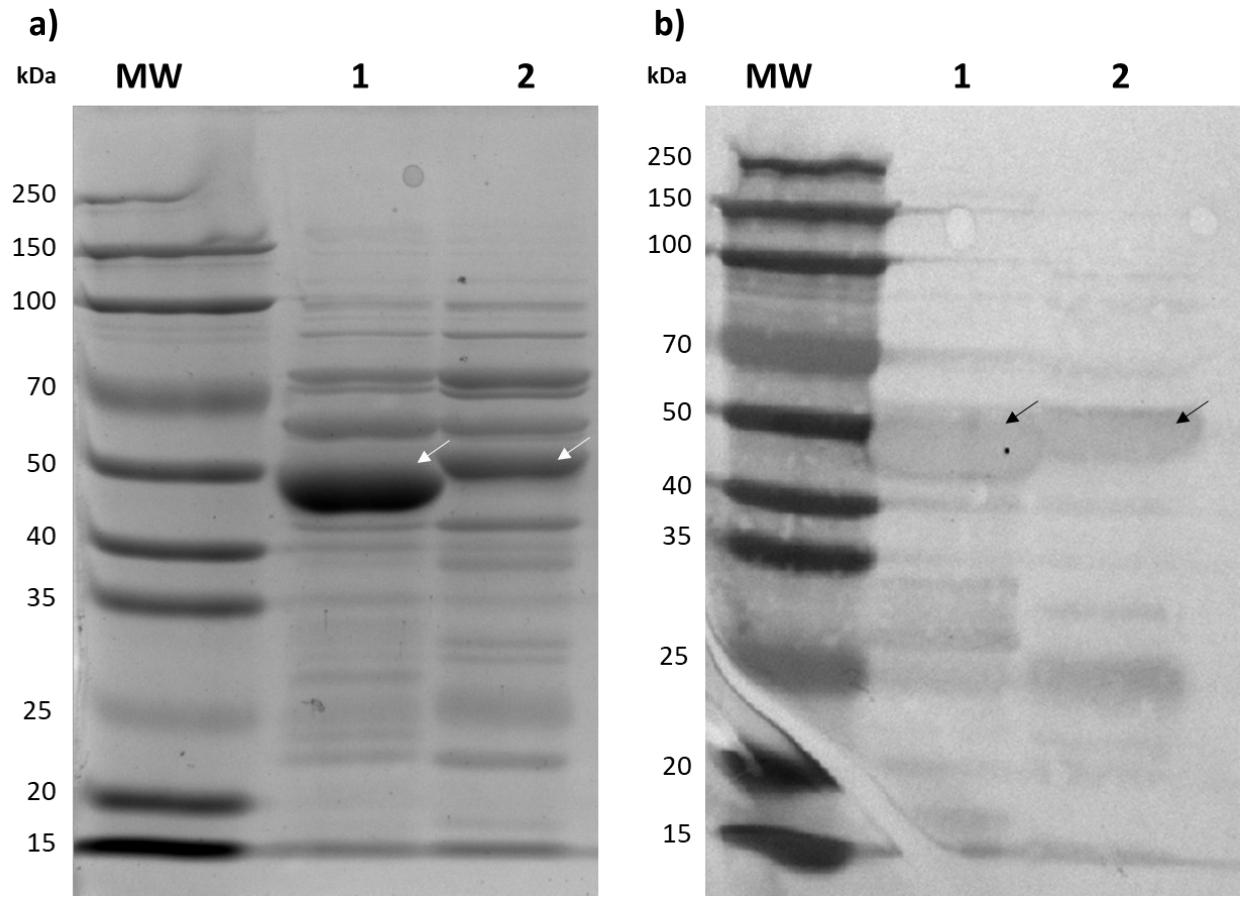

Figure 4.5. Analysis of purified recombinant proteins by SDS-PAGE. a) Coomassie stain and b) Western blot. Lanes 1-2 were loaded with purified protein preparations of recombinant Podel.13G080100 (49.39 kDa) and Podel.14G175800 (48.95 kDa), respectively. The MW lane represents the molecular weight ladder. The arrows indicate the recombinant protein bands.

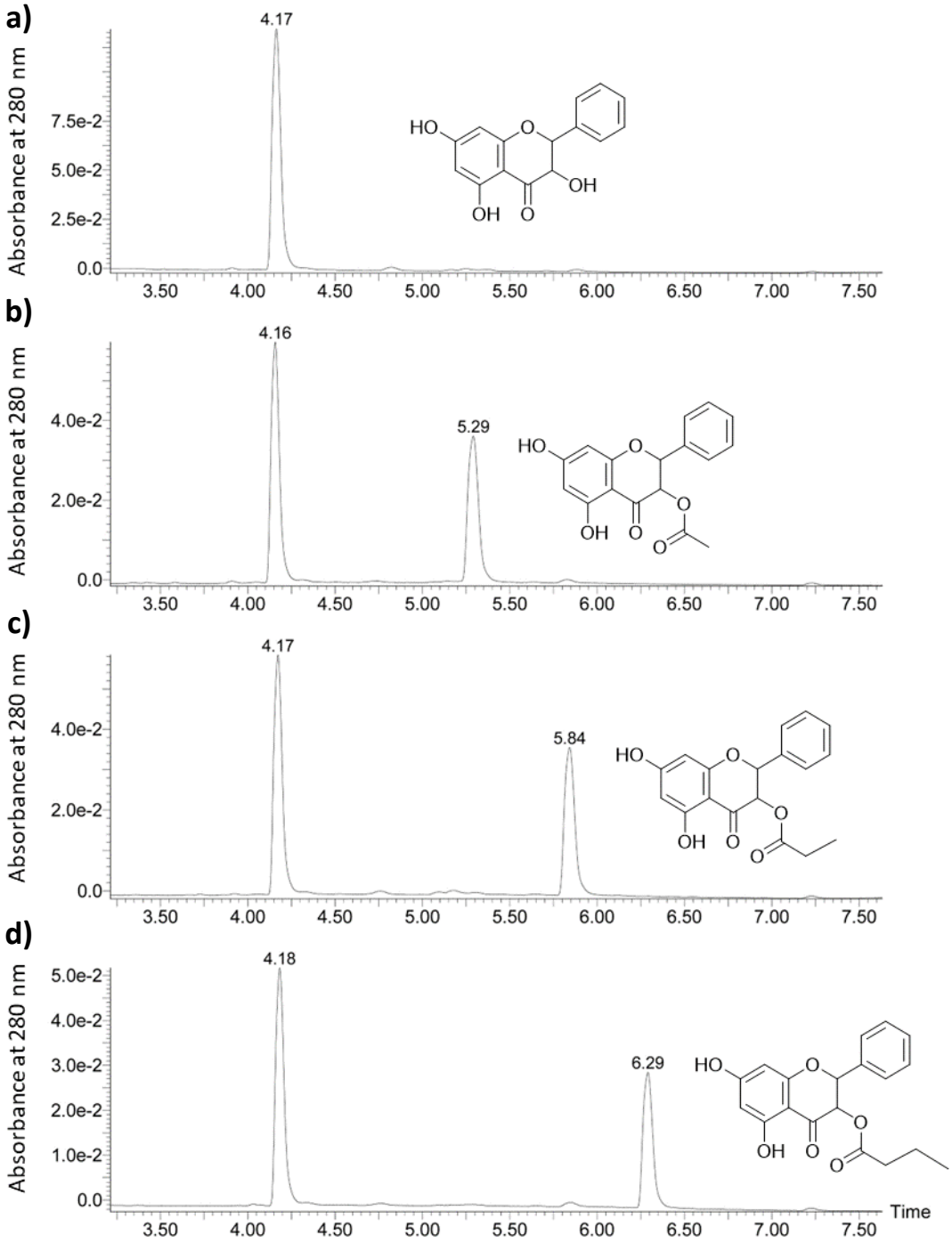

Figure 4.6. UPLC-DAD chromatograms of Podel.13G080100 (PdDAT1) enzyme assay products. The reaction products of a) pinobanksin with b) acetyl-CoA, c) propionyl-CoA, and d) butyryl-CoA were analyzed using UPLC-DAD at 280 nm. The reaction products and chemical structures shown for b-d correspond to pinobanksin-3-acetate, pinobanksin-3-propionate, and pinobanksin-3-butyrate.

4.5. Discussion

The chemical analysis of *P. deltoides* leaf buds and flower buds confirmed the presence of acylated dihydroflavonols. In addition to previously characterized series of acylated dihydroflavonols (English et al., 1992; Wilson et al., 2017), we putatively identified pinobanksin-3-heptanoate, pinobanksin-3-decanoate, and pinobanksin-3-dodecanoate, based on the observed molecular weights. These compounds have not been previously reported in *P. deltoides* buds. While the acylated dihydroflavonols were abundant in different bud tissues, including embryonic leaves, leaf bud scales, and flower bud scales, they were largely absent in flowers. These results allowed us to use differential expression analysis to select candidate genes expressed in all bud tissues except the flowers. One of these candidate genes, Podel.13G080100, could acylate pinobanksin with three different acyl donors. This is the first identified AT involved in the biosynthesis of acylated flavonoids in bud resin in *P. deltoides*.

4.5.1 PdDAT1 produces acylated pinobanksin derivatives

Preliminary biochemical characterization of PdDAT1 indicated this enzyme shows activity with pinobanksin and the capacity to utilize a range of different acyltransferases. The acylation presumably occurs on the 3-OH position on the C-ring, indicated by the matching fragmentation patterns of the observed reaction products and previously reported acylated pinobanksin derivatives (Dimkić et al., 2016). However, the substrate-specificity of PdDAT1 needs to be tested with a broader range of substrates. Other dihydroflavonols such as aromadendrin and taxifolin, which differ from pinobanksin by additional hydroxylation of the B-ring, could be potential substrates for PdDAT1. Other flavonoid classes possessing the 3-OH group, including flavan-3-ols and flavonols, could also be considered theoretical candidate substrates. However, PdDAT1 did not show activity with galangin, a flavonol substrate. Furthermore, acylated products of flavan-3-ols and other dihydroflavonols have not been previously reported in poplar, suggesting that the activity of PdDAT1 with substrates other than pinobanksin is likely limited.

The putative identification of a series of acylated pinobanksin derivatives with increasing acyl group size in *P. deltoides* buds suggests that PdDAT1 may use larger aliphatic acyl donors, such as hexanoyl-CoA in addition to the tested acyl donors. BAHD-type ATs with the capacity to utilize similar acyl donors have been characterized in many plant species (Kruse et al., 2022). For example, SlAAT1 identified in *Solanum lycopersicum* can utilize acetyl-CoA, propionyl-CoA, butyryl-CoA, and hexanoyl-CoA with 2-methyl-1-butanol to form volatile esters, including 2-methylbutyl acetate, propionate, butyrate, and hexanoate (Goulet et al., 2015). Additionally, CmAAT1, identified in *Cucumis melo* has been shown to use propionyl-CoA and hexanoyl-CoA as acyl donors to produce esters with alcohol substrates, such as hexanol, to yield propyl hexanoate and hexyl hexanoate (El-Sharkawy et al., 2005). These results support the hypothesis that a single BAHD-ATs can produce a series of acylated compounds. This remains to be tested experimentally for PdDAT1, however.

Phylogenetic analysis of PdDAT1 indicated that it belongs in the same clade as two previously identified poplar BAHD-ATs, PtBEBT and PtSABT (Chedgy et al., 2015). The substrates accepted by these two enzymes are quite different than those we identified for PdDAT1. While PtBEBT and PtSABT can utilize acetyl-CoA as an acyl donor, PtBEBT primarily catalyzes the reaction between benzyl alcohol as well as 3-hydroxy benzyl alcohol and benzoyl-CoA. By contrast, PtSABT catalyzes the reaction between salicyl alcohol and benzoyl-CoA producing salicyl benzoate, but also works with other acceptors, including 3-hydroxy benzyl alcohol, cinnamyl alcohol, and *p*-coumaryl alcohol. These enzymes are postulated to be part of the biosynthesis of salicinoids in poplar (Chedgy et al., 2015; Fellenberg et al., 2020). The surprising closeness of PdDAT1 to these two vastly different genes in the phylogenetic analysis underlines that in the context of the characterized BAHD-ATs, PdDAT1 seems to be unique. Contrary to our expectation, PdDAT1 does not group with any previously identified flavonoid-related BAHD-ATs.

Despite the wide range of identified previously characterized BAHD-type ATs that are active with other types of phenolic, including anthocyanins and glycosylated flavonols, BAHD ATs using acyl-CoAs as an acyl donor for flavonoid aglycones have not been previously reported. Flavonoid BAHD-ATs commonly use caffeoyl-CoA, coumaroyl-CoA, and malonyl-CoA as the primary acyl donors (Bontpart et al., 2015; Kruse et al., 2022). Furthermore, the

acylation reaction occurs on glycosyl moieties on flavonoid glycosides instead of directly acting on the core flavonoid structure (Bontpart et al., 2015). For example, NtMAT1 identified in *Nicotiana tabacum* can catalyze malonylation of flavonoid-7-*O* or 3-*O*-glucosides (Taguchi et al., 2005). Hence, the biochemical characterization of PdDAT1 establishes a new acyltransferase activity specific for flavonoid aglycone-specific BAHD-ATs.

4.5.2 Localization of PdDAT1 suggests resin synthesis in embryonic leaves and bud scales

During the manual dissection of the leaf buds and flower buds, the inner leaves, referred to as embryonic leaves, leaf bud scales, and flower bud scales were visibly resinous, while the flower tissues themselves lacked resin. Consistently, the highest accumulation of dihydroflavonols was detected in the flower bud scales, while the flowers lacked these compounds. The synthesis of bud resin in *Populus* is associated with the leaf buds, consistent with their ecological role of protecting vegetative tissues inside of the bud from frost or other stressors over the dormancy period (Curtis and Lersten, 1974). The role of bud resin in flower buds has not been previously studied, but the resin synthesized in the flower bud scales likely functions similarly. However, the ecological and physiological reasons why the poplar flowers do not appear to be coated in resin in the same way as the leaves have not been investigated but likely relate to their roles in pollination.

In *P. deltoides* leaf buds, the production of resin was inferred to be in cells resembling a secretory epidermis of bud scales (Curtis and Lersten, 1974). In addition, the embryonic leaves possess trichomes, which appear to contain resin droplets. Whether these trichomes are involved in resin synthesis or simply accumulating resin secreted from the surrounding bud scales is not known. The RNA-seq analysis indicated that the expression of PdDAT1 was higher in embryonic leaves and leaf bud scales than in flower bud scales. This suggests that embryonic leaves and bud scales both contain structures capable of resin synthesis. However, the tissue-specific expression of PdDAT1 needs to be verified by qPCR analysis or other methods to confirm its localization.

Overall, PdDAT1 appears to be related to the biosynthesis of acylated pinobanksin derivatives in poplar bud resin. The tissue-specific and time-course gene expression analyses of PdDAT1 should allow for the elucidation and localization of other flavonoid genes in poplars, which are involved in the synthesis of bud resin upstream in the flavonoid pathway. While the chalcone synthases (CHS), chalcone isomerases (CHI), and flavanone 3-hydroxylases (F3H) in poplar have been identified (Tsai et al., 2006), the genes which may be specifically related to bud resin biosynthesis are not known. For example, in our analysis, we identified Podel.03G190100 as the only CHS-type gene matching the expression pattern of PdDAT1, suggesting that it may be specialized to the synthesis of some of the precursors in the biosynthesis of bud resin of *P. deltoides*. Expanding on the analysis of the coexpressed genes will enable elucidation of the genes related to bud resin biosynthesis in *P. deltoides*, allowing further studies into the mechanisms of poplar bud resin production and secretion.

4.6 Conclusions

This study demonstrated the identification of BAHD-type acyltransferase in *P. deltoides* buds. PdDAT1 can directly catalyze the acylation of pinobanksin, producing acylated dihydroflavonols associated with the bioactivity of bud resins against destructive bee diseases, such as American foulbrood and chalkbrood disease. Identifying this enzyme establishes the first characterized step in the biosynthesis of *P. deltoides* bud resin. In the context of BAHD-type ATs, PdDAT1 establishes a novel activity within the family of flavonoid-related BAHDs based on its activity with flavonoid aglycones rather than flavonoid glycosides. Therefore, PdDAT1 may be leveraged for the identification of other flavonoid aglycone-specific BAHD-ATs.

4.7 Acknowledgments

We thank Dr. Raju Soolanayakanahally and Chris Stefner (AAFC) for providing *P. deltoides* cuttings, Brad Binges for the upkeep and maintenance of the greenhouse and research compound facilities, Dr. Ori Granot for the maintenance of the UPLC-MS system, and Dr. Dawei Ma for preparing RNA-seq libraries. Work in the Constabel laboratory is supported by the Natural Sciences and Engineering Research Council of Canada (NSERC).

4.8 Supplemental information

Supplemental Figure S4.1. Leaf buds of *P. deltoides*. Whole leaf buds were collected from *P. deltoides* cuttings after a) day 0, b) day 2, c) day 4, and d) day 10 of induced bud flushing in a growth chamber.

Supplemental Figure S4.2. Leaf buds and flower buds of *P. deltoides*. a) Leaf buds and b) flower buds of *P. deltoides* photographed after four days of induced bud flushing in a growth chamber. The embryonic leaves and flower tissues are surrounded by bud scales.

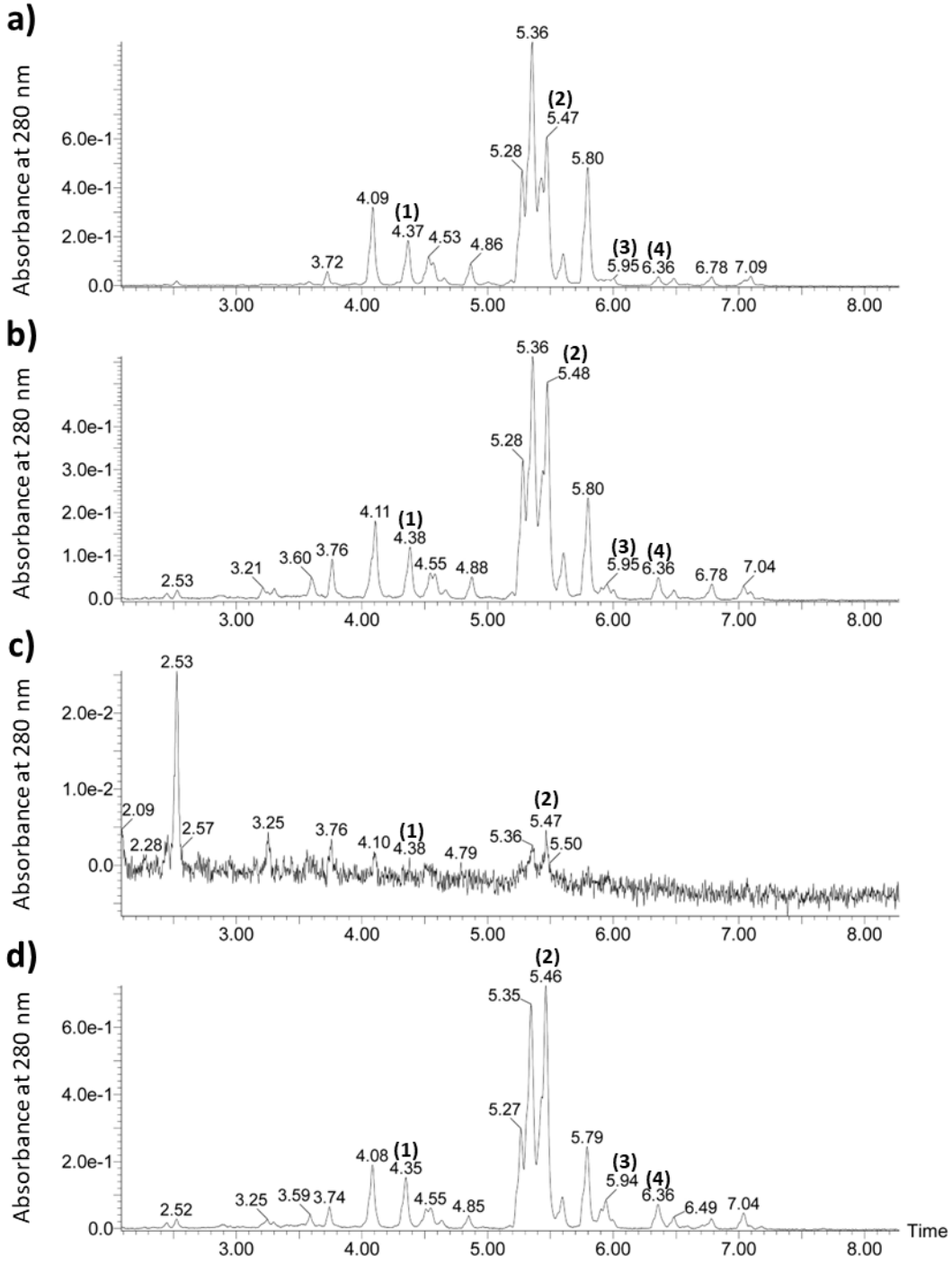

Supplemental Figure S4.3. UPLC-DAD analysis of *P. deltoides* buds. Methanolic extracts of *P. deltoides* lateral bud tissues were analyzed by UPLC-DAD at 280 nm. a) Embryonic leaves, b) leaf bud scales, c) flowers, and d) flower bud scales. Identified numbered peaks correspond to 1) pinobanksin, 2) pinobanksin-3-acetate, 3) pinobanksin-3-propionate, and 4) pinobanksin-3-butyrate.

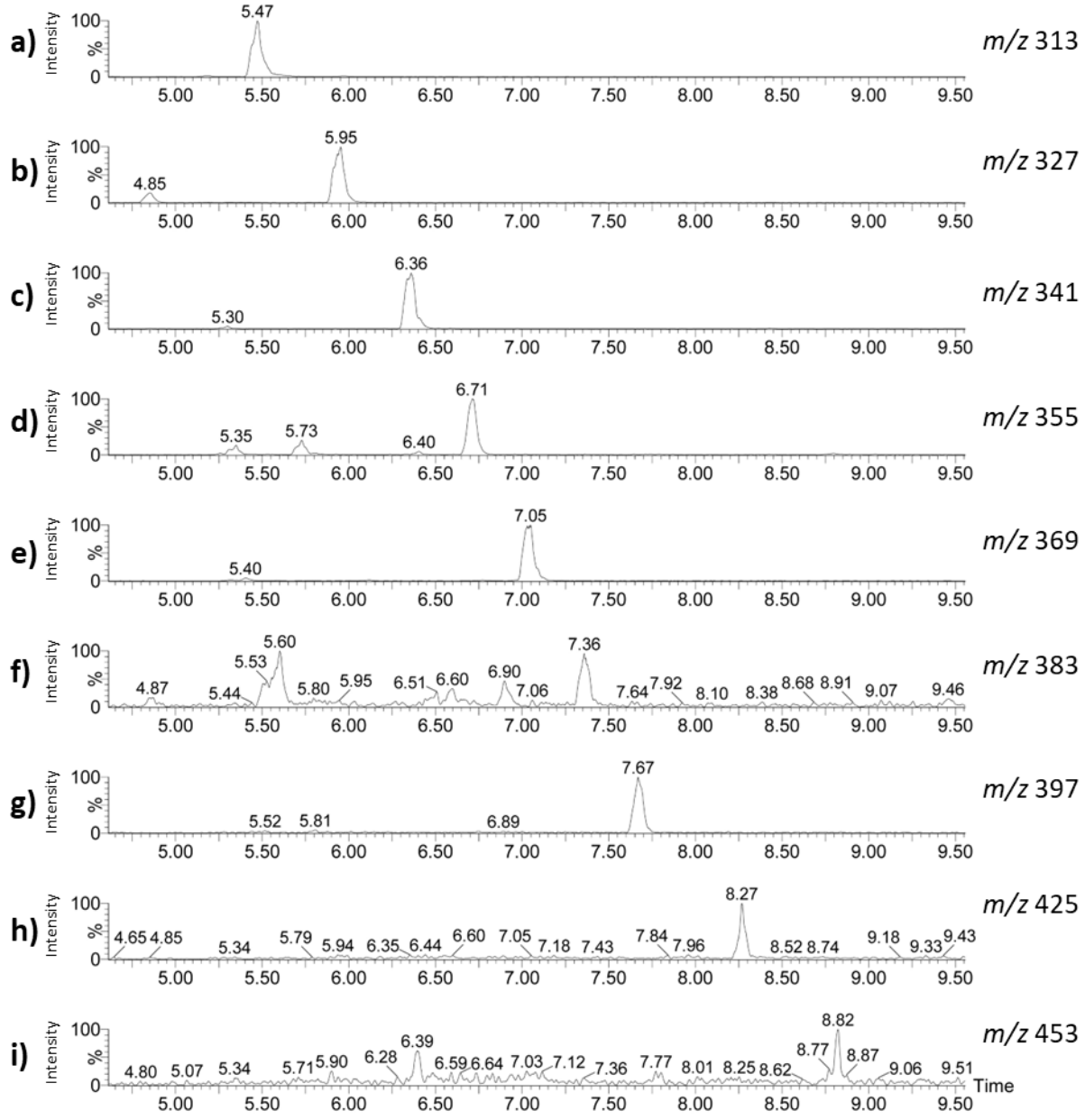

Supplemental Figure S4.4. UPLC-MS analysis of acylated dihydroflavonols in *P. deltoides* buds. Extracted ion chromatograms of the predicted molecular ions $[M+H]^-$ of acylated dihydroflanovols detected in *P. deltoides* flower bud scales. a) Pinobanksin-3-acetate (*m/z* 313), b) pinobanksin-3-propionate (*m/z* 327), c) pinobanksin-3-butyrate (*m/z* 341), d) pinobanksin-3-pentanoate (*m/z* 355), e) pinobanksin-3-hexanoate (*m/z* 369), f) pinobanksin-3-heptanoate (*m/z* 383), g) pinobanksin-3-octanoate (*m/z* 397), h) pinobanksin-3-decanoate (*m/z* 425), and i) pinobanksin-3-dodecanoate (*m/z* 453).

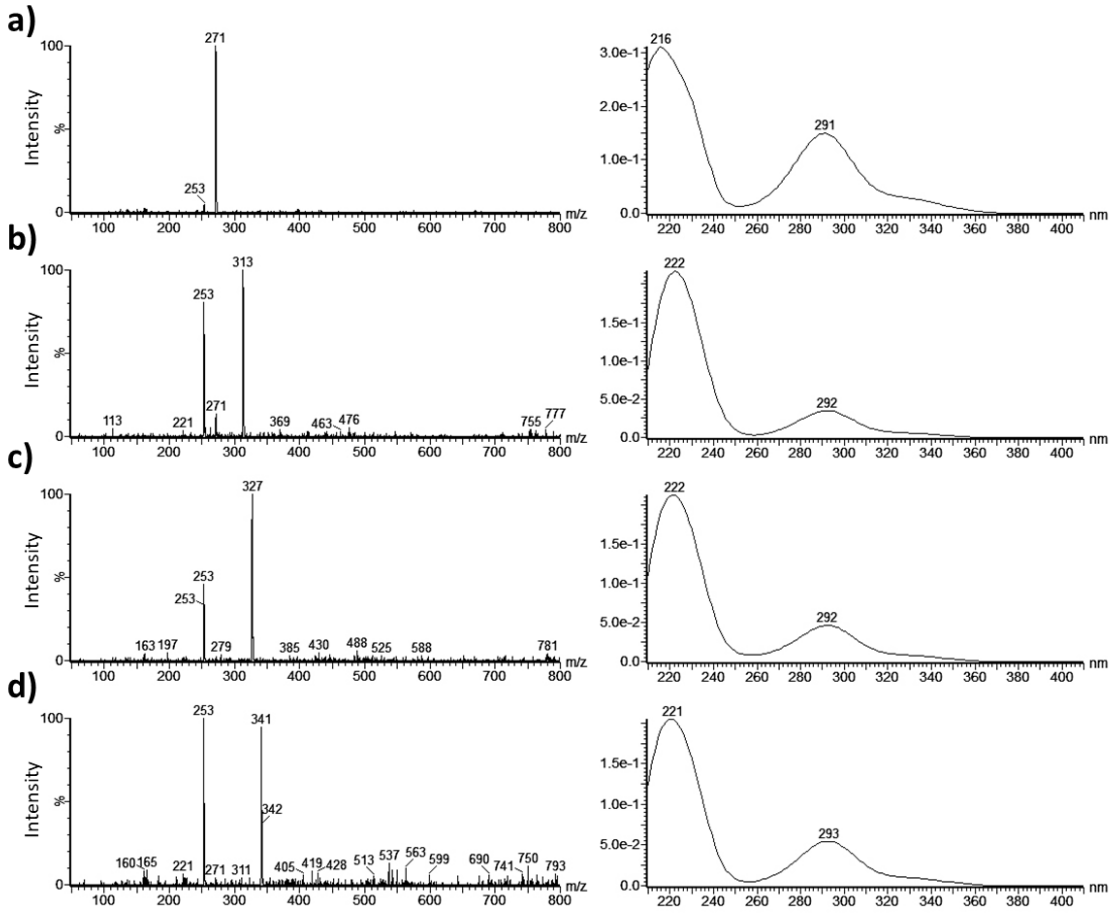

Supplemental Figure S4.5. UPLC-MS analysis of enzyme assay reaction products. Reaction products of a) pinobanksin with b) acetyl-CoA, c) propionyl-CoA, and d) butyryl-CoA were analyzed using UPLC-MS. The following spectra display the MS and UV spectra of the reaction products shown in Figure 4.6.

Supplemental Table S4.1. Relative activity of PdDAT1 with different substrates. The relative activity of PdDAT1 with different substrates and acyl donors was measured by UPLC-DAD. Relative activities are calculated based on the peak area of the products at 280 nm. The reaction product of pinobanksin and acetyl-CoA was set to 100 %.

	Acyl donor		
Substrate	**Acetyl-CoA**	**Propionyl-CoA**	**Butyryl-CoA**
Pinobanksin	100%	97%	75%
Galangin	-	-	-

Chapter 5 – General conclusions

In this thesis, I conducted chemical and transcriptomic analyses of *P. trichocarpa*, *P. balsamifera*, and *P. deltoides* buds. The chemical analyses indicated that modified flavonoid aglycones are abundant components in the leaf bud resin of *P. trichocarpa*, *P. balsamifera*, and *P. deltoides*. Through transcriptomic analyses, I identified flavonoid genes related to the biosynthesis of *O*-methylated dihydrochalcones in *P. trichocarpa* and *P. balsamifera* and *O*-acylated dihydroflavonols in *P. deltoides*, accounting for some of the characteristic major components in poplar bud resin. Identifying these genes establishes the first characterized steps in the biosynthesis of poplar leaf bud resin flavonoids.

5.1 Connection between chemistry and biochemistry of poplar bud resin

The analysis of the chemical composition of *P. trichocarpa* leaf buds and the abundance of the resin-related dihydrochalcones (Chapter 2) revealed that the accumulation and composition of leaf bud resin follow seasonal patterns. The dihydrochalcone-rich resin accumulated in the whole leaf buds in the summer during the early bud development. Interestingly, the dihydrochalcones on the surface of the bud resin display different dynamic patterns compared to the amount of accumulated resin in the whole leaf buds. The dihydrochalcones seem to accumulate on the surface of the leaf buds in the fall and spring, which suggests that the resin secretion is controlled by regulatory mechanisms responding to environmental factors or as a part of the bud development.

In addition to dihydrochalcones, we detected changes in other metabolites at different stages of the leaf bud development of *P. trichocarpa*. The dormant leaf buds were consistently rich in *O*-methoxylated flavonoids in contrast to developing leaf buds. This suggests that despite the leaf bud being dormant during the winter, the resin components may undergo biochemical modifications, including methoxylation, which adjust the lipophilicity of the resin components. Such seasonal patterns are likely to also exist in *P. balsamifera*, as well as in *P. deltoides* bud

resin, in the context of the accumulation of *O*-acylated dihydroflavonols. However, these patterns need to be confirmed.

The differences in the characteristic bud resin components in *P. trichocarpa* and *P. deltoides* highlight differences in the biosynthesis of bud resin flavonoids between poplar species. Identification of PtDOMT1 (Chapter 3) and PdDAT1 (Chapter 4) revealed that flavonoid-specific genes expressed in bud scales are involved in the biosynthesis of *O*-methylated dihydrochalcones (Fig. 5.1) and *O*-acylated dihydroflavonols (Fig. 5.2) in poplar buds.

Interestingly, while the genes were highly expressed in the bud scales, suggesting that the bud scales are the primary site for the modification of the flavonoid aglycones in both species, the *O*-methylated dihydrochalcones in *P. trichocarpa* and *O*-acylated dihydroflavonols in *P. deltoides* seem to accumulate in different tissues of the buds. The *O*-methylated dihydrochalcones accumulated in the embryonic leaves, while the concentration of *O*-acylated dihydroflavonols was consistently higher in the bud scales. The differences between the localization of the synthesis and accumulation of the resin components suggest the existence of unidentified underlying mechanisms involved in the secretion and transport of these metabolites. Understanding these mechanisms is essential for elucidating how the bud resin makes its way to the surface of the buds, where it functions as a defensive barrier for the buds but also becomes bioavailable for other species, such as honey bees, which benefit from poplar bud resins.

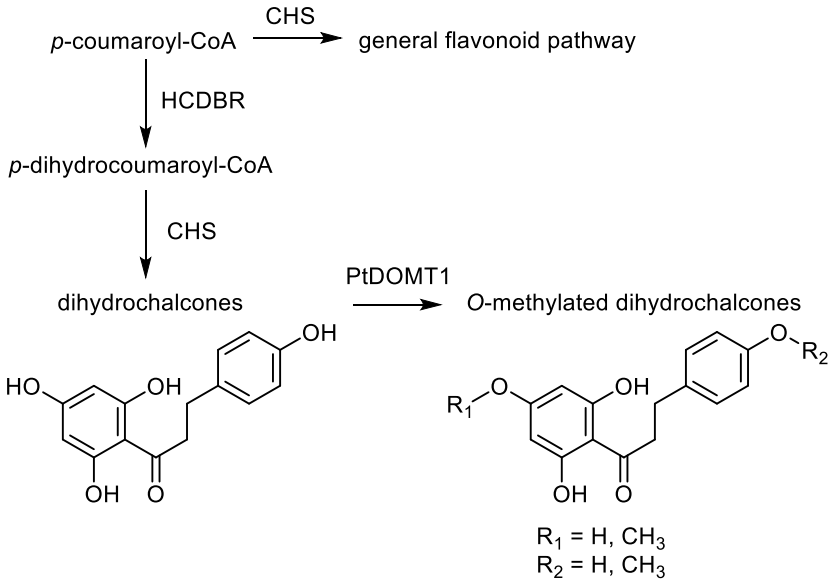

Figure 5.1. Proposed biosynthetic pathway of *O*-methylated dihydrochalcones. Enzymes involved in the biosynthesis of *O*-methylated dihydrochalcones in *P. trichocarpa* and *P. balsamifera* leaf bud resin. Name abbreviations: HCDBR, hydroxycinnamoyl-CoA double-bond reductase; CHS, chalcone synthase; PtDOMT1, *P. trichocarpa* dihydrochalcone *O*-methyltransferase 1.

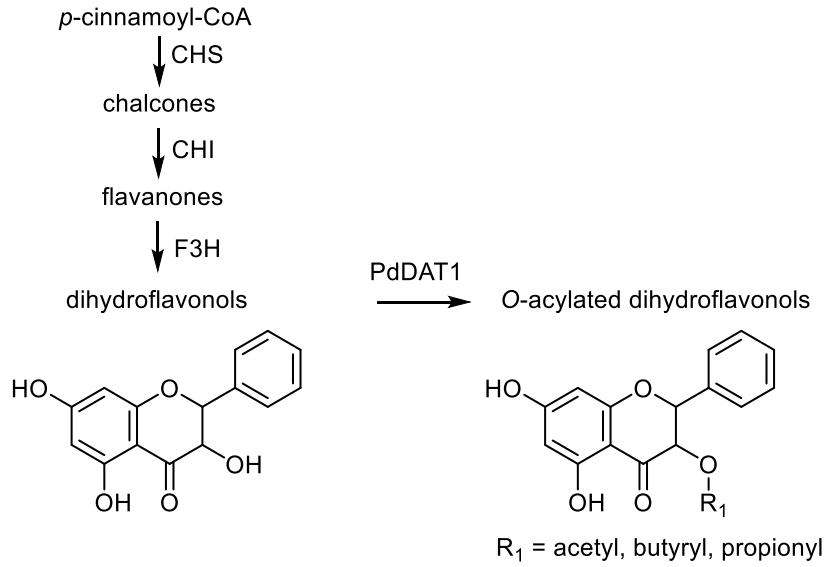

Figure 5.2. Proposed biosynthetic pathway of *O*-acylated dihydroflavonols. Enzymes involved in the biosynthesis of different *O*-acylated dihydroflavonols in *P. deltoides* bud resin. Name abbreviations: CHS, chalcone synthase; CHI, chalcone isomerase; F3H, flavanone 3-hydroxylase; PdDAT1, *P. deltoides* dihydroflavonol acyltransferase 1.

5.2 Significance of the findings

The identification of PtDOMT1 marks the first characterized OMT specific to dihydrochalcone substrates. The seasonal expression of PtDOMT1 corresponds to the accumulation of *O*-methylated dihydrochalcones in *P. trichocarpa* leaf buds, establishing the first connection between the chemistry and biochemistry of poplar bud resin flavonoids. In a broad sense, the identification of PtDOMT1 also established a new branch in the network of phenylpropanoid-related pathways previously in poplar (Tsai et al., 2006). PtDOMT1 belongs to a pathway yielding dihydrochalcones, diverging from the main flavonoid pathway (Ibdah et al., 2018), which has not been described in poplar. These findings increase the complexity of the biosynthesis network of phenylpropanoids in poplar and provide the foundation for studying other genes involved in this pathway.

Similarly to PtDOMT1, the identification of PdDAT1 establishes the first known step of bud resin biosynthesis in another poplar species, *P. deltoides*. In the context of BAHD-type ATs, PdDAT1 is unique in regard to its substrate specificity towards flavonoid aglycones. This specificity indicates the existence of a new subclade within the flavonoid BAHD-AT family (Kruse et al., 2022). Hence, PdDAT1 may be leveraged for the identification of other BAHD-ATs within this subclade.

My work outlines the first attempt to establish the connection between the chemistry and biochemistry of poplar bud resin. The use of verified female clones of *P. trichocarpa* (Nisqually-1), *P. balsamifera* (LOV-5), and *P. deltoides* (9573) in my work provides the most validated characterization of the major resin components between the studied poplar species to date. In addition to previously identified resin components, I putatively identified seasonal patterns in modified flavonoid aglycones not previously associated with resin components, suggesting that the diversity of specialized metabolites in poplar bud resins is even more expansive than we thought. These discoveries expand on the work initiated by English and Greenaway in characterizing poplar resin components of different poplar species.

Overall, this research on the chemistry of poplar bud resins contributes significantly to understanding the specialized metabolism-related defence mechanisms employed by poplars.

The knowledge of the resin components and their accumulation patterns may be leveraged to elucidate additional enzymes involved in the biosynthesis of poplar bud resin. This strategy was successfully employed in Chapters 3 and 4, leading to the identification of the two novel flavonoid genes. In addition, the seasonal patterns identified in the specialized metabolism of poplar buds suggest new directions in studying how the phenylpropanoid pathway and biosynthesis of flavonoids are regulated by environmental factors, such as abiotic stress during winter (Francini et al., 2019).

5.3 Future direction of poplar bud resin research

While this research established the terminal steps of the biosynthesis of poplar resin flavonoids, the genes involved in the upstream and production of the flavonoid aglycones are still unknown. The HCDBR and CHS genes specifically involved in the production of dihydrochalcones have not been characterized in poplar. Dihydrochalcone-related HCDBR (Ibdah et al., 2014), as well as CHS-like genes (Yahyaa et al., 2017), identified in apple (*Malus x domestica* Brokh.), which diverge the dihydrochalcones from the main flavonoid pathway, could be leveraged for the identification of similar genes in poplar to establish the complete pathway for dihydrochalcone biosynthesis. Similarly, the bud resin-specific flavonoid genes preceding PdDAT1, including CHS, CHI, and F3H, in *P. deltoides* have not been identified. Characterizing these pathways would add a new chapter to the already vast network of phenylpropanoids in poplars.

Another aspect of future poplar resin research involves studying the spatial gene expression of the resin-related genes and more accurate localization of the sites of resin synthesis. My research indicates that the resin synthesis is primarily localized in the bud scales. However, both identified genes were also expressed in the embryonic leaves, although to a lesser extent, which suggests that some of the resin synthesis could also occur on the glandular trichomes of the embryonic leaves, as previously described (Curtis and Lersten, 1974). This has not been previously studied using molecular methods. A finer dissection of the bud tissues, including the secretory epidermis of the bud scales and parts of the embryonic leaves, would provide further insight into the specific localization of the secretory structures involved in the

resin synthesis. Identifying the secretory structures could be leveraged to elucidate the mechanisms of secretion and transport. This would enable in-depth studies into how environmental effects impact resin production and secretion.

In a broader sense, investigating how resin biosynthesis is affected by the climate is an important part of understanding the environmental adaptation of perennial trees. Since the production of leaf bud resin is commonly associated with cold resistance, will the quantity or quality of resin synthesis be affected by the warming climate? In turn, how would reduced resin synthesis affect the herbivory and survival of the developing poplar buds? These questions regarding the ecological significance of poplar bud resins highlight that understanding the connection between the chemistry of the plant resins and the biochemistry involved in the resin synthesis is the key to truly understanding the novelties of the plant resins.

References

Akao, Y., Maruyama, H., Matsumoto, K., Ohguchi, K., Nishizawa, K., Sakamoto, T., Araki, Y., Mishima, S., and Nozawa, Y. (2003). Cell growth inhibitory effect of cinnamic acid derivatives from propolis on human tumor cell lines. Biol Pharm Bull **26**: 1057–1059.

Babst, B.A., Chen, H.Y., Wang, H.Q., Payyavula, R.S., Thomas, T.P., Harding, S.A., and Tsai, C.J. (2014). Stress-responsive hydroxycinnamate glycosyltransferase modulates phenylpropanoid metabolism in *Populus*. J Exp Bot **65**: 4191–4200.

Babst, B.A., Harding, S.A., and Tsai, C.J. (2010). Biosynthesis of phenolic glycosides from phenylpropanoid and benzenoid precursors in *Populus*. J Chem Ecol **36**: 286–297.

Bankova, V., Popova, M., and Trusheva, B. (2018). The phytochemistry of the honeybee. Phytochemistry **155**: 1–11.

Bankova, V.S., De Castro, S.L., and Marcucci, M.C. (2000). Propolis recent advances in chemistry and plant origin. Apidologie **31**: 3–15.

Barakat, A., Choi, A., Yassin, N.B.M., Park, J.S., Sun, Z., and Carlson, J.E. (2011). Comparative genomics and evolutionary analyses of the *O*-methyltransferase gene family in *Populus*. Gene **479**: 37–46.

Basler, D. and Körner, C. (2014). Photoperiod and temperature responses of bud swelling and bud burst in four temperate forest tree species. Tree Physiol **34**: 377–388.

Bastos, E.M.A.F., Simone, M., Jorge, D.M., Soares, A.E.E., and Spivak, M. (2008). In vitro study of the antimicrobial activity of Brazilian propolis against *Paenibacillus larvae*. J Invertebr Pathol **97**: 273–281.

Beekwilder, J., Alvarez-Huerta, M., Neef, E., Verstappen, F.W.A., Bouwmeester, H.J., and Aharoni, A. (2004). Functional characterization of enzymes forming volatile esters from strawberry and banana. Plant Physiol **135**: 1865–1878.

Berim, A. and Gang, D.R. (2016). Methoxylated flavones: occurrence, importance, biosynthesis. Phytochemistry Reviews **15**: 363–390.

Berim, A., Hyatt, D.C., and Gang, D.R. (2012). A set of regioselective *O*-methyltransferases gives rise to the complex pattern of methoxylated flavones in sweet basil. Plant Physiol **160**: 1052–1069.

Biva, I.J., Ndi, C.P., Griesser, H.J., and Semple, S.J. (2016). Antibacterial constituents of *Eremophila alternifolia*: An Australian aboriginal traditional medicinal plant. J Ethnopharmacol **182**: 1–9.

Boeckler, G.A., Gershenzon, J., and Unsicker, S.B. (2011). Phenolic glycosides of the Salicaceae and their role as anti-herbivore defenses. Phytochemistry **72**: 1497–1509.

Böhlenius, H., Huang, T., Charbonnel-Campaa, L., Brunner, A.M., Jansson, S., Strauss, S.H., and Nilsson, O. (2006). CO/FT regulatory module controls timing of flowering and seasonal growth cessation in trees. Science (1979) **312**: 1040–1043.

Bontpart, T., Cheynier, V., Ageorges, A., and Terrier, N. (2015). BAHD or SCPL acyltransferase? What a dilemma for acylation in the world of plant phenolic compounds. New Phytologist **208**: 695–707.

Braakhuis, A. (2019). Evidence on the health benefits of supplemental propolis. Nutrients **11**: 2705.

Burdock, G.A. (1998). Review of the biological properties and toxicity of bee propolis (propolis). Food and Chemical Toxicology **36**: 347–363.

Cabanillas, B.J., Le Lamer, A.C., Castillo, D., Arevalo, J., Estevez, Y., Rojas, R., Valadeau, C., Bourdy, G., Sauvain, M., and Fabre, N. (2012). Dihydrochalcones and benzoic acid derivatives from *Piper dennisii*. Planta Med **78**: 914–918.

Céline, V., Adriana, P., Eric, D., Joaquina, A.C., Yannick, E., Augusto, L.F., Rosario, R., Dionicia, G., Michel, S., Denis, C., and Geneviève, B. (2009). Medicinal plants from the Yanesha (Peru): Evaluation of the leishmanicidal and antimalarial activity of selected extracts. J Ethnopharmacol **123**: 413–422.

Chedgy, R.J., Köllner, T.G., and Constabel, C.P. (2015). Functional characterization of two acyltransferases from *Populus trichocarpa* capable of synthesizing benzyl benzoate and salicyl benzoate, potential intermediates in salicinoid phenolic glycoside biosynthesis. Phytochemistry **113**: 149–159.

Cheng, J., Wei, G., Zhou, H., Gu, C., Vimolmangkang, S., Liao, L., and Han, Y. (2014). Unraveling the mechanism underlying the glycosylation and methylation of anthocyanins in peach. Plant Physiol **166**: 1044–1058.

Clausen, T.P., Chen, J., Bryant, J.P., Provenza, F.D., and Villalba, J. (2010). Dynamics of the volatile defense of winter "dormant" balsam poplar (*Populus balsamifera*). J Chem Ecol **36**: 461–466.

Colombini, M.P., Modugno, F., Giannarelli, S., Fuoco, R., and Matteini, M. (2000). GC-MS characterization of paint varnishes. Microchemical Journal **67**: 385–396.

Conde, D., Le Gac, A.L., Perales, M., Dervinis, C., Kirst, M., Maury, S., González-Melendi, P., and Allona, I. (2017). Chilling-responsive DEMETER-LIKE DNA demethylase mediates in poplar bud break. Plant Cell Environ **40**: 2236–2249.

Constabel, C. and Lindroth, R. (2010). The Impact of Genomics on Advances in Herbivore Defense and Secondary Metabolism in *Populus*. In Genetics and Genomics of *Populus*, S. Jansson, R.P. Bhalerao, and A.T. Groover, eds (Springer-Verlag Inc.: New York, NY, USA), pp. 279–305.

Cooke, J.E.K., Eriksson, M.E., and Junttila, O. (2012). The dynamic nature of bud dormancy in trees: Environmental control and molecular mechanisms. Plant Cell Environ **35**: 1707–1728.

Cooke, J.E.K. and Rood, S.B. (2007). Trees of the people: The growing science of poplars in Canada and worldwide. Canadian Journal of Botany **85**: 1103–1110.

Curtis, J.D. and Lersten, N.R. (1974). Morphology, seasonal variation, and function of resin glands on bud and leaves of *Populus deltoides* (Salicaceae). Amer. J. Bot. **61**: 835–845.

Dare, A.P., Tomes, S., Cooney, J.M., Greenwood, D.R., and Hellens, R.P. (2013). The role of enoyl reductase genes in phloridzin biosynthesis in apple. Plant Physiology and Biochemistry **72**: 54–61.

D'Auria, J.C. (2006). Acyltransferases in plants: a good time to be BAHD. Curr Opin Plant Biol **9**: 331–340.

Dimkić, I., Ristivojević, P., Janakiev, T., Berić, T., Trifković, J., Milojković-Opsenica, D., and Stanković, S. (2016). Phenolic profiles and antimicrobial activity of various plant resins as potential botanical sources of Serbian propolis. Ind Crops Prod **94**: 856–871.

Donaldson, J.R., Stevens, M.T., Barnhill, H.R., and Lindroth, R.L. (2006). Age-related shifts in leaf chemistry of clonal aspen (*Populus tremuloides*). J Chem Ecol **32**: 1415–1429.

Druart, N., Johansson, A., Baba, K., Schrader, J., Sjödin, A., Bhalerao, R.R., Resman, L., Trygg, J., Moritz, T., and Bhalerao, R.P. (2007). Environmental and hormonal regulation of the activity-dormancy cycle in the cambial meristem involves stage-specific modulation of transcriptional and metabolic networks. Plant Journal **50**: 557–573.

Dudareva, N., D'Auria, J.C., Nam, K.H., Raguso, R.A., and Pichersky, E. (1998). Acetyl-CoA:benzylalcohol acetyltransferase - An enzyme involved in floral scent production in *Clarkia breweri*. Plant Journal **14**: 297–304.

Dudonné, S., Poupard, P., Coutiére, P., Woillez, M., Richard, T., Mérillon, J.M., and Vitrac, X. (2011). Phenolic composition and antioxidant properties of poplar bud (*Populus nigra*) extract: Individual antioxidant contribution of phenolics and transcriptional effect on skin aging. J Agric Food Chem **59**: 4527–4536.

El-Sharkawy, I., Manríquez, D., Flores, F.B., Regad, F., Bouzayen, M., Latché, A., and Pech, J.C. (2005). Functional characterization of a melon alcohol acyl-transferase gene family involved in the biosynthesis of ester volatiles. Identification of the crucial role of a threonine residue for enzyme activity. Plant Mol Biol **59**: 345–362.

English, S., Greenaway W., and Whatley, F.R. (1992). Analysis of phenolics in bud exudates of *Populus deltoides*, *P. fremontii*, *P. sargentii* and *P. wislizenii* by GC-MS. Phytochemistry **31**: 1255–1260.

English, S., Greenaway, W., and Whatley, F.R. (1991). Analysis of phenolics of *Populus trichocarpa* bud exudate by GC-MS. Phytochemistry **30**: 531–533.

Fang, J.-M., Su, W.-C., and Cheng, Y.-S. (1988). Flavonoids and stilbenes from armand pine. Phytochemistry **27**: 1395–1397.

Fellenberg, C., Corea, O., Yan, L.H., Archinuk, F., Piirtola, E.M., Gordon, H., Reichelt, M., Brandt, W., Wulff, J., Ehlting, J., and Peter Constabel, C. (2020). Discovery of salicyl benzoate UDP-glycosyltransferase, a central enzyme in poplar salicinoid phenolic glycoside biosynthesis. Plant Journal **102**: 99–115.

Francini, A., Giro, A., and Ferrante, A. (2019). Biochemical and molecular regulation of phenylpropanoids pathway under abiotic stresses. In Plant Signaling Molecules: Role and Regulation under Stressful Environments (Elsevier), pp. 183–192.

Fujiwara, H., Tanaka, Y., Yonekura-Sakakibara, K., Fukuchi-Mizutani, M., Nakao, M., Fukui, Y., Yamaguchi, M., Ashikari, T., and Kusumi, T. (1998). cDNA cloning, gene expression and subcellular localization of anthocyanin 5-aromatic acyltransferase from *Gentiana triflora*. Plant Journal **16**: 421–431.

Gallai, N., Salles, J.M., Settele, J., and Vaissière, B.E. (2009). Economic valuation of the vulnerability of world agriculture confronted with pollinator decline. Ecological Economics **68**: 810–821.

Ghisalberti, E.L. (1979). Propolis: A Review. Bee World **60**: 59–84.

Goffinet, M.C. and Larson, P.R. (1981). Structural changes in *Populus deltoides* terminal buds and in the vascular transition zone of the stems during dormancy induction. Source: American Journal of Botany **68**: 118–129.

Goodstein, D.M., Shu, S., Howson, R., Neupane, R., Hayes, R.D., Fazo, J., Mitros, T., Dirks, W., Hellsten, U., Putnam, N., and Rokhsar, D.S. (2012). Phytozome: A comparative platform for green plant genomics. Nucleic Acids Res **40**: 1178–1186.

Gordon, H., Fellenberg, C., Lackus, N.D., Archinuk, F., Sproule, A., Nakamura, Y., K Llner, T.G., Gershenzon, J., Overy, D.P., and Constabel, C.P. (2022). CRISPR/Cas9 disruption of UGT71L1 in poplar connects salicinoid and salicylic acid metabolism and alters growth and morphology. Plant Cell **34**: 2925–2947.

Goulet, C., Kamiyoshihara, Y., Lam, N.B., Richard, T., Taylor, M.G., Tieman, D.M., and Klee, H.J. (2015). Divergence in the enzymatic activities of a tomato and *Solanum pennellii* alcohol acyltransferase impacts fruit volatile ester composition. Mol Plant **8**: 153–162.

Gourlay, G. and Constabel, C.P. (2019). Condensed tannins are inducible antioxidants and protect hybrid poplar against oxidative stress. Tree Physiol **39**: 345–355.

Greenaway, W., English, S., May, J., and Whatley, F.R. (1991). Analysis of phenolics of bud exudate of *Populus sieboldii* by GC-MS. Phytochemistry **30**: 3005–3008.

Greenaway, W., English, S., Weber, E.W., and Whatley, F.R. (1989a). Series of novel flavanones identified by gas chromatography-mass spectrometry in bud exudate of *Populus fremontii* and *Populus maximowiczii*. J Chromatogr **481**: 352–357.

Greenaway, W., May, J., Scaysbrook, T., and Hatley, F.R.W. (1992a). Compositions of bud and leaf exudates of some *Populus* species compared. Z. Naturforsch **47**: 329–334.

Greenaway, W., May, J., and Whatley, F.R. (1992b). Analysis of phenolics of bud exudate of *Populus laurifolia* by GC-MS. Zeitschrift für Naturforschung C **47**: 776–778.

Greenaway, W., May, J., and Whatley, F.R. (1989b). Flavonoid aglycones identified by gas chromagraphy-mass spectometry in bud exudate of *Populus balsamifera*. J Chromatogr **472**: 393–400.

Greenaway, W. and Whatley, F.R. (1990). Resolution of complex mixtures of phenolics in poplar bud exudate by analysis of gas chromatography-mass spectrometry data. J Chromatogr **519**: 145–158.

Holdsworth, D. and Damas, K. (1986). Medicinal plants of Morobe province, Papua New Guinea part III: The Finschhafen coast. Pharm Biol **24**: 217–225.

Ibdah, M., Berim, A., Martens, S., Valderrama, A.L.H., Palmieri, L., Lewinsohn, E., and Gang, D.R. (2014). Identification and cloning of an NADPH-dependent hydroxycinnamoyl-CoA double bond reductase involved in dihydrochalcone formation in *Malus* × *domestica* Borkh. Phytochemistry **107**: 24–31.

Ibdah, M., Martens, S., and Gang, D.R. (2018). Biosynthetic pathway and metabolic engineering of plant dihydrochalcones. J Agric Food Chem **66**: 2273–2280.

Ibrahim, R.K., Bruneau, A., and Bantignies, B. (1998). Plant *O*-methyltransferases: molecular analysis, common signature and classification. Plant Mol Biol **36**: 1–10.

Irmisch, S., Jiang, Y., Chen, F., Gershenzon, J., and Köllner, T.G. (2014). Terpene synthases and their contribution to herbivore-induced volatile emission in western balsam poplar (*Populus trichocarpa*). BMC Plant Biol **14**: 1–16.

Ishizu, E., Honda, S., Vongsak, B., and Kumazawa, S. (2018). Identification of plant origin of propolis from Thailand stingless bees by comparative analysis. NPC Natural Product Communications **13**: 973–975.

Isidorov, V.A. and Vinogorova, V.T. (2003). GC-MS analysis of compounds extracted from buds of *Populus balsamifera* and *Populus nigra*. Z. Naturforsch **58**: 355–360.

Jansson, S. and Douglas, C.J. (2007). *Populus*: A model system for plant biology. Annu Rev Plant Biol **58**: 435–458.

Jerković, I. and Mastelić, J. (2003). Volatile compounds from leaf-buds of *Populus nigra* L. (Salicaceae). Phytochemistry **63**: 109–113.

Johnson, R. (2010). Honey bee colony collapse disorder. Washington: Congressional Research Service.

Kane, J.M. and Kolb, T.E. (2010). Importance of resin ducts in reducing ponderosa pine mortality from bark beetle attack. Oecologia **164**: 601–609.

Kim, B.G., Kim, H., Hur, H.G., Lim, Y., and Ahn, J.H. (2006). Regioselectivity of 7-*O*-methyltransferase of poplar to flavones. J Biotechnol **126**: 241–247.

Kim, B.G., Sung, S.H., Chong, Y., Lim, Y., and Ahn, J.H. (2010). Plant flavonoid *O*-methyltransferases: Substrate specificity and application. Journal of Plant Biology **53**: 321–329.

Kim, D., Paggi, J.M., Park, C., Bennett, C., and Salzberg, S.L. (2019). Graph-based genome alignment and genotyping with HISAT2 and HISAT-genotype. Nat Biotechnol **37**: 907–915.

Kruse, L.H., Weigle, A.T., Irfan, M., Martínez-Gómez, J., Chobirko, J.D., Schaffer, J.E., Bennett, A.A., Specht, C.D., Jez, J.M., Shukla, D., and Moghe, G.D. (2022). Orthology-based analysis helps map evolutionary diversification and predict substrate class use of BAHD acyltransferases. Plant Journal **111**: 1453–1468.

Kujumgiev, A., Tsvetkova, I., Serkedjieva, Y., Bankova, V., Christov, R., and Popov, S. (1999). Antibacterial, antifungal and antiviral activity of propolis of different geographic origin. J Ethnopharmacol **64**: 235–240.

Kumazawa, S., Hamasaka, T., and Nakayama, T. (2004). Antioxidant activity of propolis of various geographic origins. Food Chem **84**: 329–339.

Kuś, P.M., Okińczyc, P., Jakovljević, M., Jokić, S., and Jerković, I. (2018). Development of supercritical CO2 extraction of bioactive phytochemicals from black poplar (*Populus nigra* L.) buds followed by GC–MS and UHPLC-DAD-QqTOF-MS. J Pharm Biomed Anal **158**: 15–27.

Lambert, J.B., Santiago-Blay, J.A., Wu, Y., Contreras, T.A., Johnson, C.L., and Bisulca, C.M. (2021). Characterization of phenolic plant exudates by nuclear magnetic resonance spectroscopy. J Nat Prod **84**: 2511–2524.

Langenheim, J.H. (1990). Plant Resins. Am Sci **78**: 16–24.

Langenheim, J.H. (2003). Plant resins: Chemistry, evolution, ecology, and ethnobotany (Timber Press: Portland, Oregon).

Lavoie, S., Legault, J., Simard, F., Chiasson, É., and Pichette, A. (2013). New antibacterial dihydrochalcone derivatives from buds of *Populus balsamifera*. Tetrahedron Lett **54**: 1631–1633.

Leonhardt, S.D. and Blüthgen, N. (2009). A sticky affair: resin collection by Bornean stingless bees. Biotropica **41**: 730–736.

Lex, A., Gehlenborg, N., Strobelt, H., Vuillemot, R., and Pfister, H. (2014). UpSet: Visualization of intersecting sets. IEEE Trans Vis Comput Graph **20**: 1983–1992.

Liu, C., Wang, X., Shulaev, V., and Dixon, R.A. (2016). A role for leucoanthocyanidin reductase in the extension of proanthocyanidins. Nat Plants **2**: 1–7.

Love, M.I., Huber, W., and Anders, S. (2014). Moderated estimation of fold change and dispersion for RNA-seq data with DESeq2. Genome Biol **15**: 1–21.

Ma, D., Reichelt, M., Yoshida, K., Gershenzon, J., and Constabel, C.P. (2018). Two R2R3-MYB proteins are broad repressors of flavonoid and phenylpropanoid metabolism in poplar. Plant Journal **96**: 949–965.

Mitton, J.B. and Grant, M.C. (1996). Genetic variation and the natural history of quaking aspen. Bioscience **46**: 25–31.

Moerman, D.E. (1998). Native American Ethnobotany (Timber Press: Portland, Oregon).

Muoki, R.C., Paul, A., Kumari, A., Singh, K., and Kumar, S. (2012). An improved protocol for the isolation of RNA from roots of tea (*Camellia sinensis* (L.) O. Kuntze). Mol Biotechnol **52**: 82–88.

Nagel, J., Culley, L.K., Lu, Y., Liu, E., Matthews, P.D., Stevens, J.F., and Page, J.E. (2008). EST analysis of hop glandular trichomes identifies an O-methyltransferase that catalyzes the biosynthesis of xanthohumol. Plant Cell **20**: 186–200.

Nissinen, K., Virjamo, V., Randriamanana, T., Sobuj, N., Sivadasan, U., Mehtätalo, L., Beuker, E., Julkunen-Tiitto, R., and Nybakken, L. (2017). Responses of growth and leaf phenolics in European aspen (*Populus tremula*) to climate change during juvenile phase change. Canadian Journal of Forest Research **47**: 1350–1363.

Orjala, J., Wright, A.D., Behrends, H., Folkers, G., Sticher, O., Rüegger, H., and Rali, T. (1994). Cytotoxic and antibacterial dihydrochalcones from Piper aduncum. J Nat Prod **57**: 18–26.

Paiva, E.A.S. (2016). How do secretory products cross the plant cell wall to be released? A new hypothesis involving cyclic mechanical actions of the protoplast. Ann Bot **117**: 533–540.

Pang, Z., Chong, J., Zhou, G., De Lima Morais, D.A., Chang, L., Barrette, M., Gauthier, C., Jacques, P.É., Li, S., and Xia, J. (2021). MetaboAnalyst 5.0: Narrowing the gap between raw spectra and functional insights. Nucleic Acids Res **49**: 388–396.

Philippe, R.N. and Bohlmann, J. (2007). Poplar defense against insect herbivores. Canadian Journal of Botany **85**: 1111–1126.

Phillips, M.A. and Croteau, R.B. (1999). Resin-based defenses in conifers. Trends Plant Sci **4**: 184–190.

Pluskal, T., Castillo, S., Villar-Briones, A., and Orešič, M. (2010). MZmine 2: Modular framework for processing, visualizing, and analyzing mass spectrometry-based molecular profile data. BMC Bioinformatics **11**: 1–11.

Pramsohler, M. and Neuner, G. (2013). Dehydration and osmotic adjustment in apple stem tissue during winter as it relates to the frost resistance of buds. Tree Physiol **33**: 807–816.

Rinne, P.L.H., Welling, A., and van der Schoot, C. (2010). Perennial Life Style of *Populus*: Dormancy Cycling and Overwintering. In Genetics and Genomics of *Populus*, S. Jansson, R.P. Bhalerao, and A.T. Groover, eds (Springer-Verlag Inc.: New York, NY, USA), pp. 171–200.

Rivière, C. (2016). Dihydrochalcones: occurrence in the plant kingdom, chemistry and biological activities. In Studies in Natural Products Chemistry (Elsevier B.V.), pp. 253–381.

Rogers, P.C. et al. (2020). A global view of aspen: Conservation science for widespread keystone systems. Glob Ecol Conserv **21**: 1–21.

Rohde, A., Prinsen, E., De Rycke, R., Engler, G., Van Montagu, M., and Boerjan, W. (2002). PtABI3 impinges on the growth and differentiation of embryonic leaves during bud set in poplar. Plant Cell **14**: 1885–1901.

Rohde, A., Ruttink, T., Hostyn, V., Sterck, L., Van Driessche, K., and Boerjan, W. (2007). Gene expression during the induction, maintenance, and release of dormancy in apical buds of poplar. J Exp Bot **58**: 4047–4060.

Roje, S. (2006). S-Adenosyl-*L*-methionine: Beyond the universal methyl group donor. Phytochemistry **67**: 1686–1698.

Rubiolo, P., Casetta, C., Cagliero, C., Brevard, H., Sgorbini, B., and Bicchi, C. (2013). *Populus nigra* L. bud absolute: A case study for a strategy of analysis of natural complex substances. Anal Bioanal Chem **405**: 1223–1235.

Russo, E.B. (2007). History of cannabis and its preparations in saga, science, and sobriquet. Chem Biodivers **4**: 1614–1648.

Ruttink, T., Arend, M., Morreel, K., Storme, V., Rombauts, S., Fromm, J., Bhalerao, R.P., Boerjan, W., and Rohde, A. (2007). A molecular timetable for apical bud formation and dormancy induction in poplar. Plant Cell **19**: 2370–2390.

Salatino, A., Fernandes-Silva, C.C., Righi, A.A., and Salatino, M.L.F. (2011). Propolis research and the chemistry of plant products. Nat Prod Rep **28**: 925–936.

Schmidt, A., Li, C., Jones, A.D., and Pichersky, E. (2012). Characterization of a flavonol 3-*O*-methyltransferase in the trichomes of the wild tomato species *Solanum habrochaites*. Planta **236**: 839–849.

Schmidt, A., Li, C., Shi, F., Jones, A.D., and Pichersky, E. (2011). Polymethylated myricetin in trichomes of the wild tomato species Solanum habrochaites and characterization of trichome-specific 3'/5'- and 7/4'-myricetin *O*-methyltransferases. Plant Physiol **155**: 1999–2009.

Shim, D., Ko, J.H., Kim, W.C., Wang, Q., Keathley, D.E., and Han, K.H. (2014). A molecular framework for seasonal growth-dormancy regulation in perennial plants. Hortic Res **1**: 14059.

Silim, S., Nash, R., Reynard, D., White, B., and Schroeder, W. (2009). Leaf gas exchange and water potential responses to drought in nine poplar (*Populus* spp.) clones with contrasting drought tolerance. Trees - Structure and Function **23**: 959–969.

Simone-Finstrom, M., Borba, R.S., Wilson, M., and Spivak, M. (2017). Propolis counteracts some threats to honey bee health. Insects **8**: 1–20.

Simone-Finstrom, M. and Spivak, M. (2010). Propolis and bee health: The natural history and significance of resin use by honey bees. Apidologie **41**: 295–311.

Singh, R.K., Svystun, T., AlDahmash, B., Jönsson, A.M., and Bhalerao, R.P. (2017). Photoperiod- and temperature-mediated control of phenology in trees – a molecular perspective. New Phytologist **213**: 511–524.

Sjödin, A., Street, N.R., Sandberg, G., Gustafsson, P., and Jansson, S. (2009). The *Populus* Genome Integrative Explorer (PopGenIE): A new resource for exploring the *Populus* genome. New Phytologist **182**: 1013–1025.

St-Pierre, B., Laflamme, P., Alarco, A.M., and De Luca, V. (1998). The terminal O-acetyltransferase involved in vindoline biosynthesis defines a new class of proteins responsible for coenzyme A-dependent acyl transfer. Plant Journal **14**: 703–713.

Sturgeon, K.B. (1979). Monoterpene variation in Ponderosa pine xylem resin related to western pine beetle predation. **33**: 803–814.

Taguchi, G., Shitchi, Y., Shirasawa, S., Yamamoto, H., and Hayashida, N. (2005). Molecular cloning, characterization, and downregulation of an acyltransferase that catalyzes the malonylation of flavonoid and naphthol glucosides in tobacco cells. Plant Journal **42**: 481–491.

Tanino, K.K., Kalcsits, L., Silim, S., Kendall, E., and Gray, G.R. (2010). Temperature-driven plasticity in growth cessation and dormancy development in deciduous woody plants: A

working hypothesis suggesting how molecular and cellular function is affected by temperature during dormancy induction. Plant Mol Biol **73**: 49–65.

Trapnell, C., Roberts, A., Goff, L., Pertea, G., Kim, D., Kelley, D.R., Pimentel, H., Salzberg, S.L., Rinn, J.L., and Pachter, L. (2012). Differential gene and transcript expression analysis of RNA-seq experiments with TopHat and Cufflinks. Nat Protoc **7**: 562–578.

Trapp, S. and Croteau, R. (2001). Defensive resin biosynthesis in conifers. Annu. Rev. Plant Physiol. Plant Mol. Biol **52**: 689–724.

Tsai, C.J., Harding, S.A., Tschaplinski, T.J., Lindroth, R.L., and Yuan, Y. (2006). Genome-wide analysis of the structural genes regulating defense phenylpropanoid metabolism in *Populus*. New Phytologist **172**: 47–62.

Tuominen, L.K., Johnson, V.E., and Tsai, C.J. (2011). Differential phylogenetic expansions in BAHD acyltransferases across five angiosperm taxa and evidence of divergent expression among *Populus* paralogues. BMC Genomics **12**: 1–17.

Tuskan, G.A. et al. (2012). The genome of black cottonwood, *Populus trichocarpa* (Torr. & Gray). Science (1979) **313**: 1596–1604.

Tyśkiewicz, K., Konkol, M., Kowalski, R., Rój, E., Warmiński, K., Krzyżaniak, M., Gil, Ł., and Stolarski, M.J. (2019). Characterization of bioactive compounds in the biomass of black locust, poplar and willow. Trees - Structure and Function **33**: 1235–1263.

Uprety, Y., Asselin, H., Dhakal, A., and Julien, N. (2012). Traditional use of medicinal plants in the boreal forest of Canada: Review and perspectives. J Ethnobiol Ethnomed **8**: 1–14.

Valkama, E., Salminen, J.P., Koricheva, J., and Pihlaja, K. (2004). Changes in leaf trichomes and epicuticular flavonoids during leaf development in three birch taxa. Ann Bot **94**: 233–242.

Veloz, J.J., Alvear, M., and Salazar, L.A. (2019). Antimicrobial and antibiofilm activity against *Streptococcus* mutans of individual and mixtures of the main polyphenolic compounds found in Chilean propolis. Biomed Res Int **2019**: 1–8.

Vogt, T. (2010). Phenylpropanoid biosynthesis. Mol Plant **3**: 2–20.

Wang, L., Chen, K., Zhang, M., Ye, M., and Qiao, X. (2022). Catalytic function, mechanism, and application of plant acyltransferases. Crit Rev Biotechnol **42**: 125–144.

Wang, X., Liu, Y.-S., Nair, U.B., Armstrong, D.W., Ellis, B., and Williams, K.M. (1997). Enantiomeric composition of monoterpenes in conifer resins. Tetrahedron Asymmetry **8**: 3977–3984.

Whetten, R. and Sederoff, R. (1995). Lignin biosynthesis. Plant Cell **7**: 1001–1013.

Wilson, M.B., Brinkman, D., Spivak, M., Gardner, G., and Cohen, J.D. (2015). Regional variation in composition and antimicrobial activity of US propolis against *Paenibacillus larvae* and *Ascosphaera apis*. J Invertebr Pathol **124**: 44–50.

Wilson, M.B., Pawlus, A.D., Brinkman, D., Gardner, G., Hegeman, A.D., Spivak, M., and Cohen, J.D. (2017). 3-Acyl dihydroflavonols from poplar resins collected by honey bees

are active against the bee pathogens *Paenibacillus larvae* and *Ascosphaera apis*. Phytochemistry **138**: 83–92.

Wilson, M.B., Spivak, M., Hegeman, A.D., Rendahl, A., and Cohen, J.D. (2013). Metabolomics reveals the origins of antimicrobial plant resins collected by honey bees. PLoS One **8**: 77512.

Winkel-Shirley, B. (2001). Flavonoid biosynthesis. A colorful model for genetics, biochemistry, cell biology, and biotechnology. Plant Physiol **126**: 485–493.

Witte, T.E., Harris, L.J., Nguyen, H.D.T., Hermans, A., Johnston, A., Sproule, A., Dettman, J.R., Boddy, C.N., and Overy, D.P. (2021). Apicidin biosynthesis is linked to accessory chromosomes in *Fusarium poae* isolates. BMC Genomics **22**: 591.

Wollenweber, E. and Dietz, V.H. (1981). Occurrence and distribution of free flavonoid aglycones in plants. Phytochemistry **20**: 869–932.

Yahyaa, M., Ali, S., Davidovich-Rikanati, R., Ibdah, M., Shachtier, A., Eyal, Y., Lewinsohn, E., and Ibdah, M. (2017). Characterization of three chalcone synthase-like genes from apple (*Malus x domestica* Borkh.). Phytochemistry **140**: 125–133.

Yang, Q., Reinhard, K., Schiltz, E., and Matern, U. (1997). Characterization and heterologous expression of hydroxycinnamoyl/benzoyl-CoA:anthranilate N-hydroxycinnamoyl/benzoyltransferase from elicited cell cultures of carnation, *Dianthus caryophyllus* L. Plant Mol Biol **35**: 777–789.

Yonekura-Sakakibara, K., Higashi, Y., and Nakabayashi, R. (2019). The origin and evolution of plant flavonoid metabolism. Front Plant Sci **10**: 943.